UNIVERSIDAD COMPLUTENSE DE MADRID

FACULTAD DE CIENCIAS FÍSICAS

Departamento de Física de la Tierra, Astronomía y Astrofísica II

(Astrofísica y Ciencias de la Atmósfera)

TESIS DOCTORAL

Reliability analysis and radiation hardness assurance for the Extreme Universe Space Observatory (EUSO)

Análisis de fiabilidad y resistencia a la radiación espacial del Observatorio del Universo Extremo (EUSO)

MEMORIA PARA OPTAR AL GRADO DE DOCTOR

PRESENTADA POR

Héctor Prieto Alfonso

Directores

María Dolores Rodríguez Frías y
Luis del Peral Gochicoa

Madrid, 2017

Universidad Complutense de Madrid
Facultad de CC. Físicas
Dpto. de Física de la Tierra, Astronomía y Astrofísica II
(Astrofísica y cc. de la Atmósfera)

Tesis Doctoral

Reliability Analysis and Radiation hardness assurance for the Extreme Universe Space Observatory (EUSO)

Análisis de fiabilidad y resistencia a la radiación espacial del Observatorio del Universo Extremo (EUSO)

Dirigida por los doctores:

M. D. Rodríguez Frías y L. del Peral Gochicoa

Héctor Prieto Alfonso

Madrid, September 1, 2016

Contents

List of Figures

List of Tables

Listings

Abstract

The main objective of this Doctoral Thesis was to perform a reliability prediction of the JEM-EUSO space telescope due to the impact of Total Ionizing Dose (TID) and Single Event Effects (SEE) on its focal surface electronics when on-board the International Space Station (ISS)). The aim of this analysis was to evaluate its present and potential reliability of the instrument so as to ensure its mission success during its 5 years of operation. By implementing pre existing models, a computational tool for estimating such failure rates has been created.

JEM-EUSO is a large imaging telescope that will study Extremely-High Energy Cosmic Rays (EHECR) from space by imaging the UV light generated by Extensive Air Showers (EAS) particles. These EAS are produced by cosmic rays with energies that can reach and exceed 10^{20} eV. Looking downward the Earth from the International Space Station (ISS) will detect such particles observing the UV light generated by Extensive Air Showers (EAS) the UHECRs develop in the atmosphere. Among the objectives of JEM-EUSO are: setting up a new window for observing the Universe never used before and therefore opening the Particle Astronomy Era; extend the measurement of the energy spectrum of the cosmic radiation beyond Greisen-Zatsepin-Kuzmin (GZK) suppresion energy; observe Extremely High Energy Gamma Rays (EHEGR) and Extremely High Energy Neutrinos (EHEN) opening the field of EHEGR & EHEN Astronomy.

The analysis of the reliability of a system is particularly useful in engineering at any time of the system operating life. In this case, the JEM-EUSO space telescope, will be operating at least 5 years. Therefore, the reliability analysis of this system is considered crucial, especially when the environment is the outer space.

Thus, the evaluation of the performance of the electronics components of the JEM-EUSO space telescope has been carried out. This assessment included the Photomultiplier tubes of its focal surface. With this analysis, their likelihood of failure and the consequences of these failures were obtained. During the analysis of the degradation of the performance of this kind of equipment it was observed that the degradiation effects were not appropriately or completely addressed by the main reliability prediction models: 217 and 217 Plus. Therefore, responsivity, sensitivity and other degradation factors related to PMTs were needed to be developed. It is therefore suggested that these models being considered in further versions of these reliability prediction models or any other methods further released.

Although the principal components of PMTs are semiconductors, and their operation is that of a linear circuit (whose purpose is to amplify the current from photoemissive materials) they are not considered as a semiconductor-based electronic equipment. It is well known that PMTs are affected by high brightness effect. This phenomenon reduces the transmittance of the Crystal Window: the lower the transmittance the less the photoelectrons observed when a high energy cosmic ray event occurred. The PMTs also suffer degradation due to secondary electron emission by ionizing particles. Effect that wears out the equipment and generates noise at the output of these components.

As a result of this study, taking into account the values produced by the model based on the TID, as well as the darkening of the glass, they show similar values in terms of degradation or aging. Therefore, as a preliminary result, it is possible to conclude that the TID model proposed herein for PMTs can be "validated". In other words, the TID model proposed can give us an approach of possible radiation effects on these components.

The design and use of a reliability analysis tool designed for JEM-EUSO space telescope, may significantly increase the knowledge of components implemented on the focal surface of the instrument as well as their behavior. This computational tool is able to provide basic reliability data from the statistical distribution of failures. It should not be unnecessarily restricted, but as flexible as possible.

Keywords: Reliability, Electronic Systems, Space Radiation, JEM-EUSO.

Resumen

El objetivo principal de esta tesis es el análisis de la fiabilidad del telescopio espacial JEM-EUSO considerando para ello los fallos asociados a Dosis Total de Ionización (TID) y Efectos de Evento Único (SEE). Eventos y/o partículas presentes en la órbita espacial LEO. Órbita en la cual transita la estación espacial internacional (ISS) quien llevará a bordo al telescopio JEM-EUSO. Durante el desarrollo de este trabajo y utilizando métodos actuales de predicción de fiabilidad, se ha creado una herramienta computacional con el fin de sistematizar cualquier evaluación futura de fiabilidad de electrónica espacial.

JEM-EUSO ("Extreme Universe Space Observatory on the Japanese Experiment Module") es un nuevo telescopio espacial que utilizará grandes volúmenes de atmósfera de la Tierra como detector de las partículas más energéticas en el Universo (E $> 10^{19}$ eV). JEM-EUSO observa los destellos breves de luz de fluorescencia en la atmósfera de la Tierra causados por las partículas provenientes de las profundidades del espacio. Se espera que este instrumento permita, por fin, desvelar las incógnitas aun existentes acerca del origen y propagación de esta radiación. Cada 90 minutos, JEM-EUSO orbitará la Tierra, a bordo de la estación espacial internacional (ISS, por sus siglas en inglés) a una altitud de aproximadamente 400 km. Dicho entorno de funcionamiento, hace de un análisis de fiabilidad un estudio crucial en estos equipos. JEM-EUSO, por otra parte, no cuenta con apoyo externo de los astronautas que se encuentran en la ISS. Es decir, el reemplazo de piezas u/o componentes no sería posible a lo largo de la misión. Para ello, estudios de fiabilidad como los llevado a cabo en este trabajo son fundamentales. Estas evaluaciones aportan datos esenciales que permiten construir equipos e instrumentos adaptados a las necesidades de funcionamiento.

Estudios del rendimiento de los equipos electrónicos de JEM-EUSO se han llevado a cabo a lo largo de este trabajo. Estas evaluaciones incluyen a su vez, los tubos fotomultiplicadores del instrumento. Dicho sea, el corazón del Telescopio. Con este análisis, las probabilidades de fallo y sus respectivas consecuencias han sido obtenidas. Sin embargo y para poder llevar a cabo este estudio, ha sido necesario el desarrollo de modelos que permitiesen comprender las degradaciones de sensibilidad y respuesta de los tubos fotomultiplicadores. Estos tipos de cálculo no están comprendidos entre los dos principales modelos de análisis de fiablidad: 217 Plus y 217F. Como contribución, se propone que en futuras versiones de estos modelos antes mencionados, sean considerados los estudios que en este trabajo han sido desarrollados. Con esto se permitiría tener una visión más realista de la degradación de estos equipos tan singulares como los PMTs.

Aunque los componentes principales de los tubos fotomultiplicadores sean semiconductores, y su modo de operación sea la de un circuito lineal, éstos no son considerados equipos semiconductores. Es ampliamente conocido que uno de los effectos que más puede afectar a un PMTs es el brillo (exceso de luz). Este fenómeno reduce la transmitancia del cristal de la ventana de este equipo: mientras menor sea la transmitancia, peor será la observación de un evento producido por un rayo cósmico de altas energías. Los PMTs también sufren de degradación de su funcionamiento debido a emisión secundaria de electrones producida por partículas ionizantes. Efecto que degrada el equipo y genera señales de ruido innecesario a la salida de estos equipos.

Como resultado de este estudio, al comparar los resultados arrojados por el modelo TID, y los del oscurecimiento del cristal de los PMTs, éstos muestran valores similares en terminos de degradación o envejecimiento. Por lo tanto, como resultados preliminares, es posible concluir que el modelo TID propuesto en este estudio puede ser utilizado como un modelo "válido" para estos tipos de evaluaciones. En otras palabras, el modelo TID propuesto nos permite conocer más de cerca los efectos de radiación en este tipo de componentes.

El diseño y uso de un sistema computacional de análisis de fiabilidad desarrollado para la misión espacial JEM-EUSO, incrementaría de forma significativa la comprensión del funcionamiento de los componentes utilizados en la superficie focal del instrumento,

así como su desempeño. Este sistema será capaz de aportar datos básicos y esenciales de fiabilidad. Dicho sistema será tan flexible y abierto a futuras mejoras y actualizaciones como sean necesarias.

Palabras Clave: JEM-EUSO, Fiabilidad, Sistemas electrónicos, Radiación espacial.

Agradecimientos

Venezuela

Mi casa. El lugar desde donde se me ha apoyado enormemente durante la bella aventura que ha supuesto este trabajo. A mis padres Carmen y José. Mis Amados padres y mi adorado hermano Javito que no han descansado hasta hacer de este sueño una realidad como es ahora. Gracias por tanto amor y dedicación. A mis tías, tíos y primos que no han olvidado a su sobrino y primo y siempre tienen esa sonrisa de amor infinito. A mi ángel Virginia, que siempre me envía esas bendiciones tan bien guardadas y que no paran de estar presentes todos los días de mi vida. ¡Gracias, abuelita! A todos, Gracias por ser lo que son y por permitirme tenerlos. ¡Gracias! A María Juana, Barranco y Joyce, mi otra familia, vamos, el amor de toda una vida juntos. Gracias por ese calor humano desde siempre. A mis colegas y grandes amigos de la Uni y de siempre: Pedro, Paula, Marcel, Marco, Kimi, Jose, Vanessa. Gracias chicos por tantas sonrisas y abrazos sinceros.

A Iriana, Jesús y Mariana... ¡¡¡GRACIAS por todo el amor y amistad sincera!!!

Gracias por enseãrme que la distancia no es más que un mito.

España

Esto parece un tren de cercanías que parte desde Atocha pasa por Campomanes, con parada en Gijón, Alcalá y Guadalajara y Madrid como destino final... Ya bien lo dijo Sabina: yo me bajo en Atocha, yo me quedo en Madrid. Pues eso, yo me quedé en Madrid.

Y vaya si tengo que decir. ¡Más que Encarta!

A Miri: artifice de mis sueños. Tú, el amor más bonito que haya podido tener Jamás.

¡Gracias, princesa!

A Maricarmen: mi madre asturiana. A ti, ¿qué no te debo? ¡Gracias!

A Jose Alberto: Gracias por tu amor incondicional y por haber sido complice de este trabajo. ¡Gracias, gran amigo!

A mi nueva familia: Miri, Malena, Paco, Alberto, Mario, Ana, Irma. Más que una familia, un todo.

A mis amigos de la UAH: Mihaela, Sandra, Germán, Cristina, Sara, Noelia, Lupe, Jorge, Miguel, Noelita, Nacho, Judit, Antonio, Belén, María, Eugenio, Borja, Paloma, Laura, Isabel, Asier, Silvia y Pablo. Gracias por tan hermosos momentos compartidos, y por estar allí cuando las cosas se ponían más feas que un coche por debajo. Gracias de todo corazón.

A Loly y Luis: Gracias por depositar vuestra confianza en mi. Sin vuestro apoyo y esfuerzo esto no hubiese sido posible. Infinitas gracias!

A Mi hermano Hatu, Gea, Julio, Mari, Jhonny y Helena: gracias por acortar las distancias. Gracias por tanto amor!

Italia

Grazie mile, Marco Casolino. Eternamente agradecido y orgulloso de haberte conocido y. Gracias por tu apoyo y consejos a lo largo de este trabajo.

Suecia

A Oscar Larsson: Gracias por la dedicación y el amor fraterno que me has regalado. Han sido increibles. Gracias, amigo!

Japón

A Ohata, Tsuno, Toshi, Ohata, Francesco, Lech, Hiroko, Yuka, Stefano, Erin. ¡¡Gracias por hacer de mi vida en Japón una maravillosa aventura!!

Francia, Canadá y USA

A todos mis colegas que con tanto cariño siempre recuerdo: Camille, Michele, Jean, Guillaume, Peter, Brian y Tom. Gracias de todo corazón.

¡Gracias por ese amor infinito!

Chapter 1

Introduction

1.1 Objectives

The objective of this Ph.D Thesis is to test the validity of concepts and technical choices made today for the JEM-EUSO space telescope mission scheduled for 2020, as well as for any subsequent project aimed at observing giant air showers induced by energetic cosmic rays from Space.

The design and construction of this telescope is indeed a technical challenge, as it involves the use of new technologies from laboratories of both industry and research in areas as diverse as large optical and accurate Fresnel lenses, a technique of photo detection highly sensitive and with good resolution, and very innovative analog and digital electronics.

This work will focus on the development of a statistical methods in order to comprehend the nature of the impact of Space environment on electronics devoted for Space applications. With this statistical methods we pretend to build a computational tool which to assess the reliability assessment of the Space experiment JEM-EUSO focal surface electronics.

1.2 About Reliability analysis of Space electronics components

In this thesis the field of the reliability of space electronic components is investigated. As the name suggests, the methods developed in this field tries to predict the behavior of electronic components when exposed to different situations during their missions. A space mission leads to huge technological challenges. Developing new measurement techniques of the reliability in terms of failure rates is a constantly evolving field, growing and changing every day since electronics and space engineering development never stops.

The huge potential the reliability field has is tremendous, saving both the resources necessary to create new electronics due to the data extracted from statistical studies, as well as money in terms of redundancy of elements and space within the aircraft, rocket, shuttles or satellites.

The first attempts to develop a reliability standard was the american military handbook 217 (MIL-HDBK-217), its first compilation was established in 1962 by the U.S Army. MIL-HDBK-217 latest version dates from 1991. These standards are far of being completed. Finding no standards for new components is a common issue in the field of reliability. Developing new models for instruments designed for space applications is the challenge of this science.

The difficulties and duties faced in producing high quality statistical models in order to evaluate the reliability of space components, are related to the lack of statistical information in order to understand their behavior in a mathematical concept. Attempts to replicate the behavior of these components under multiple failure sources are mostly done in private laboratories and results obtained are considered classified information.

As a result, in terms of reliability, the space research community when designing a new instrument has to trust in the information provided by the private industry. Therefore a new statistical method is investigated and developed in this thesis. The methods proposed herein are focused on the Photo-Multiplier Tubes (PMTs) failure rates. These failure rates are based on the the impact and influence the radiation sources have on the electronics in

Low Earth Orbit (LEO) environment as well as the failure rates due to the most important failing sources -wear out- of the PMT, considering, adapting and improving part of the MIL-217 Plus prediction model related to semiconductors, vacuum tubes and different kind of electronics.

1.3 Contribution of this thesis

The main contributions of this thesis fall into 4 categories: evaluation of the different standards for space applications, adaptation and enhancement of the MIL-217 Plus prediction model for semiconductors family, evaluation of radiation sources and statistical model so as to perform a reliability and radiation hardness assurance for PMT component and finally developing a computational model which includes the development of the techniques previously mentioned to evaluate in a computational perspective the reliability of the PMT under the influences of sources of failure while working in Space. To achieve these goals, an extensive research and review of existing statistical methods currently used in space electronics has been carried out. This section presents the main original contributions and how they can be achieved.

The **main contribution** of this thesis is devoted to perform a comparative, qualitative and quantitative evaluation of the reliability standards for space applications. The goals of this evaluation are:

- To uncover the influence of different standards on the reliability analysis.
- To comprehend the impact of modifications of their parameters can lead to changes in the quality of the statistical reliability analysis method. A general overview of this contribution has been presented in section 1.2.

The **second contribution** of this thesis refers to the study of the principal influence of space radiation environment in electronic components, condition expressed in terms of failing rates. Moreover, the scope of this study is related to the comprehension of the multiple sources of radiation and their mechanism in the orbit where the instruments are supposed to be operating. In terms of reliability, an electronic component should be at least assessed by a failure rate analysis based on statistical methods, including a radiation

hardness assurance, to statistically guarantee the successful performance of the component selected for the experiment. With this research it is intended to demonstrate that a statistical evaluation of the reliability of space electronic components provides a vital prediction and knowledge of the behavior and performance of the electronics components before mission is started. A method to identify the most critical failing sources of the PMT is proposed in order to demonstrate its limits.

The **third contribution** refers to the development of statistical methods which to assess the reliability of any electronic component devoted to Space applications.

The contributions listed above are achieved by setting the following list of goals:

Goal 1 is to conduct a study of the whole electrical and electronic components of the focal surface of JEM-EUSO space telescope, in order to understand the behavior of the instrument as a whole. Thus detecting the most critical elements, and focusing mainly on the focal surface electronics, which leads the understanding of the performance of the PMT.

Goal 2 is to deeply analyze the main and current methods and space and military standards for the reliability assessment performance. A required review toward to select the appropriate methods to be investigated during this thesis. The selection of these methods is determined by their applicability.

Goal 3 is to review the existing evaluation methods of reliability analysis in terms of space radiation. A step toward developing a suitable evaluation strategy based on the characteristics of radiation sources that may affect the PMT performance. An impact given in terms of failing rates; how to reduce it and how feasible it is to apply it. This evaluation strategy assesses the main mechanism of influence, the available tools, and the application of these tools.

Goal 4 is to integrate the most important mechanism of failure of PMTs. Thereafter performing a reliability analysis of the PMTs in terms of failure rates with respects to the main failing sources. The implementation of the statistical analysis is done in such a way that it is highly customizable, so that a comprehensive evaluation can

be performed.

Goal 5 is to perform qualitative, quantitative and comparative evaluations of the reliability analysis.

Goal 6 is to create a computational tool to perform a statistical reliability analysis in terms of failure rate model based on the requirements of the JEM-EUSO space telescope.

Goal 7 is to identify the main weaknesses of the methods developed in this thesis and propose improvements.

1.4 Scientific motivation

Most of the work described in this thesis was conducted at the University of Alcalá (UAH) in Alcalá de Henares, Madrid, Spain. The reason for conducting the research work at this university was in principle due to the important role the SPAS group of UAH plays as one of the main contributor and collaborator and developer of the JEM-EUSO Space Telescope. Secondly due to our highly involvement into the development of the electronics and IR Camera of the JEM-EUSO Space telescope. These two reasons had lead us to comprehend the crucial role the PMTs play on the focal surface of the telescope. Assessing their performance is a mandatory task that we at the SPAS group took.

1.5 Personal motivation

(1) I have served as a Junior Researcher at the Faculty of Physics of the UAH for more than 4 years involved in the JEM-EUSO space telescope project. Thus, I have gained a good understanding of the instrument and its scientific goals; (2) I have been actively involved in the development and design of High Voltage Power Supplies prototypes for the JEM-EUSO space telescope focal surface. Being my prototype one of the candidates to be considered for the JEM-EUSO space telescope collaboration in the near future; (3) Over the past three years, I have been involved in the development of reliability and risk analysis for the Infra Red Camera. Prototype developed and tested in Spain; (4) I

participated as the reliability engineer of the IR Camera and the responsible of the power supply design of the EUSO-BALLOON pathfinder;

1.6 Thesis Outline

This Thesis is structured in 7 chapters; including this general introduction, chapter 1 contains a brief introduction of the dissertation and Chapter 7 contains the conclusions and discussion of the results regarding the research of this thesis as well as an outlook.

The Thesis Outline will be explained regarding its main goals.

Chapter 2 presents a description of JEM-EUSO space telescope mission, so as to comprehend the electronics of JEM-EUSO space telescope focal surface. This chapter leads to know the extent of all systems and subsystems that encompasses it, as well as predicting their behavior while performing their tasks. An interesting, necessary and crucial information as it allows us to comprehend those aspects to consider when creating the model for reliability estimation.

Chapter 3 presents the study of current standards and methods used to perform a reliability analysis.

Chapter 4 presents the first "prototype" of the statistical methods to perform the reliability analysis of the JEM-EUSO PMTs. It includes the radiation failure mechanism sources study for being considered within the novel statistical analysis method.

Chapter 5 focuses on the development and the implementation of a method of reliability analysis which determines the performance degradation of PMTs.

Chapter 6 presents the software engineering used while developing the computational tool.

1.7 Limitations

The research work is about failures due to radiation and electronic performance in PMTs components related to complex mechanical systems and infrastructures for which the environment is Space. The degradation process in mechanical systems is not considered.

Failures initiated on account of human errors are also not considered.

Chapter 2

JEM-EUSO

2.1 Objectives of JEM-EUSO

JEM-EUSO space observatory [1] is planned with a very large exposure factor which will exceed the critical exposure factor required for observing the most of the sources within the propagating horizon of about one hundred Mpc. The main science objective of JEM-EUSO is the source-identifying astronomy in particle channel with extremely-high-energy particles.

Quasi-linear tracking of the source objects through galactic magnetic field should become feasible at energy 10^{19} eV for all-sky. The individual GZK profile in high statistics experiments should differ from source to source due to different distance unless Lorentz invariance is somehow limited. In addition, JEM-EUSO has three exploratory test observations:

1. Extremely high energy neutrinos beginning at E$>10^{19}$ eV: neutrinos as being expected to have a slowly increasing cross section in the Standard Model. In particular, hundreds of times more in the extra dimensions model.

2. Fundamental physics at extreme super LHC (Large Hadronic Collider) energies with the hierarchical unified energy much below the GUT scale.

3. Global atmospheric observation. Including large scale and local plasma discharges,

night glow, meteorites and others.

2.2 The Mission

The JEM-EUSO mission [2] illustrated in Figure 2.1 explores the origin of the EHECRs above 100 EeV and explores the limits of the fundamental physics, through the observations of their arrival directions and energies. It is designed to open a new particle astronomy channel.

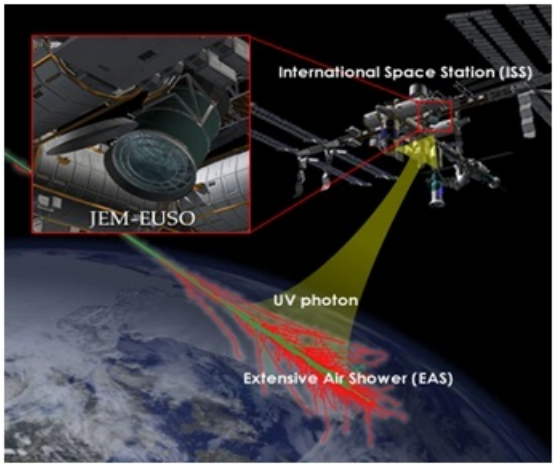

Figure 2.1: JEM-EUSO On-board the International Space Station, [3]

This super-wide-field of view (60 degrees) telescope with a diameter of about 2.5 m looks down from space onto the night sky to detect near UV photons (330-400 nm, both fluorescence and Cherenkov photons) emitted from the giant air showers produced by EHECRs. The arrival direction map with more than five hundred events will tell us the origin of the EHECRs and allow us to identify the nearest EHECR sources with known astronomical objects. It will allow them to be examined in other astronomical channels. This is likely to lead to an understanding of the acceleration mechanisms perhaps producing discoveries in Astrophysics and/or Fundamental Physics.

The comparison of the energy spectra among the spatially resolved individual sources will help to clarify the acceleration/emission mechanism, and also finally confirm the Greisen-Zatsepin-Kuz'min process for the validation of Lorentz invariance up to $\gamma \sim 10^{11}$.

Neutral components (neutrinos and gamma rays) can also be detected as well, if their fluxes are high enough. The JEM-EUSO mission is planned to be launched by a H2B rocket and transferred to ISS by H2 Transfer Vehicle (HTV) or by the Dragon. It will be attached to the Exposed Facility external experiment platform of "KIBO".

Table 2.1 lists the main parameters of the JEM-EUSO mission .

Parameter	**Value**
Mission Lifetime	3+2 years
Launch Rocket	H2B or Dragon
Transport Vehicle	HTV
Accommodation on JEM	EF 2 (or 9)
Instrument mass	1938 kg
Power	926(op), 352(non op)
Data rate	285 kbps (+ on board storage)
Height of the orbit	400 km
Inclination of the orbit	51.6°

Table 2.1: Main parameters of the JEM-EUSO Mission , [3]

2.3 International Space Station

The International Space Station is the largest and most complex international scientific project in history. The station represents a move of unprecedented scale off the home planet that began in 1998 with the launch of the first two components, the Unity and Zarya modules. Led by the United States, the International Space Station draws upon the scientific and technological resources of 16 nations: Canada, Japan, Russia, 11 nations of the European Space Agency and Brazil [4], illustrated in Figure 2.2.

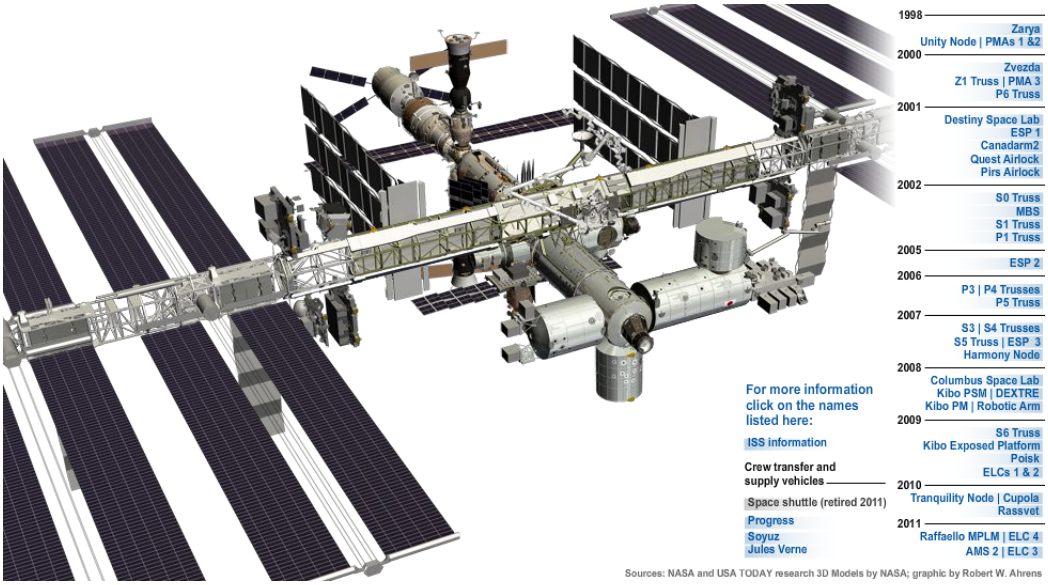

Figure 2.2: International Space Station, [5]

The station is in an orbit with an altitude of 250 statute miles with an inclination of 51.6 degrees. This orbit allows the station to be reached by the launch vehicles of all the international partners to provide a robust capability for the delivery of crews and supplies. The orbit also provides excellent Earth observations with coverage of 85 percent of the globe and over flight of 95 percent of the population. Already, about 500,000 pounds of station components have been built at factories around the world. The two-module complex now in orbit has a mass of more than 74,000 pounds and measures 76 feet long with a 78-foot wingspan tip to tip of the solar arrays. The current station's internal pressurized volume is 4,635 cubic feet. The Space Shuttle Discovery performed the first

docking with the new station in May 1999 on mission STS-96, delivering almost two tons of internal and external supplies.

The Japanese Experiment Module (JEM) [6], known as "Kibo" which means hope in Japanese as illustrated in figure 2.3, is Japan's first human-rated space facility and the Japan Aerospace Exploration Agency's (JAXA's) first contribution to the International Space Station (ISS) program.

Kibo was designed and developed with a view to conducting scientific research activities on orbit. In Kibo, a maximum of four astronauts can perform experimental activities. Currently, educational, cultural and commercial uses of Kibo are also planned. Thus, as a part of the ISS, Kibo will provide extensive opportunities for utilization of the space environment.Resources necessary for Kibo's on-orbit operation, such as air, power, data, and cooling fluid, are provided from the US segment of the ISS.

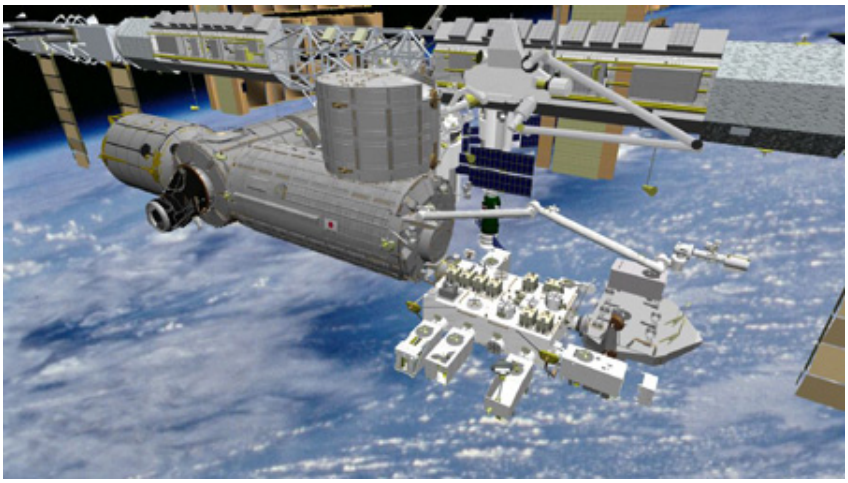

Figure 2.3: ISS and KIBO, the Japanese Experiment Module (JEM), [6]

2.3.1 Major Component

Kibo is a complex facility consisting of the following six major elements:

- Pressurized Module (PM)
- Exposed Facility (EF)
- Experiment Logistics Module-Pressurized Section (ELM-PS)
- Experiment Logistics Module-Exposed Section

- Japanese Experimental Module Remote Manipulator System (JMRMS)
- Inter-orbit Communication System (ICS)

Since JEM-EUSO will be located on the Exposed Facility of JEM, a deeply look at this facility is mandatory in order to have a best understanding to comprise the operation of the instrument onboard the ISS.

2.3.2 Exposed Facility (EF)

The Exposed Facility (EF) illustrated in figure 2.4 provides a multipurpose platform where science experiments can be deployed and operated in the exposed environment. The payloads attached to the EF can be exchanged or retrieved by Kibo's robotic arm, the JEM Remote Manipulator System (JEMRMS).

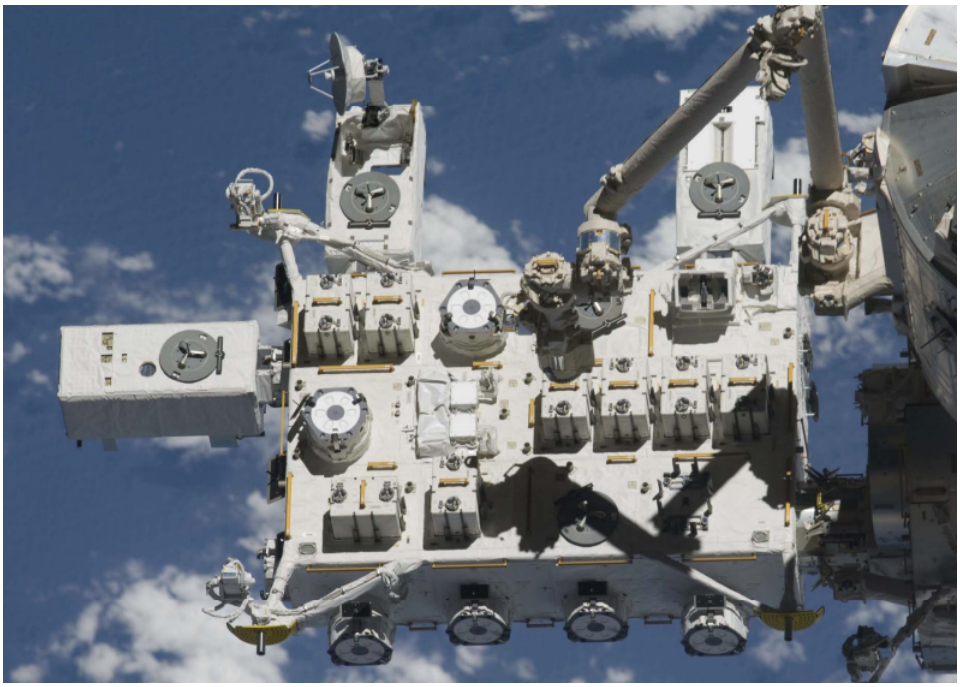

Figure 2.4: Exposed Facility of the Japanese Experimental Module (KIBO), [7]

The electrical and mechanical specification of the Exposed facility is provided by table 2.2.

Item	Specification
Shape	Box Shaped
Width	5.0m
Height	3.8m
Length	5.2m
Mass (at launch)	4.1 tons
Payloads attached	12 (including 2 for JEM system 1 for temporary storage
Power	Max. 11kW 120V (Direct Current)
Lifetime	More than ten years

Table 2.2: Main Specifications of the Exposed Facility of the Japanese Experimental Module (KIBO) , [6]

2.3.3 Exposed Facility (EF) Structure

The EF will be operated while berthed to the Pressurized Module (PM). The Equipment Exchange Units (EEUs) located on the EF can accommodate a maximum of 12 payloads, as illustrated in figure 2.5 including the EF experiments, Experiment Logistics Module-Exposed Section (ELM- ES), HTV-EP and the Inter-Orbit Communication System (ICS).

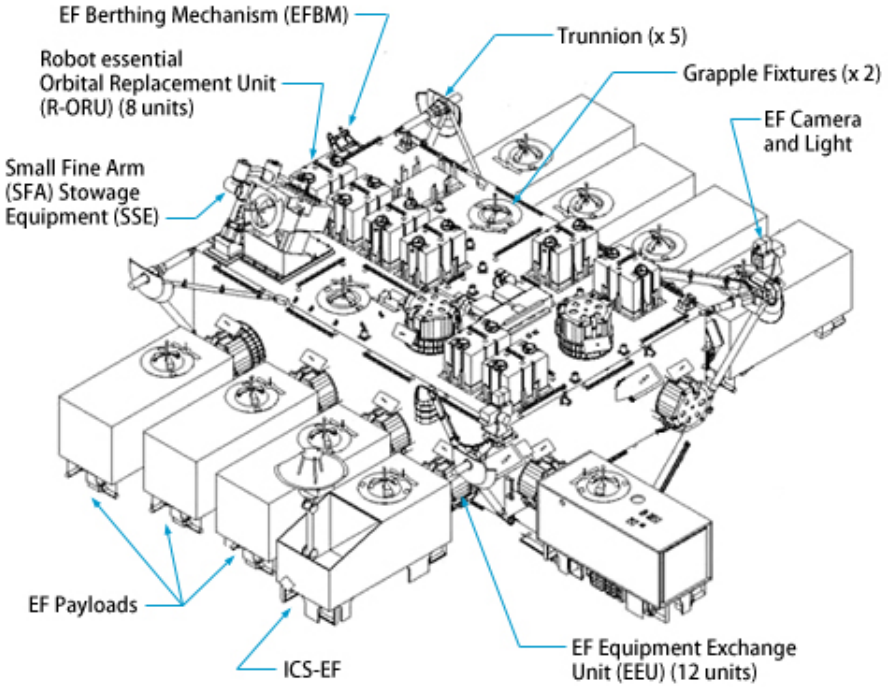

Figure 2.5: Structure of the EF, [6]

2.4 JEM-EUSO Telescope

The JEM-EUSO instrument [2] consists of the main telescope, an atmosphere monitoring system, and a calibration system [8]. The main telescope of the JEM-EUSO mission is an extremely-fast (μs) and highly-pixelized (3×10^5 pixels) digital camera with a large diameter (about 2.5 m) and a wide-FoV($\pm 30°$). It works in near UV wavelength (330-400 nm) with single-photoncounting mode.

The telescope consists of four parts: the optics, the focal surface detector and electronics, and the structure. The optics focuses the incident UV photons onto the focal surface with an angular resolution of 0.07 degrees [9]. The focal surface detector converts the incident photons to photoelectrons and then to electric pulses [10, 11].

The data electronics issues a trigger for airshower event or other transient event in the atmosphere and send necessary data to ground for further analysis. Atmospheric Monitoring System (AMS) monitors the Earth's atmosphere continuously inside the FoV of the JEM-EUSO telescope [12]. The AMS uses IR camera, Lidar, and the slow data

of the main telescope to measure the cloud-top height with accuracy better than 500 m. The calibration system measures the efficiencies of the optics, the focal surface detector, and the data acquisition electronics [13].

The list of the main parameters of JEM-EUSO telescope is reported in table 2.3.

Parameter	**Value**
Field of View	$\pm 30^{\circ}$
Observational area	$> 1.9 \times 10^5$ km^2
Optical Bandwidth	330 - 400 nm
Focal Surface Area	4.5 m^2
Number of pixels	3.2×10^5
Pixel size	2.9 mm
Pixel size at ground	$\sim$ 550 m
Spatial resolution	0.07°
Event time sampling	2.5 μs
Duty Cycle $\times$ cloud impact	$\sim$ 14%

Table 2.3: Parameters of the JEM-EUSO telescope , [3]

2.4.1 Mission duration

JEM-EUSO is planned to be launched by an H2B rocket and will be conveyed to the ISS by the H-II Transfer Vehicle (HTV) illustrated by figure 2.6a. It may also be taken to the ISS by the SpaceX Dragon delivery system ilustrated in figure 2.6b. Once at the ISS, it will be attached to one of the ports for non-standard payloads of the Exposure Facility (EF) of the Japanese Experiment Module (JEM). Data will be transmitted via TDRS to the Mission Operation Center hosted by JAXA in the Tsukuba Space Centre.

The mission will last at least 5 years. JEM-EUSO will be operated for three years in Nadir configuration to maximize statistics at the lowest energies in order to cross calibrate with the current generation of ground-based detectors. The instrument will be then tilted (about 30°) with respect to Nadir in order to exploit a larger amount of atmosphere and to maximize the statistics of events at the highest energies. JEM-EUSO will significantly increase the exposure to UHECRs compared to the largest ground-based air shower arrays presently in operation. [14]

(a) H-II Transfer Vehicle [15]

(b) SpaceX Dragon Delivery System, [16]

Figure 2.6: Modules in charge of delivering and transfer JEM-EUSO instrument onboard the International Space Station. Kounotori as the Space Transfer Vehicle and Dragon devoted to deliver the instrument to the ISS.

2.4.2 Operation modes

In the JEM-EUSO concept [17], the Earth's atmosphere is a giant detector. UHECRs collide with atmospheric nuclei and produce Extended Air Showers (EAS). JEM-EUSO observes the fluorescence light emitted by the Nitrogen molecules excited by the EAS charged particles and the reflected signal at ground of the Cherenkov emission associated with the shower development. Viewing from the ISS orbit, the ($\pm$ 30°) Field of View (FoV) of the telescope corresponds to an observational area at ground larger then 1.9$\times$ 10^5 km^2.

The threshold energy of the detector is around 3 $\times$ 10^{19} eV. Increase in exposure and energy threshold is realized by inclining the telescope from nadir to tilted mode illustrated by figure 2.7, to extend the range of observation up to 10^{21}eV.

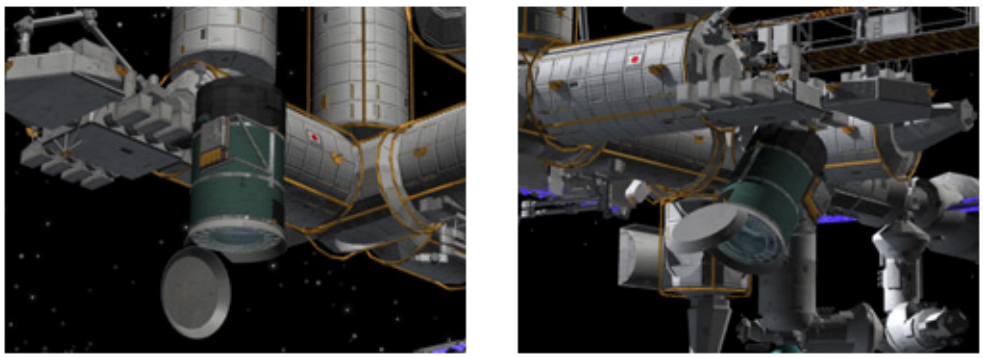

Figure 2.7: Artistic illustration of the JEM-EUSO telescope attached to the Japanese Experiment Module of the International Space Station, under nadir (left) and tilt (right) mode of observation. [3]

2.4.3 Observational Technique

The main advantages of JEM-EUSO compared to any existing or planned ground-based experiment are the significant increase of aperture and the full-sky coverage with an almost uniform exposure [17]. Moreover, as the EAS maximum develops for most zenith angles at altitudes higher than 3-5 km from ground, the measurements will be possible even in cloudy sky conditions.

Compared to ground-based detectors, the duty cycle will be, therefore, mostly limited by the moon phase, while the cloud impact will be less important than for ground-based observations. One of the key elements to estimate the performance of JEM-EUSO is the evaluation of its exposure. This can be factorized into three main contributions: the trigger aperture, the observational duty cycle and the cloud impact.

The observational duty cycle, meant as the fraction of time in which EAS observation is not hampered by the brightness of the sky, has been evaluated by analyzing the measurements of the Russian satellite Tatiana and rescaling them to the ISS orbit [18] and it accounts for $\sim$20%.

The peculiarity of the observation from space is the possibility of observing CRs also in some cloudy conditions (i.e. if the shower maximum is above the cloud top), which is typically not the case for ground-based telescopes. Studies and simulations on cloud distributions and evaluation of cloud impact have been carried out [19, 20]. The result indicates that the average fraction of the observational time where the measurement will not be hampered by atmospheric factors is $\sim$ 70%. This number, convoluted with the 20% duty cycle observational time, provides a final 14% multiplication factor to be applied to the aperture to determine the exposure. Fig 2.8 shows the full aperture, and annual exposure of JEM-EUSO in nadir mode for the full FoV of the detector together with different quality cuts [21] 80-90% aperture is already reached at energies $\sim$ 2-3$\times 10^{19}$ eV when the foot print of the shower is located in the central part of the FoV (R$<$125 km from nadir) and with zenith angles $\theta > 60^{\circ}$, and it slightly increases at $\sim$5 $\times 10^{19}$ eV if the entire FoV is considered. In the most stringent conditions JEM-EUSO has an annual exposure equivalent to Auger ($\sim$7000 km^2 sr yr) while it reaches $\sim$60000 km^2 sr yr at 10^{20} eV, 9 times Auger equivalent.

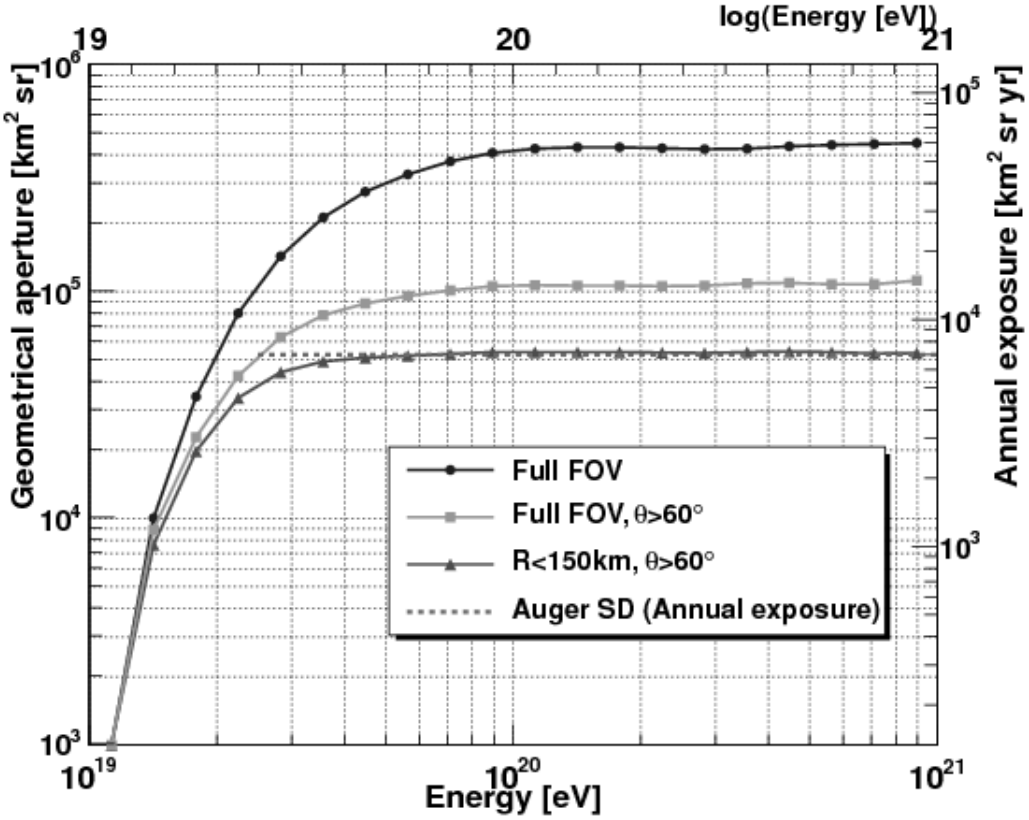

Figure 2.8: Aperture and annual exposure of JEM-EUSO for different quality cuts, [3]

2.5 Atmospheric Monitoring System

An Atmospheric Monitoring System (AMS) is mandatory and a key element of a space-based mission which aims to detect Ultra-High Energy Cosmic Rays (UHECR) using the Earth's atmosphere as a huge calorimeter. JEM-EUSO has a dedicated atmospheric monitoring system that plays a fundamental role in our understanding of the atmospheric conditions in the Field of View (FoV) of the telescope [22].

The goal of the AMS of JEM-EUSO is to provide information on the distribution and optical properties of the cloud and aerosol layers within the telescope FoV [12, 23]. The basic requirements on the precision of measurements of the cloud and aerosol layer characteristics are determined by the requirements on the precision of measurement of EAS parameters (A1) measurement of EHECR energy with precision 30%; (A2) measurement

of the depth of the shower maximum with precision 120 g/cm^2.

Precision of the measurement of the energy of EHECR is affected by the absorption of UV light cloud and aerosol layers. Precision of the measurement of the depth of shower maximum is additionally affected by the uncertainties of location of clouds and aerosols in the atmosphere. Imposing the requirements on the performance of the AM system: (B1)measurement of the optical depth of atmospheric features with precision down to $\Delta_\tau \leq 0.15$; (B2) measurement of the altitude of the boundaries of atmospheric features with precision Δ_H $\leq$500 m. assures that the systematic error of the measurement of the energy and the depth of the EAS maximum introduced by the uncertainty of atmospheric conditions is significantly below that of requirements A1, A2, The required precision od measurement of the altitude and optical depth of the cloud and aerosol layers will be achieved with the following dedicated AM system which will consist of (ilustrated by Figure 2.9).

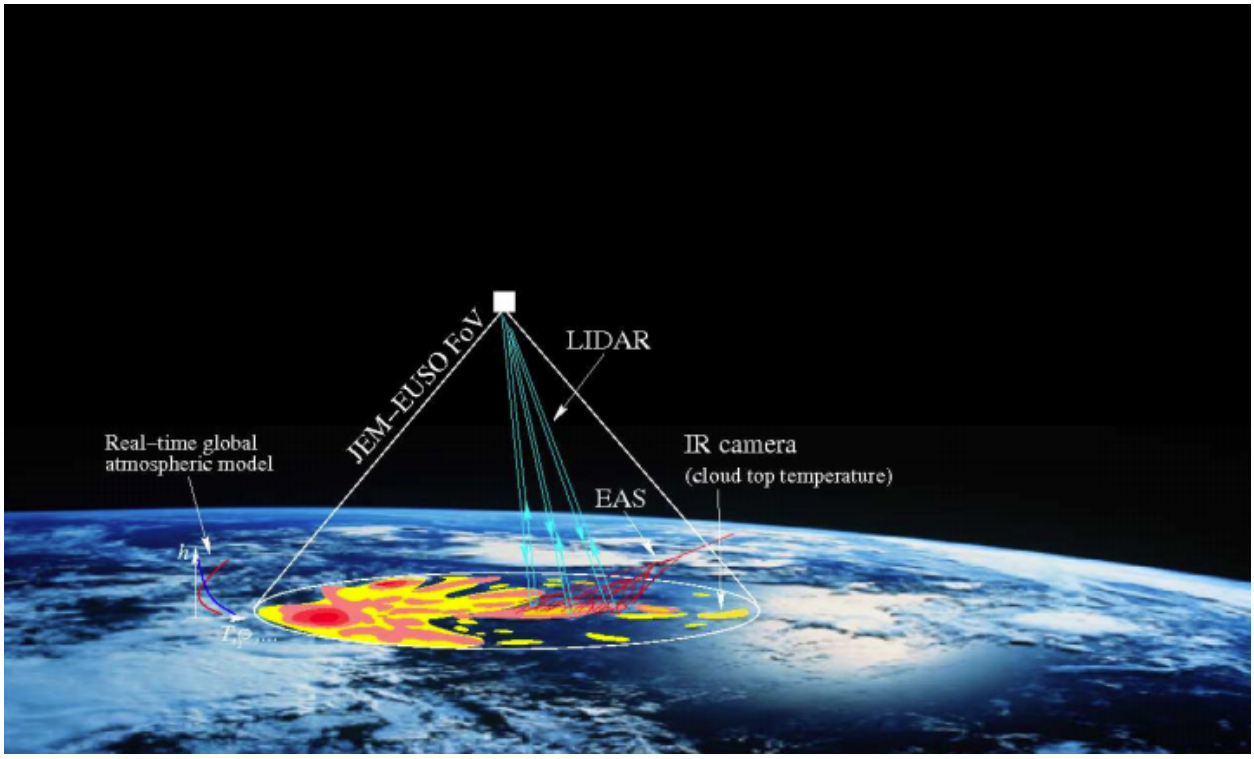

Figure 2.9: The principle of Atmospheric Monitoring in JEM-EUSO, [12]

- Laser Imaging Detector and Ranging (LIDAR)

- Infrared Camera (IR) and
- Global atmospheric models from the post-analysis of all available meteorological data by global weather prediction services.

JEM-EUSO will take the cosmic ray data during the ISS nighttime. To reveal the overall picture of cloud distribution in the FoV an IR camera will be used. The IR camera is an infrared imaging system used to detect the presence of clouds and to obtain the cloud coverage and cloud top altitude during the observation period of the JEM-EUSO main instrument. Measurement of the temperature of the clouds will be used to estimate the altitude of the cloud top layers. Such an estimate is possible in the troposphere in the altitude range 0-10 km where the atmosphere is characterized by a steady temperature gradient of $\mathrm{d}T/\mathrm{d}H \simeq 6^{\circ}/\mathrm{km}$. To achieve he precision of measurement of the cloud top altitude $\Delta H \simeq 0.5$ km the precision of the temperature measurements by the IR camera will be $\Delta T = (\mathrm{d}T/\mathrm{d}H)\ \Delta H = 3\mathrm{K}$.

The AM system will additionally use a LIDAR device. The Lidar will measure the optical depth profiles of the atmosphere in selected directions, with the ranging accuracy of $375/cos(\theta_z)$m, where $\theta_z$is the angle between the direction of the laser beam and nadir direction. The power of the laser will be in such a way that cloud/aerosol layers with optical depth $\tau \geq 355$ nm wavelength will be detectable.

The IR camera and LIDAR measurements will provide complementary information with the amount of details sufficient to:

- Select the EAS events appearing in the clear sky conditions;
- provide information on the optical properties of the clouds needed for correction of the cloud affected EAS profiles which could be retained for further analysis;
- rejects EAS events occurring in the complicated atmospheric conditions (multi-layer cloud/aerosol structures).

2.5.1 Laser Imaging Detector And Ranging

JEM-EUSO is a next-generation fluorescence telescope which will observe UV emission from UHECR induced Extensive Air Showers (EAS) from space, experiencing all possible

weather conditions. It has been estimated that $\sim 70\%$ of EAS detected by JEM-EUSO will be affected by scattering and absoprtion in the clouds and aerosol layers [19, 20]. Proper interpretation of the EAS signal, including the reconstruction of the energy, direction and identity of the UHECR particle requires a detailed knowledge of the influence of the scattering of UV light in clouds and aerosols on the detected fluorescence signal. Cloud and aerosol induced variations of the scattering and absorption properties ar the location of EAS events distort the UV signal from EAS detected by JEM-EUSO.

In the absence of detailed information on the presence and physical properties of the cloud and aerosol layers in the JEM-EUSO Field of View (FoV), distortions of the UV signal from EAS lead to systematic errors on the determination of the properties of UHECR from the UV light profiles. The distortion of the EAS profiles could be corrected if detailed information on distribution and optical properties of the cloud/aerosol layers in the JEM-EUSO FoV is known. This information will be provided by the Atmospheric Monitoring (AM) system of JEM-EUSO. The most relevant information about the absorption and scattering properties of clouds and aerosols is at the location around the EAS events and it will be provided by the LIDAR. The laser beam will be shot several times in the direction in which the EAS trigger ocurred directly after the trigger is generated. With this pointing capability, the LIDAR device will be able to measure the backscattered signal in several directions around the supposed EAS maximum.

A LIght Detection And Ranging (LIDAR) device is foreseen as a part of the Atmospheric Monitoring system for the JEM-EUSO mission. The goal of the LIDAR is to provide measurements of extinction and scattering properties of the atmosphere along the EAS development path and between the EAS and JEM-EUSO [24].

The list of the main parameters of JEM-EUSO LIDAR is reported in table 2.4.

2.5.2 Infrared Camera

The IR-Camera will be the instrument devoted to detect clouds and determine their top height in the FoV of the JEM-EUSO main instrument. The camera will provide a 2D image of the cloud top temperature, and using this image, with the LIDAR and the global

Parameter	Value
Wavelenght	355nm
Pulse repetition rate	> 1Hz
Pulse width	15ns
Pulse energy	20mJ/Pulse
Steering of output beam	$\pm 30°$
Receiver	JEM-EUSO telescope
Detector	MAPMT (JEM-EUSO)
Range resolution	375 m
Mass	17 kg
Power	< 70 W

Table 2.4: Parameters of JEM-EUSO LIDAR, [12]

models, the cloud top height under investigation will be achieved with an accuracy better than 500 m during the observation period of the JEM-EUSO main instrument [25].

The IR-Camera [26], illustrated in figure 2.10 is a microbolometer based infrared imaging system aimed to obtain the cloud coverage and cloud top altitude during the observation period of the JEM-EUSO main instrument. Its preliminary design can be divided into three main blocks: the Telescope Assembly, the Electronic Assembly and the Calibration Unit. The main function of the Telescope Assembly is to acquire the infrared radiation by means of an uncooled microbolometer and to convert it into digital counts. A dedicated optical design has been developed as well, with a huge angular field to complain with the wide FoV of the JEM-EUSO main telescope. Meanwhile the Electronic Assembly provides mechanisms to process and transmit the obtained images, the electrical system, the thermal control and to secure the communication with the platform computer. To assure the high demanding accuracy, a dedicated on-board calibration system is foreseen. Moreover, this system preliminary design is complemented by a challenging mechanical and thermal design to secure that the IR-Camera will be completely isolated. The list of the main requirements of JEM-EUSO IR Camera is reported in table 2.5.

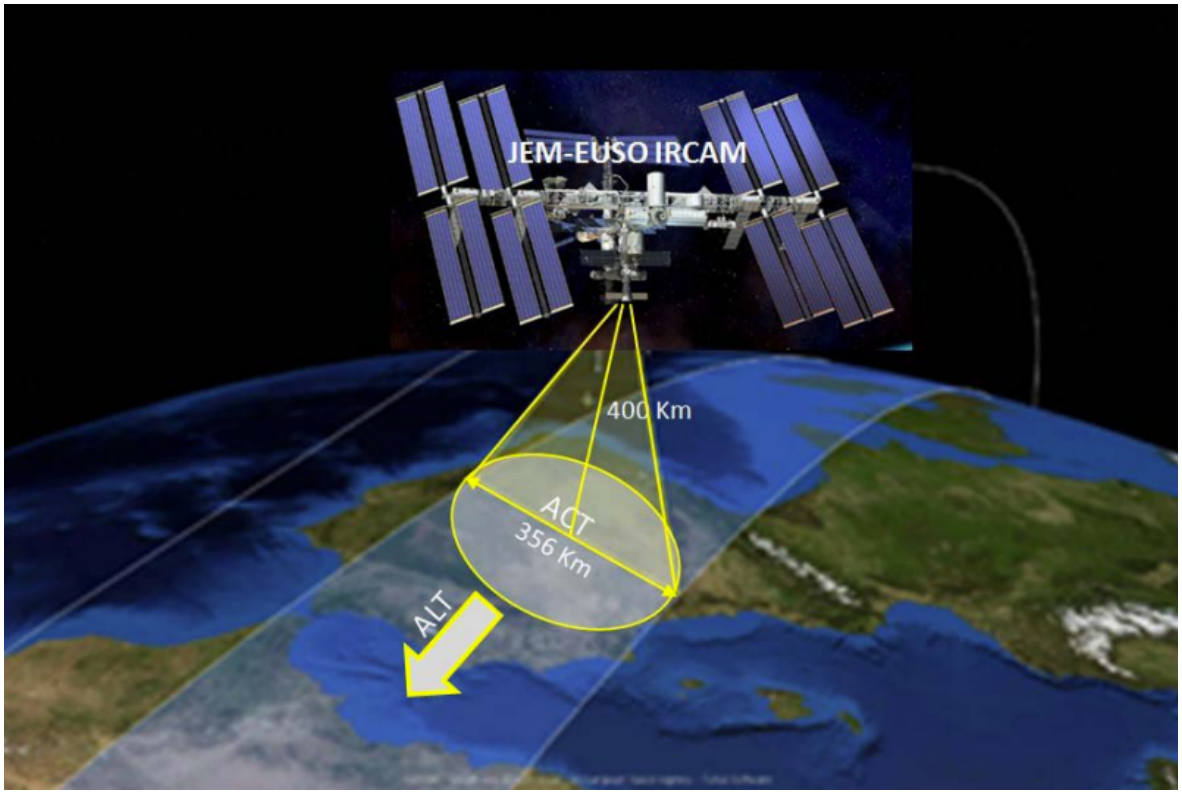

Figure 2.10: Schematic view of the IR-Camera observation concept along the International Space Station Track, [25]

2.5.2.1 The Telescope Assembly; detector and FEE

The IR-Camera Telescope assembly includes the Infrared detector (μBolometer), the FEE (Front End electronic) and the Optical lens assembly, see 2.11. The infrared detector that has been selected for the JEM-EUSO IR Camera is the UL04171 from the ULIS Company [27].

The UL04171 is an infrared opto-electronic device comprised by a μBolometer Focal Plane Array (FPA); two dimensional detector array made from amorphous silicon. The working operative temperature is around 30° and a dedicated TEC (Thermo-Electrical Cooler) has been implemented to guarantee a very stable temperature. The μBolometer is supplied by the manufacturer in a vacuum sealed package with the redaout electronics, peltier and temperature sensor integrated. Moreover, a protective window of Germanium glass has been implemented in the optical design.

Parameter	Target Value	Comments
Measurement Range	220 K - 320 K	Annual variation of cloud temperature plus 20 K margin
Wavelength	10 - 12 μm	Two atmospheric windows available: 10.3-11.3 μm and 11.5-12.5 μm respectively
FoV	48°	Same as main instrument
Spatial resolution	0.1° (Goal) 0.2° (Threshold)	@ FoV Center
Absolute temperature accuracy	3 K	500 m in altitude
Mass	$\leq$ 11 kg	Inc 20% margin.
Dimensions	400× 400× 370	w/o Insulation and mountaing bracket.
Power	$\leq$ 15 W	Inc 20% margin.
Lifetime	5 years In-orbit	+ 2 years On-ground

Table 2.5: Requirements of JEM-EUSO IR Camera, [25]

The FEE (Front End Electronics) manages and drives the μBolometer; It provides the bias and the sequencer and manages the images acquisition modes. The FEE communicates with the ICU and provides it the uncompressed raw images. The core of the FEE shall be a FPGA, VIRTEX family, in charge of implementing the main FEE functions. This includes the control of the UL04171, the generation of all the synchronism including the clocks generation and the interface with the sequencer.

The polarization of the detector (bias, gain, offset generation and control) will be also controlled by the FPGA. The data acquisition will be implemented with an Analog Digital Converter (ADC) in each detector output channel previous to the FPGA input. The ADC number of bits will be chosen according to the pixel data resolution required by the IR Camera.

2.5.2.2 The Optical subsystem Preliminary Design

The Optical Assembly is one of the most critical sub-assemblies of the IR-Camera. For an optimal operation, the design of the Optical subsystem has to fulfill the following technical requirements: To acquire radiation at the mid infrared wavelength band (10-12.5) μm; To

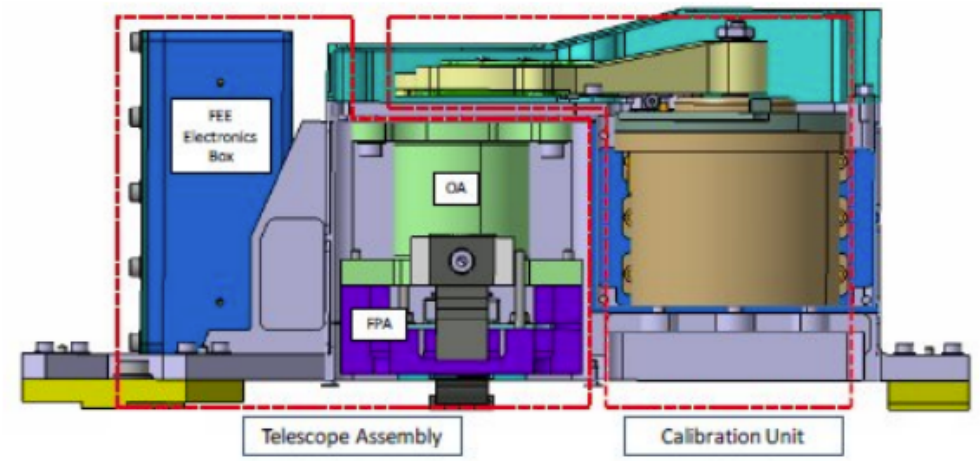

Figure 2.11: Illustration of the preliminary design of the infrared camera telescope assembly, [25]

guarantee the requested (48°) FoV; To be very fast in terms of F-number; To secure an optimal operative temperature for the ULIS (29°) detector, for both, the cold operative case (-15°) and the hot operative case (15°); The thermal excursion of the lenses has to be less than 20° and finally, to keep the Cold Stop temperature 15° below the ULIS μBolometer temperature.

Presently, the optical system design, see Figure 2.12, is a refractive objective based in a triplet with one more lens close to the stop and a window for the filters cose to the focal plane. The first surface of the first lens and the second surface of the third lens are spherical that allow a better quality of the complete system. The aperture stop is situated at 0.40 mm behind the fourth lens, in order to separate the optical system to the detection module. The system, consisting of four lenses, has a focal length of 19.10 mm, and a F-number of 1, and it shall work with a FoV of 48°. The overall length between the first surface to the focal plane is 62.30 mm. All the data shown below are related to extreme fields ($\sim$ 34°), although better response is obtained for intermediate fields. The full system has been designed only with one optical material, Germanium with a refraction index of 4.003118.

A breadboard model (Figure 2.13) has been manufactured to test the optical performances of the system. The bread- board lenses have been mounted in the same way that

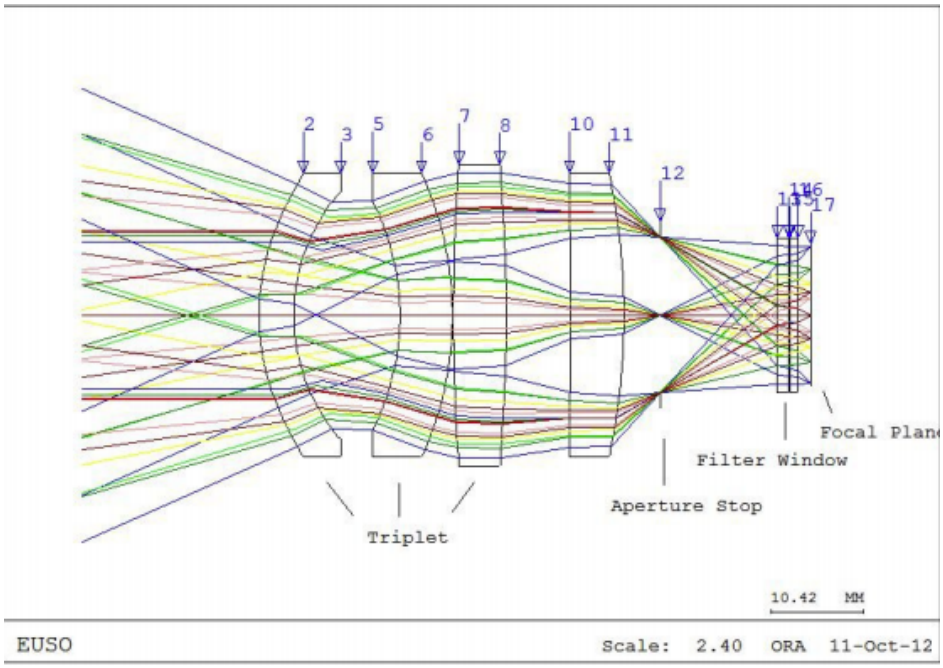

Figure 2.12: Schematic illustration of the optic preliminary design of the Infrared Camera, [25]

will be assembled in the flight model. The tolerances and optomechanic process have been successfully tested and verified at this stage of development.

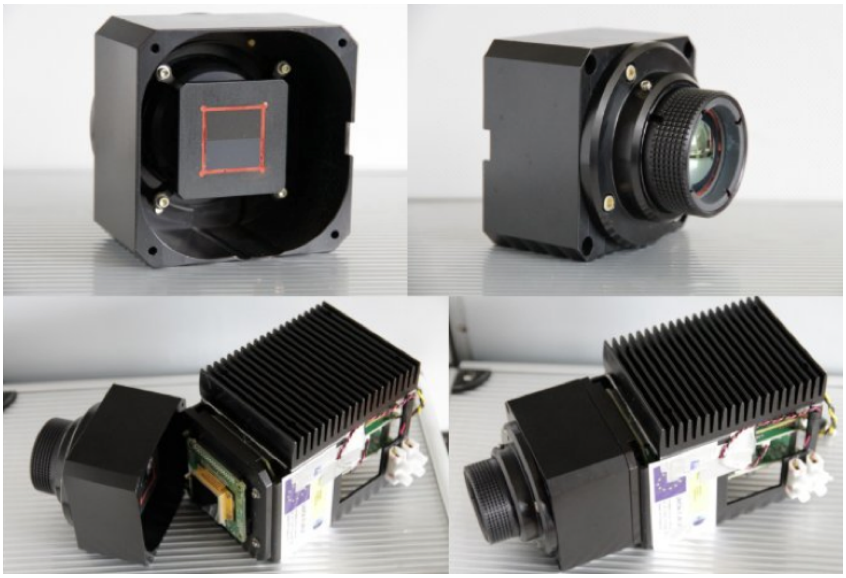

Figure 2.13: Breadboard model manufactured at INTA facilities for the Infrared Camera of JEM-EUSO, [25]

2.5.2.3 The electronic assembly

The Electronic Assembly is composed of two main sections: the Instrument Control Unit (ICU), and the Power Supply Unit (PSU). Both blocks follow cold redundancy architecture and are placed on individual PCBs so that four boards are defined: ICU Main, ICU Redundant, PSU Main, and PSU Redundant. The ICU controls and manages the overall system behavior, including the data management (compression, format), the power drivers and the mechanisms (shutter, black bodies etc.) controller FPGA. The IR-Camera electronics shall provide mechanisms to process and transmit images obtained from an IR detector controlled by a dedicated FEE board, a Firmware (FW) solution is considered as baseline for this proposal.

Data generated by the FEE is then processed by the Instrument Control Unit (ICU), which is in charge of controlling several aspects of the system management such as the electrical system, the thermal control and the communication with the platform computer. The Power Supply Unit (PSU) receives the main power bus from JEM- EUSO main telescope and it provides the required power regulation to the system and the sub-systems. The actuator will be managed by the ICU, providing control to a stepper motor and acquiring its position by means of micro-switches placed in the stable positions.

2.5.2.4 The calibration subsystem

The calibration unit (Figure 2.14) is dedicated to manage and control the IR calibration operation. This unit has to guarantee a reference internal temperature to ensure the calibration of the data coming out of the FEE. Following the strategy of operational modes, four positions are provided from this unit: Acquire, Shutter (offset correction), Calibration Hot point, and Calibration Cold point.

The position of shutter will be used to close the optic in the safe and off operation mode. Calibration unit is mainly composed of two Black Bodies with a temperature controlled Shutter, a moving mechanism and the motor, the positioning system and a calibration Thermal control.

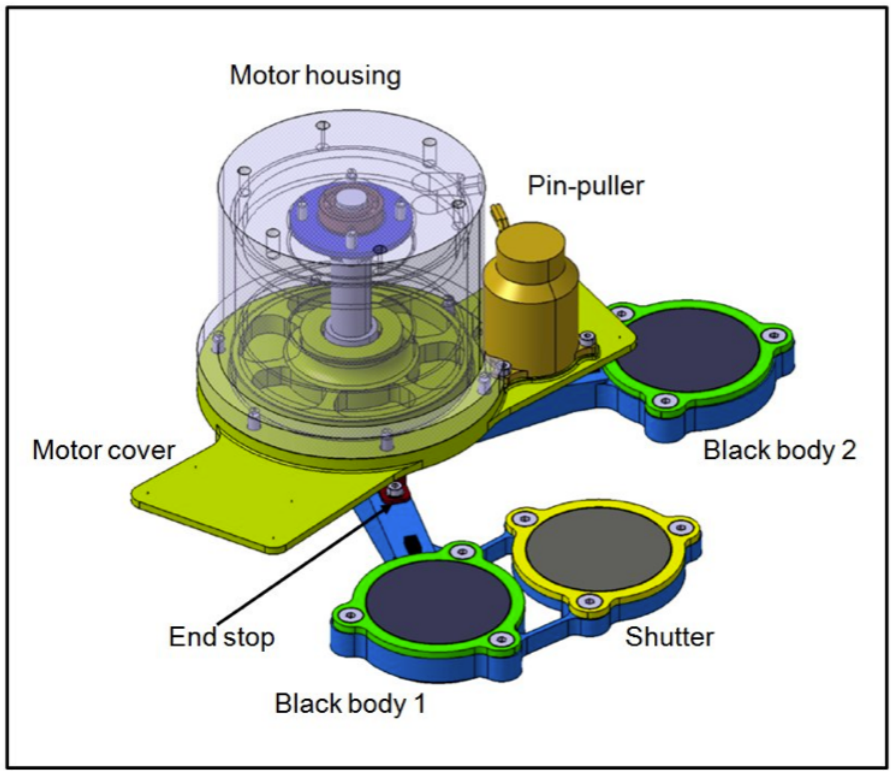

Figure 2.14: Illustration of the calibration subsystem for the Infrared Camera of JEM-EUSO, [25]

2.5.2.5 The thermal and mechanical design

The mechanical structure contains and protects the Telescope Assembly and the Calibration Unit. It is attached to the bench of the JEM-EUSO Telescope by means of three flexure-pads. The Main Housing is an aluminum Al6082 monocoque body-shell. It has three different compartments to accommodate the required subsystems and provide overall stiffness and thermal isolation of the Optical Assembly (see Figure 2.15) and FPA from the Calibration Unit and the FEE. Stiffeners have been used to optimize the mass of the Main Housing structure. This Housing contains a stiff base plate, which supports the Calibration Unit and the FEE Electronics Box, both contained in the IF plane to minimize the loads on this plane maintaining a low CoG.

The Lenses Barrel has the mission to enclose and support the lenses, which are positioned with Spacers, and they are bonded with optical adhesive EPO-TEK 301-2. The

Cold Stop is a sort of diaphragm between the last lens and the microbolometer. It is necessary for optical purposes, and its temperatue must be around 15° lower than the ULIS temperature. This is achieved by means of a passive thermal control, and two (main and redundant) thermal sensors.

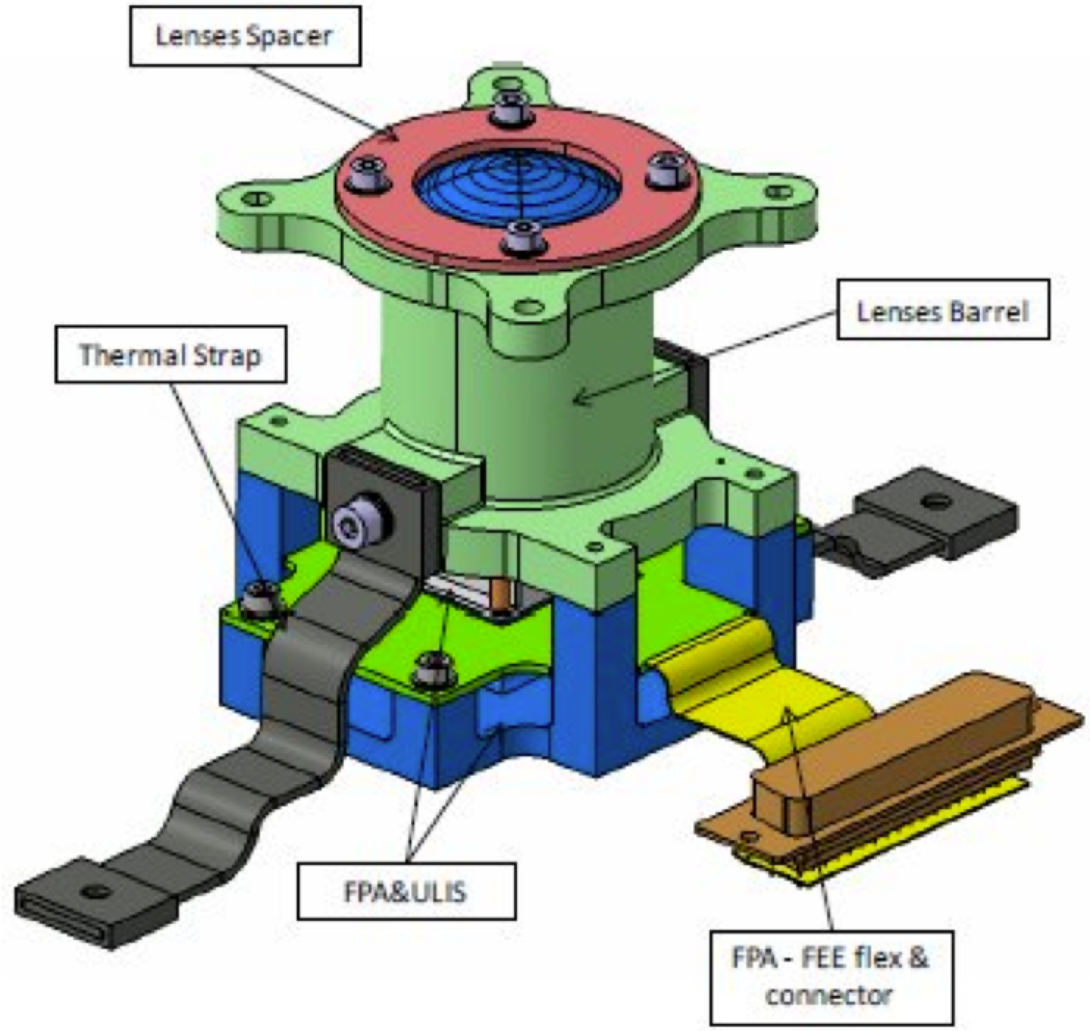

Figure 2.15: Illustration of the Optic Assembly for the Infrared Camera of JEM-EUSO, where the lenses barrel is shown [25]

2.6 The instrument

The JEM-EUSO instrument is a wide-angle refractive telescope in the near-ultraviolet wavelength region which will be mounted to the International Space Station. Its goal is to measure time-resolved fluorescence images of extensive air showers in the atmosphere. The focal surface is a spherically curved surface, and its area amounts to about 4.5 m^2 [28].

2.6.1 Focal Surface

The Focal Surface (FS) of JEM-EUSO has a curved surface of about 2.35 m in diameter, and it is covered with about 5,000 Multi-Anode Photomultipliers Tubes, MAPMTs, (Hamamatsu R11265-M64). It makes ± 30° FOV and 0.07° angular resolution. The FS detector consists of Photo-Detector Modules (PDM), each of which consists of 9 Elementary Cells (EC) arranged in an array of 3 × 3. About 1,233 ECs, corresponding to about 137 PDMs, are arranged on the whole FS (Figure 2.16) [28].

2.6.2 Photodetector

JEM-EUSO is a photon-hungry experiment; its expected photon ratio is <100 photons/μsec/pixel around shower maximum. And its FS detector should have high detection efficiency. The FS detector should have single photon counting capability in the near-ultraviolet wavelength region to avoid the systematic errors, which may be introduced through the gain drift. It should be reliably and stably operational in Space environment for at least 3 or 5 years mission period.

For the above reason, MAPMTs with UV-glass entrance window are employed as sensors of the FS detector.Current baseline choice is the Hamamatsu R11265-03-M64 (see Fig 2.17), which was developed by RIKEN in collaboration with Hamamatsu Photonics K.K. It has an ultra-bialkali photo- cathode, which transforms photons into electrons, and amplifies photo-electrons by means of a stack of metal channel dynodes. The signals are taken from the anode which is formatted as an array of 8×8. the photon detection efficiency of this is about 0.3 in the near-ultraviolet region.

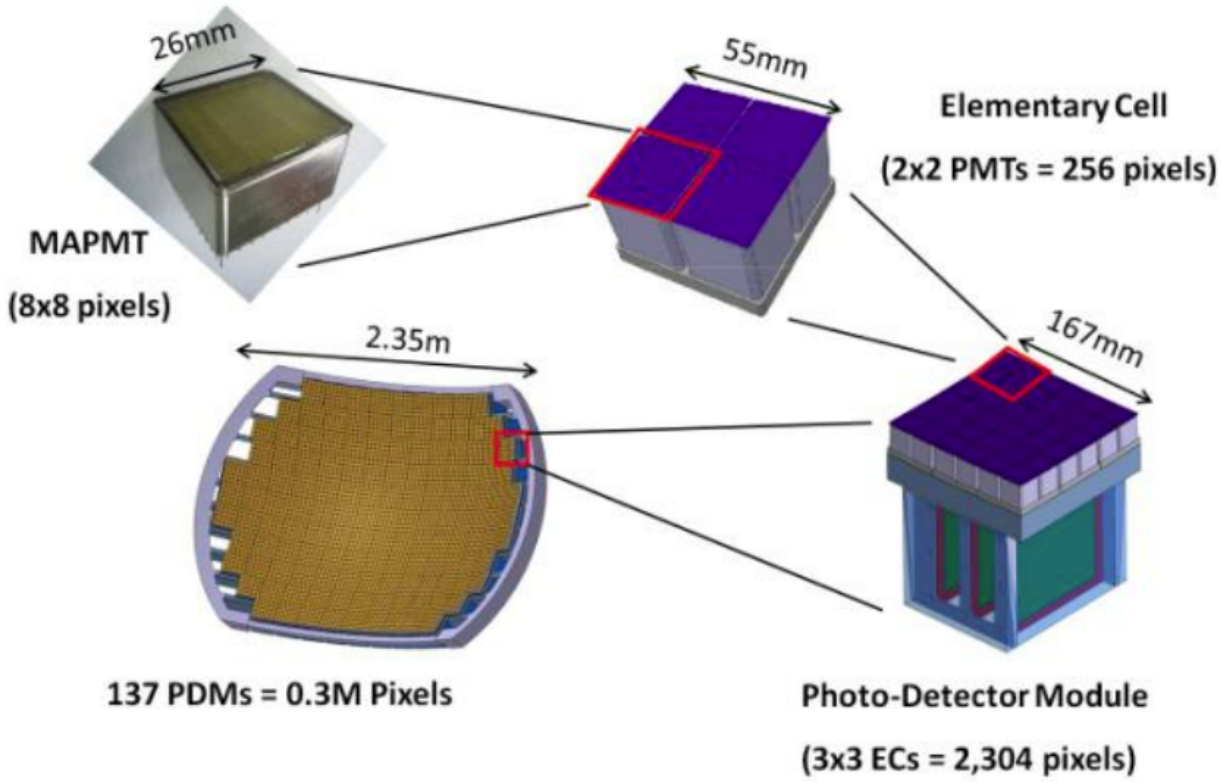

Figure 2.16: Schematic illustration of the JEM-EUSO Focal Surface, [28]

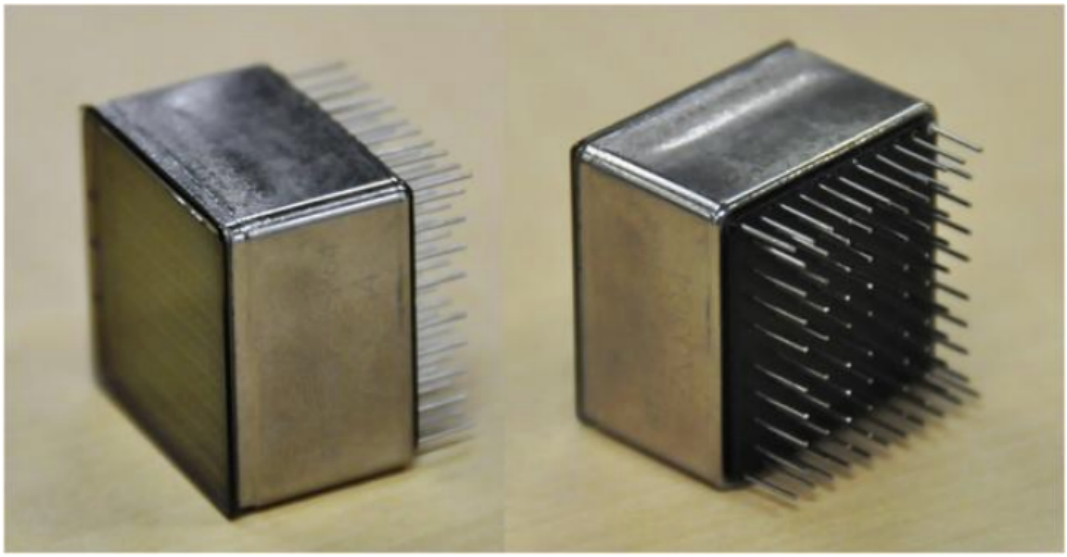

Figure 2.17: Schematic illustration of the MAPMT for the JEM-EUSO photodetector, [28]

2.7 Photo-Detector Module

PDM is the basic unit of the data acquisition of the JEM-EUSO telescope. PDM consists of the following components.

- 36 MAPMTs
- Front-End readout ASIC boards
- Trigger board
- Power Supply board
- High Voltage Power Supply Boards
- PDM Mechanical Structure

Figure 2.18 shows the Prototype of the PDM Mechanical Structure with 12 MAPMTs.

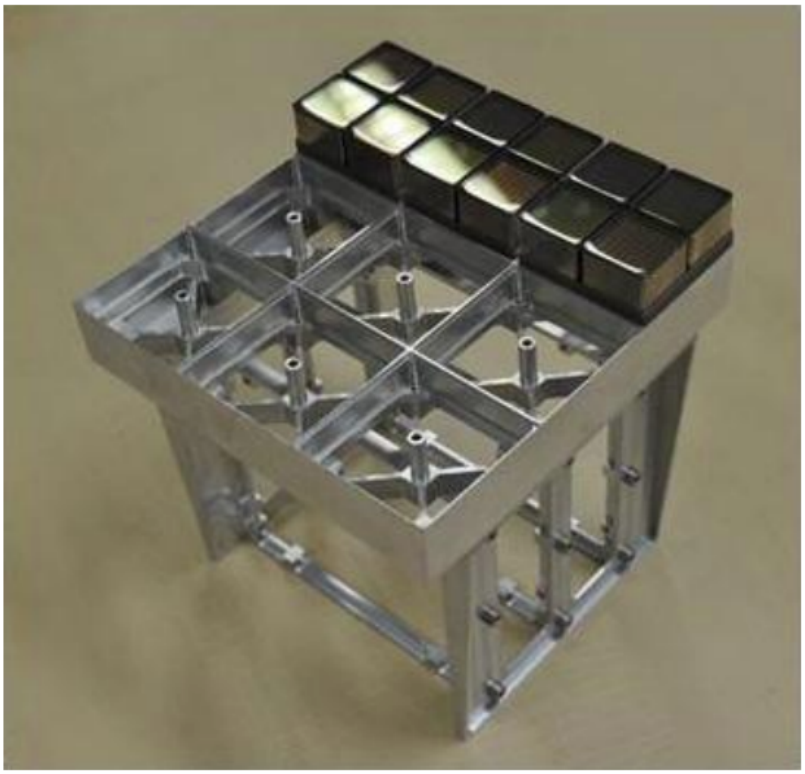

Figure 2.18: Prototype of the PDM Mechanical Structure with 12 MAPMTs, [28]

2.7.1 Focal Surface Mechanical Structure

The FS of JEM-EUSO is composed of a grid of $\sim$ 5,000 MAPMTs arranged in modular support structures, that cover all the surface to collect the light of the optical system. The FS is a portion of a sphere of radius 2785 mm, inserted within an in-plane section 2650 mm $\times$ 1900 mm (allowed by the HTV Exposed Pallet dimensions). We have studied the FS geometry and analyzed different PDMs distributions in order to maximize their number within the allocated space. The adopted configuration consists of a total of 137 PDMs lying in 11 rows along the parallels of the mentioned sphere, with one PDM located at the center of the FS geometry as shown in Figure 2.19.

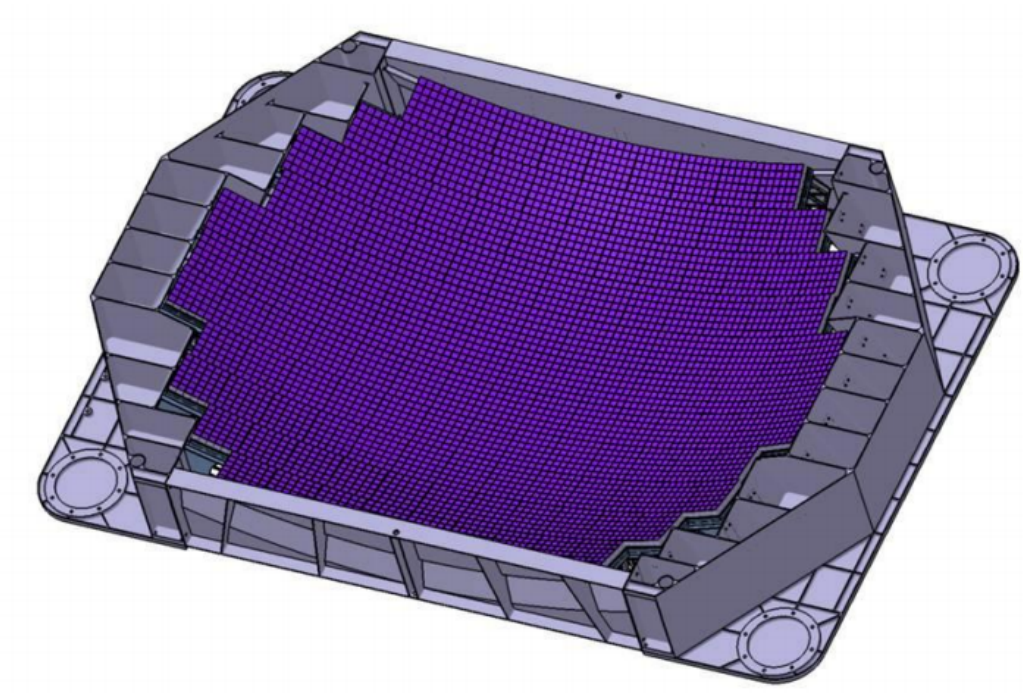

Figure 2.19: Focal Surface Assembly of JEM-EUSO telescope, [28]

2.8 Other parts of the instrument

There are also many more parts and sub-parts of the JEM-EUSO instrument not included in this dissertation. They were not considered in this chapter since they do not interact

in any way with the reliability methods develop thorough this work. In future versions of this work, they will may be included.

Some of them are enumerated below:

- Data Handling Subsystem
- Power Supply Board
- Trigger Board
- Front-End redout ASIC boards
- High Voltage Power Supply Boards
- Data Processor Power Supply
- GPS Receiver

2.9 The Mission pathfinders

2.9.1 EUSO-Balloon

EUSO-Balloon is a balloon-borne experiment performed in collaboration with the French Space Agency CNES. It is equipped with one full original JEM-EUSO PDM (Photon Detection Module with 2304 pixels) and with an optical system made of two Fresnel lenses, with a side of 1 meter covering a FOV of $\pm$ 8 degrees, which are real prototypes of those foreseen in JEM-EUSO [29]. Besides the main instrument, a stand-alone and waterproof infrared camera is on board [30] The EUSO-Balloon concept is illustrated in Figures 2.20 and 2.21.

Key objectives, in addiction to the full-scale end-to-end test of the JEM-EUSO technique, are the experimental determination of the effective UV background below 40 km, the test of the ground based calibration system, the observation of the first UV-image of an EAS looking down on the Earth's atmosphere illustrated in Figure 2.22.

On August 25, 2014, the instrument, installed on board a Gondola, has been brought by a stratospheric balloon to a float altitude of 40 km. The flight has been performed by the balloon division of the French Space Agency CNES from Timmins Balloon base (Ontario, Canada).

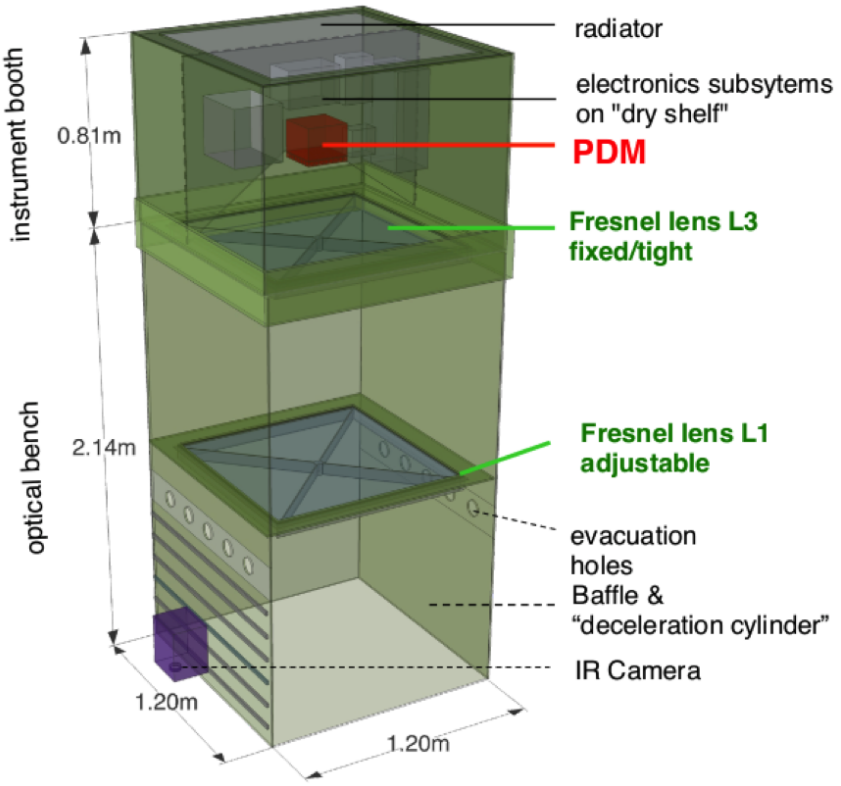

Figure 2.20: Detailed view of EUSO-Balloon and its main components [31].

Figure 2.21: Artistical concept of EUSO-Balloon [32].

The flight itself has been particularly smooth and interesting from the scientific point

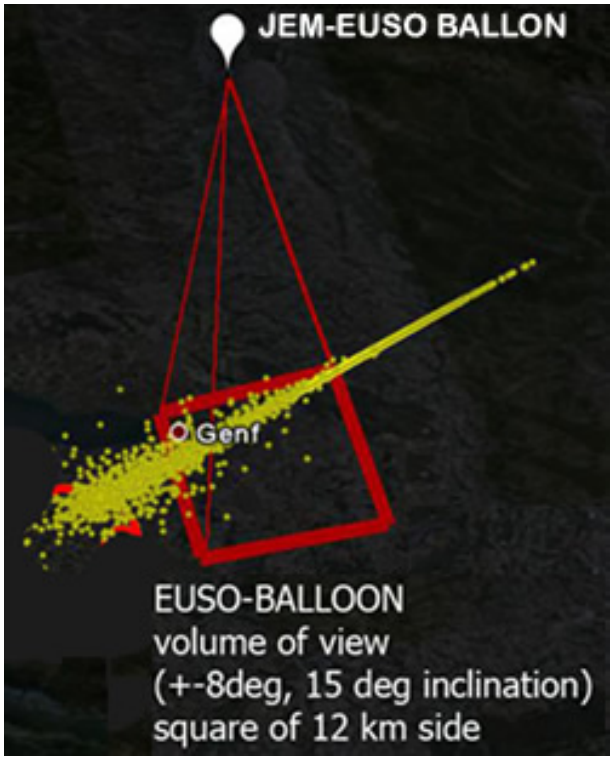

Figure 2.22: Volume of view of the EUSO-Balloon [32].

of view, since different types of grounds could be overflown, as well as regions with and without clouds of different types. This will allow the comparative study of the UV background in different conditions, which was one of the complementary goals of the mission. From the technical point of view, all the subsystems of EUSO-Balloon behaved in flight according to their nominal requirements, and the proof of concept seems to be fully validated. The good behavior of the instrument could be assessed during the flight itself, thanks to the sample data sent by telemetry, which correspond to about 1% of the total data collected. These data, quickly analyzed during the flight, were sufficient to show the changing light level on each pixel, as well as the light of a calibrated UV flasher and the track of a laser shots emitted from an helicopter, which flew under the balloon in the FOV for about two hours, as a coordinated contribution of NASA to the campaign.

The objectives of the EUSO-Balloon were:

- To test all the technologies developed for JEM-EUSO under very severe operating conditions (stratosphere), partly representative of some conditions that would have

to meet any telescope fluorescence light space (accommodated on the ISS or in free flight on a satellite).

- To measure the intensity of the atmospheric air glow with an appropriate angular resolution for JEM-EUSO, this continuous background requiring to be subtracted to any measured signal.
- To highlight the ability of such an instrument to detect air showers from space (above the measured background level from the Air glow).

Over 50 researchers from Japan (RIKEN), France (LAL, OMEGA, APC, IRAP and CNES), Poland (NCBJ), South Korea (SKKU), Italy (INFN Napoli and Frascatti), Mexico (UNAM), Spain (UAH, IAC, ULE, INTA, MULTIDARK) and Germany (IAAT and KIT) are involved in the EUSO-BALLOON mission, led by CNES.

2.9.1.1 EUSO-Balloon Spanish Contribution

The scientific groups involved in the EUSO-Balloon Space Mission are the SPace and AStroparticles group at the University of Alcala (SPAS-UAH), the Intituto de Astrofisica de Canarias (IAC), the Atmosphere Group of the University of Leon (ULE) and the Instituto Nacional de Tecnica Aeroespacial (INTA) in collaboration with the space company ORBITAL.

The Spanish contribution to the EUSO-Balloon mission is the IR camera illustrated in Figure 2.23 and 2.24, which is devoted to take IR pictures of the scenario and determine if the cosmic ray telescope measurement is affected by clouds interaction with the Extensive Air Shower. The aim of this contribution is:

- To validate the IR camera mission concept
- To obtain real data with ULIS UL 04171 micro bolometer IR camera (used in JEM-EUSO IR camera).
- To validate and optimize Temperature Retrieval Algorithms.
- To validate and optimize Stereo Vision Technique.
- To validate and assess part of Calibration Strategy (micro Shutter).

The EUSO-Balloon IR Camera took one picture every 80 seconds during the balloon flight held in August, 2014, over Timmins (Canada). It was functioning for around 17

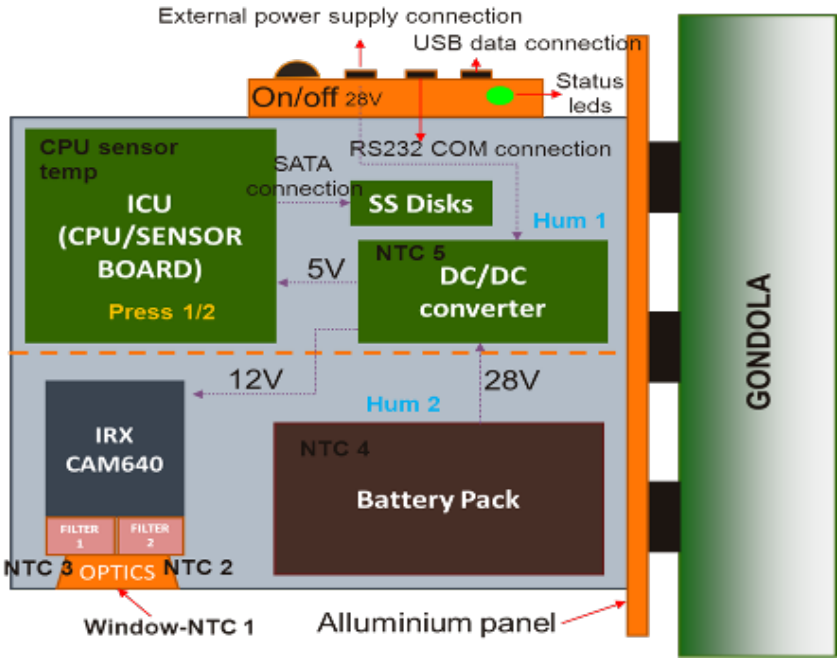

Figure 2.23: Internal distribution of EUSO-Balloon IR Camera components [32].

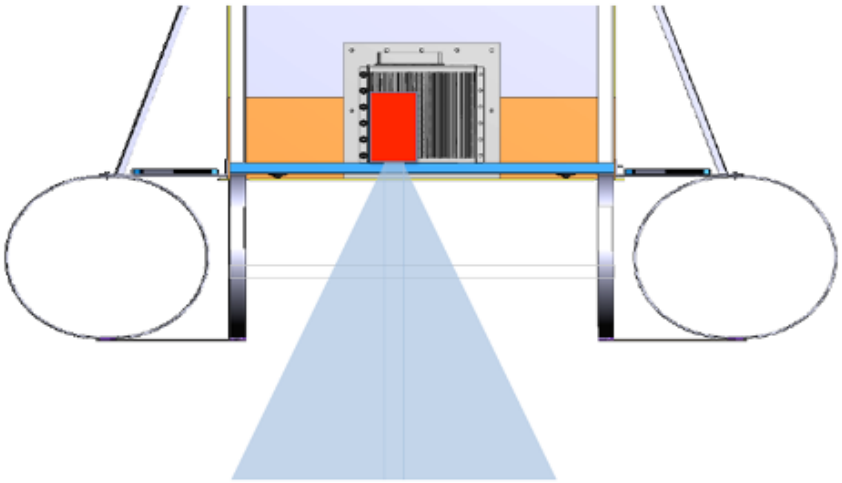

Figure 2.24: Mechanical configuration of EUSO-Balloon IR Camera [32].

hours, and therefore, took an overall of 753 images around 400 of them under the water. Although the EUSO-Balloon splashed down on a lake, the IR camera is water-proof, so all the data could be recovered.

Among the scientific results of the EUSO-Balloon IR camera we can stand out the accuracy in the calculation of the Cloud Top Height 2.25, the optical depth 2.26 and the

measurement of the UV background under different scenarios [33]

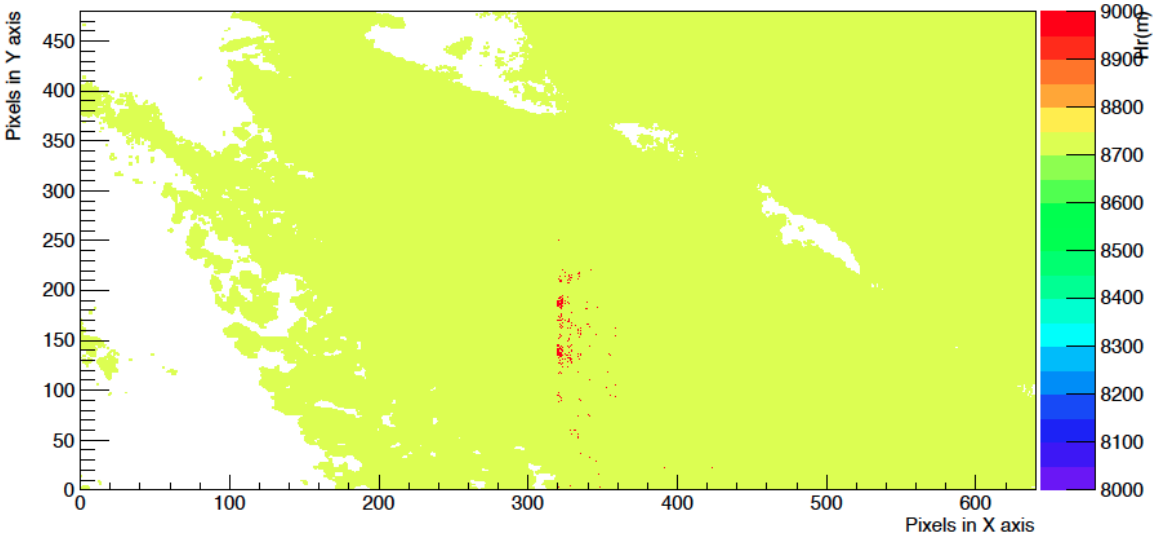

Figure 2.25: Cloud coverage and Cloud Top Height (CTH) in the Infrared. [34].

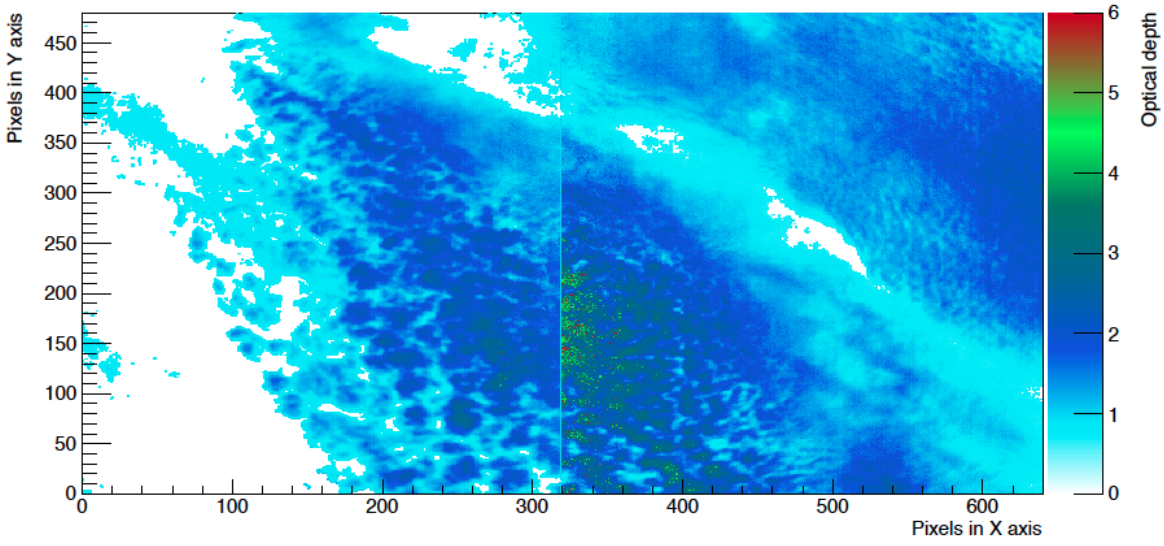

Figure 2.26: Cloud Optical depth in the Infrared. [34].

2.9.2 miniEUSO

Mini-EUSO, in the International Space Station (ISS) is a precursor of the K-EUSO main mission intended to open the path towards the Astronomy with EHECR. The mission is devised with the intention of raising the Technology Readiness Level (TRL) of the future K-EUSO mission to observe EHECRs from space. Mini-EUSO will provide a detailed mapping of the UV emissions of the Earth and the atmosphere and presents the opportunity to study a diverse range of scientific phenomena including atmospheric physics, strange quark matter, meteorites, bioluminescence and EHECRs. Moreover, it will validate the technologies already flown in the EUSO-Balloon in August 24, 2014 and will increase the technical readiness level of all of its components to a level compatible with space requirements. An exceptional opportunity to install this instrument onboard the ISS, with almost no launch and installation costs. A standalone Mini-EUSO (illustrated in Figure 2.27) to be easily handled by astronauts with assured safety and very limited human risks is foreseen.

Mini-EUSO was first approved by the Italian Space Agency (ASI) [35] in July 2013 in the framework of the VUS-2 call where it was ranked 9^{th} out of more than 70 proposals and funds for the Italian involvement in Mini-EUSO has been approved by Istituto Nazionale di Fisica Nucleare (INFN) [36] since the beginning of 2014. In June 2014 Mini-EUSO have been just approved to be placed in the Russian ISS segment by the Russian Federal Space Agency (Roscosmos) [37]. Figure 2.28 show the UV transparent window number 9 of the Russian service module Zvesda facing the Nadir direction.The transparency of the window in the UV range (300 to 400 nm) is above 80 % and close to constant over the spectral range. The Zvesda module, as a result the operational environment, will be at room temperature (nominal range 18.3 C to 26.7 C) ant at a sea level air pressure (nominal range 97.9 kPa to 102.7 kPa).

Mini-EUSO is a compact telescope with wide FOV ($\pm 19^{\circ}$) based on an optical system employing two Fresnel lenses, with a focal surface composed by an array of 6×6 MAPMTs with 64 pixels eatch, resulting in a readout of 2304 channels. Front-End Electronics (FEE) is based on SPACIROC ASIC, developed specifically for this purpose. The

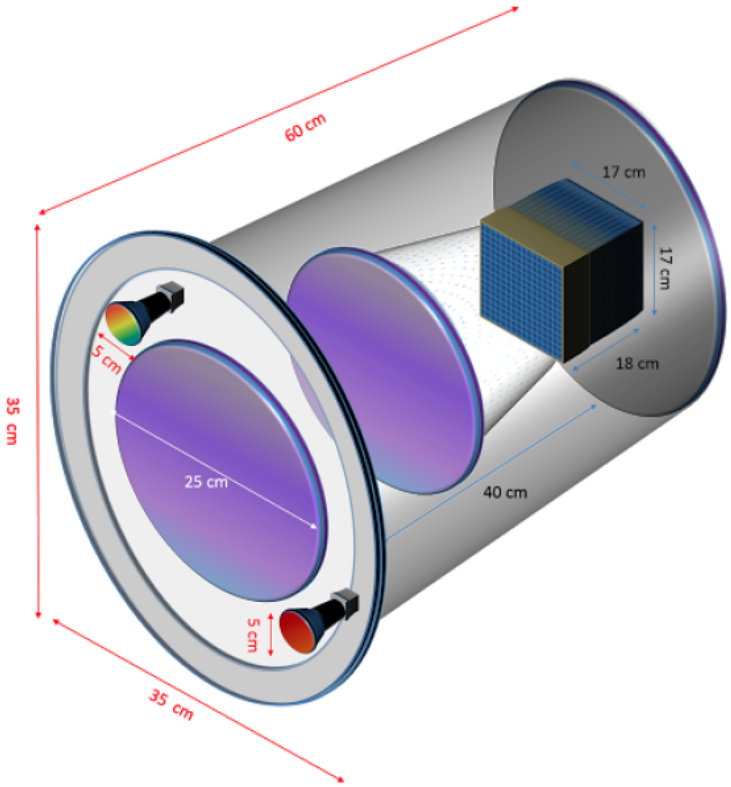

Figure 2.27: Internal Distribution of Mini-EUSO main components [29].

ASIC (64 channel, dual readout) perform the task of pre-amplification, Analog-to-Digital Conversion and readout. The signal is sent to an FPGA board (korean PDM board) and subsequently to a CPU for experiment control and storage on Solid State Disks. We will construct and test the infrared camera for Mini-EUSO telescope to perform the observation of IR light and background from space, from the interior of the ISS (WORF facility and/or Russian Service Module UV transparent window). Multiple trigger levels will be used to filter out noise and identify events of interest. Relevant data is then stored at regular time intervals depending upon the complexity of the trigger. Data transfer to Earth takes place physically via the delivery of a hard drive by the ISS astronauts and there is no telecommunication with the ISS systems or directly to ground from the instrument.

The block Scheme of Mini-EUSO is illustrated in Figure 2.29 where an infrared camera in the near infrared is considered under responsibility of the Spanish Consortium. The Near-InfraRed (NIR) bands of Mini-EUSO camera will led us to retrieve the thermody-

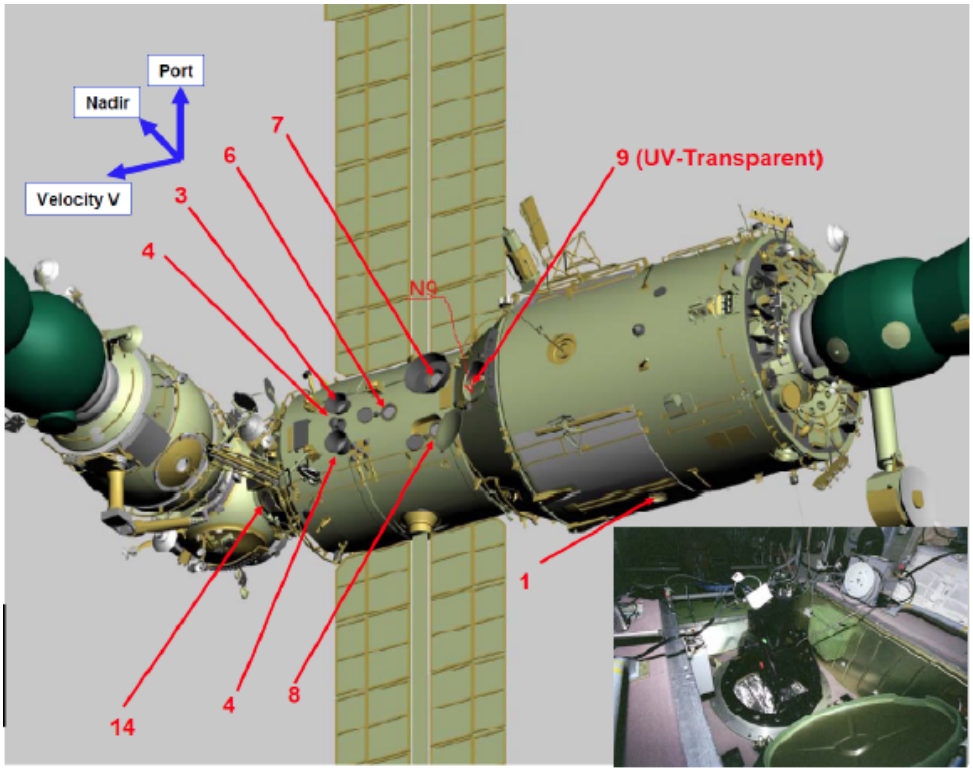

Figure 2.28: Russian service module seen from below. Port 9 is the one to be used [29].

namic cloud phase. NIR bands are useful for distinguishing the cloud phase. In this spectral band, ice and liquid-water clouds have different reflectance owing to sensitivity to cloud top effective radios and cloud top phase.

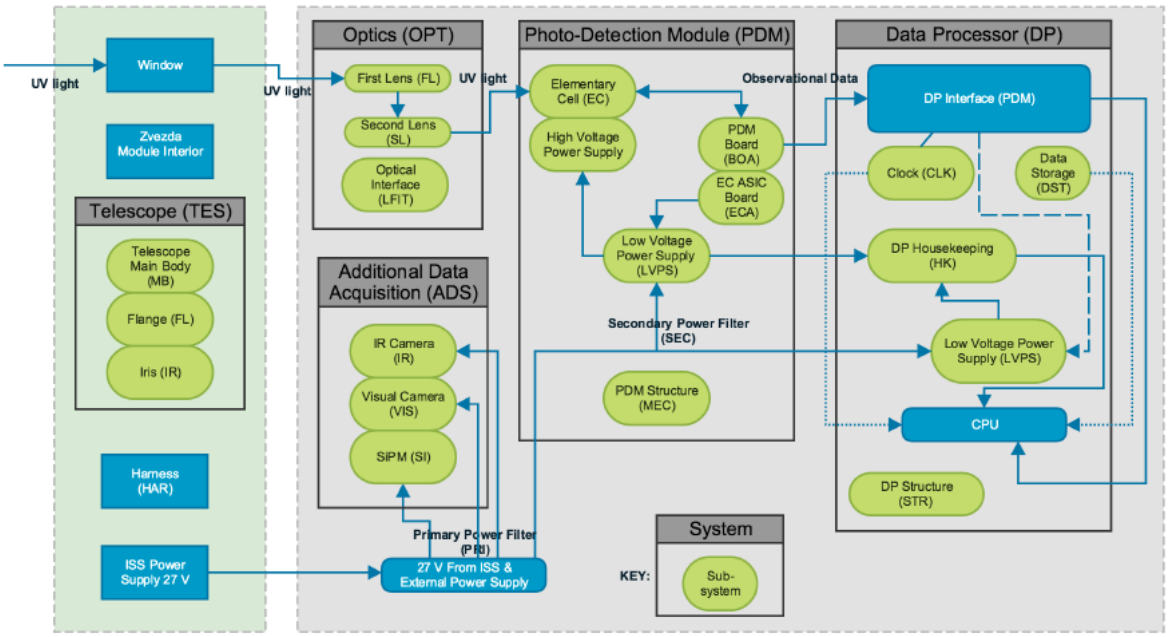

Figure 2.29: Detailed view of Mini Euso Block Scheme.

Bibliography

[1] Yoshiyuki Takahashi, Science Objectives of the JEM-EUSO mission on International Space Station. 30th International Cosmic Ray Conference, Merida, Mexico 2007. (ID 1227).

[2] T.Ebisuzaki for the JEM-EUSO collaboration. The JEM-EUSO Mission. 32nd International Cosmic Ray Conference, Beijing, China 2011. (ID 1628)

[3] JEM-EUSO web page. http://jemeuso.riken.jp/

[4] NASA Facts. The International Space Station: An overview. IS-1999-06-ISS022. June 1999.

[5] NASA and USA Today research 3D Models by NASA; graphic by Robert W. Ahrens.

[6] Japan Aerospace Exploration Agency. http://iss.jaxa.jp/en/kibo/

[7] JAXA. Kibo Exposed Facility User Handbook. September 2010.

[8] F. Kajino et. al., Overview of the JEM-EUSO Instruments. 32nd International Cosmic Ray Conference, Beijing, China 2011. (ID 1216).

[9] J.H. Adams, For the JEM-EUSO Collaboration. Testing of Large Diameter Fresnel Optics for Space Based Observations of Extensive Air Showers 32nd International Cosmic Ray Conference, Beijing, China 2011. (ID 1100).

[10] Y. Kawasaki et al., For the JEM-EUSO Collaboration, The Focal Surface of the JEM-EUSO instrument, 32nd International Cosmic Ray Conference, Beijing, China 2011.(ID 0472).

[11] Marco Casolino et al., Data acquisition System of the JEM-EUSO project, 32nd International Cosmic Ray Conference, Beijing China 2011.(ID 1219).

[12] A. Neronov et al., For the JEM-EUSO collaboration, Atmospheric Monitoring System of JEM-EUSO, 32nd International Cosmic Ray Conference, Beijing, China 2011.(ID 0301).

[13] P. Gorodetzky et al., For the JEM-EUSO collaboration, Calibration of JEM-EUSO photodetectors, 32nd International Cosmic Ray Conference, Beijing, China 2011. (ID 0218).

[14] University of Chicago. http://jem-euso.uchicago.edu/mission.php

[15] Jaxa Projects. http://www.jaxa.jp/projects/rockets/htv/

[16] California Institute of Technology. http://www.kiss.caltech.edu/workshops /exoplanet2009/presentations/croonquist.pdf

[17] M.Ricci, for the JEM-EUSO collaboration. The JEM-EUSO Mission. 12th International Conference on Topics in Astroparticle and Underground Physics (TAUP 2011).

[18] P.Bobik for the JEM-EUSO collaboration. Estimation of JEM-EUSO experiment duty cycle based on Universitetsky Tatiana measurements. 32nd internationalc Cosmic Ray Conference, Beijing, China 2011. (ID 0886).

[19] F.Garino et al., on behalf of the JEM-EUSO collaboration.Cloud Coverage and its implication for Cosmic Ray Observation from Space.32nd internationalc Cosmic Ray Conference, Beijing, China 2011. (ID 0398).

[20] G.Saez-Cano for the JEM-EUSO collaboration. ESAF Simulation of Ultra-High Energy Cosmic Rays in cloudy conditions for the JEM-EUSO (JAXA) Space Observatory.32nd internationalc Cosmic Ray Conference, Beijing, China, 2011. (ID 1034).

[21] K.Shinozaki for the JEM-EUSO collaboration. Estimation of effective aperture for extreme energy cosmic rays by space-based JEM-EUSO Mission. 32nd International Cosmic Ray Conference, Beijing, China 2011.(ID 0979).

[22] M.D.Rodríguez Frías et al., for the JEM-EUSO collaboration. The Atmospheric Monitoring System of the JEM-EUSO space mission. International Sysmposium on Future Directions in UHECR Physics. UHECR 2012. (ID 10005).

[23] A.Santangelo, Requirements and Expected Performances of the JEM-EUSO mission.32nd International Cosmic Ray Conference, Beijing, China 2011.(ID 0991).

[24] S.Toscano et al., for the JEM-EUSO Collaboration. LIDAR treatment inside the ESAF Simulation Framework for the JEM-EUSO mission. 33rd International Cosmic Ray Conference, Rio de Janeiro 2013.(ID 530).

[25] M.D.Rodríguez Frías et al., for the JEM-EUSO collaboration. Towards the Preliminary Design Review of the Infrared Camera of the JEM-EUSO Space Mission. 33rd International Cosmic Ray Conference, Rio de Janeiro 2013.(ID 0900)

[26] J.A. Morales de los Ríos et al., The IR-Camera of the JEMEUSO Space Observatory, 32nd International Cosmic Ray Conference, Beijing, China 2011.(ID 1031).

[27] UL 04171 640 $\times$ 480 VGA LWIR uncooled microbolometer Data sheet from ULIS Propietary (UL 04171)/15.10.07/UP/DVM/NTC07 1010-4 rev.4.

[28] Yoshiya Kawasaki et al., The Focal Surface of the JEM-EUSO Instrument, 32nd International Cosmic Ray Conference, Beijing, China 2011.(ID 0472).

[29] Von Valmos, P. for the JEM-EUSO Collaboration, General overview of EUSO-Balloon mission, The 34th International Cosmic Ray Conference, 30 July- 6 August, 2015. The Netherlands

[30] Rodríguez Frías, M. D. et al. for the JEM-EUSO collaboration, The Spanish Infrared Camera onboard the EUSO-Balloon (CNES) flight on Augus 24, 2015, The 34th International Cosmic Ray Conference, 30 July- 6 August, 2015. The Netherlands

[31] Lawrence Wiencke, for The JEM-EUSO Collaboration, EUSO-BALLOON mission to record extensive air showers from near space. The 34th International Cosmic Ray Conference, 30 July- 6 August, 2015. The Netherlands

[32] SPace & AStropaticle Group website of the JEM-EUSO Collaboration spas.uah.es/EUSO-balloon

[33] Mackovjak, S. et al. for the JEM-EUSO collaboration, Cloud Optical Depth obtained from the Infrared Camera data and the UV Flashers mounted on a helicopter flying under the EUSO-Balloon during its flight, The 34th International Cosmic Ray Conference, 30 July- 6 August, 2015. The Netherlands

[34] Sáez-Cano, G. et al. for the JEM-EUSO collaboration, Cloud Optical Depth obtained from the Infrared Camera data and the UV Flashers mounted on a helicopter flying under the EUSO-Balloon during its flight, The 34th International Cosmic Ray Conference, 30 July- 6 August, 2015. The Netherlands.

[35] Agenzia Spazial Italiana. http://www.asi.it/ene

[36] Istituto Nazionale di Fisica Nucleare.

[37] Russian Federal Space Agency. http://en.federalspace.ru

Chapter 3

PMT reliability analysis model

3.1 The dual nature of light

In the mid 1800s, scientists were convinced that the age-old question, «What is light?» had been answered conclusively. Light, they said, is an electromagnetic wave. Polarization, diffraction and interference offered proof of the wave nature of light. In addition, the speed of light was the same as that of electromagnetic waves. By the late 1800s, however, certain experiments showed that light behaved as though it consisted of particles. These apparently contradictory models of light, wave and particle, took decades to resolve.

When electromagnetic radiation strikes certain materials, particularly metals, electrons are ejected from them and escape into the space around the materials. This phenomenon is known as the photoelectric effect. Materials that behave in this manner are said to be photoemissive, and the emitted electrons are referred to as photoelectrons.

The more intense the electromagnetic radiation that strikes a photoemissive material, the more photoelectrons are ejected per second. Increasing the intensity of the radiation, however, does not result in more energetic photoelectrons. Instead, the kinetic energy of the emitted electrons depends on the frequency of the incident radiation and on the type of photoemissive material. The higher the frequency, the greater the energy of the photoelectrons.

For each photoemissive material there is a threshold frequency, a frequency below

which no photoelectrons will be emitted, no matter how intense the radiation. For example, a material whose threshold frequency is that of yellow light emits no electrons when bombarded by red light or radio waves, no matter how intense the radiation. But this material will emit many electrons when bombarded by even the faintest green light or by X rays.

Figure 3.1 shows the relationship between the maximum kinetic energy of photoelectrons, and the frequency of the incident radiation, ν, for two different photoemissive materials, A and B. For every photoemissive material, the maximum kinetic energy of photoelectrons varies linearly with the frequency of the incident radiation.

The slope of the graph is the same for all photoemissive materials and is equal to Planck's constant, h (6.626×10^{-34} J·S). The point at which the graph intercepts the x axis is different for different photoemissive materials and represents the threshold frequency ν_0 of the material [1].

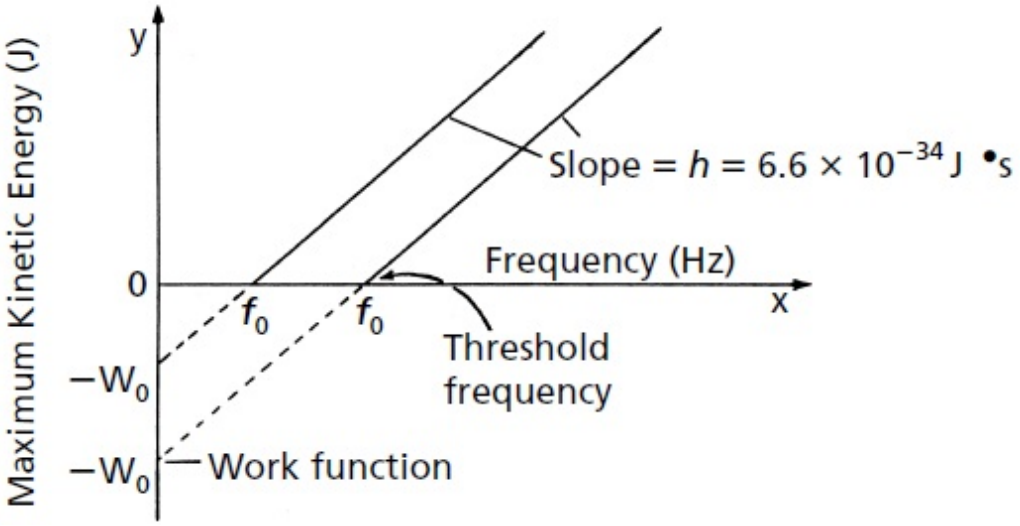

Figure 3.1: Relationship between the maximum kinetic energy of photoelectrons and the frequency of the incident radiation [1].

The relationship between K_{max} and ν can be expressed mathematically as:

$$K_{max} = h\nu - W_0 \tag{3.1}$$

where h is Planck's constant and W_0 is the absolute value of the y-intercept of the graph.

This y-intercept is different for different photoemissive materials and is known as the work function of the material.

If light and the other Electromagnetic radiations were just electromagnetic waves, the kinetic energy of the ejected electrons should depend on the intensity of the radiation, rather than the frequency, and no threshold frequency should exist. More intense radiation (brighter light) then means waves with greater amplitude that exert stronger electric and magnetic forces. As a result, the electrons should emerge with more kinetic energy when the radiation is more intense. But since frequency, not intensity, is the sole determining factor of the kinetic energy of emitted photoelectrons, to the point that a «threshold» for frequency exists, a new and improved model of light had to be devised.

The photoelectric effect was explained by Albert Einstein in 1905. He proposed that light and all forms of electromagnetic radiation consisted of particles called photons. This proposal was based on Max Planck's quantum theory which states that electromagnetic radiation is emitted in discrete amounts, or quanta, of energy. Einstein extended this idea: not only was electromagnetic radiation emitted in discrete amounts of energy, it was also absorbed in discrete amounts, because electromagnetic radiation consists of particles,each carrying a discrete amount of energy [1].

The energy of each particle, or photon, of light or any type of electromagnetic radiation is directly proportional to the frequency of the radiation.

It is found, according to Einstein, by using the formula

$$E = h \cdot \nu \tag{3.2}$$

where E is the energy in Joules, $\hbar$ is Planck's constant, and ν is the frequency of the radiation, in hertz, this formula indicates that photons of higher frequency have more energy than those of lower frequency.

Since all forms of electromagnetic radiation travel at the speed of light and satisfy the relationship c = $\lambda\nu$, the energy of a photon can be expressed as

$$E = \frac{hc}{\lambda} \tag{3.3}$$

where λ is the wavelength, and c is the speed of light. Thus, the energy of a photon is inversely proportional to its wavelength.

In the photoelectric effect, each photon acts individually on one electron. A photon gives either all of its energy, equal to $h\nu$, to the electron it interacts with, or none. An electron that gains no energy remains in the material. One that absorbs all of the energy of the photon may or may not escape from the particular material, depending on how much energy it absorbed and how much it needs to escape [1].

The minimum amount of energy an electron needs to be able to escape from a photoemissive material is the work function W_0 of that material.This is also the minimum amount of energy an electron loses as it escapes. Thus, if $h\nu$ (photon energy) is greater than W_0, the electron picks up more than enough energy to escape. After absorbing $h\nu$ Joules of energy, the escaping electron loses a minimum of W_0 Joules on the way out and emerges with, at most, $h\nu - W_0$ Joules of kinetic energy. This is why the maximum kinetic energy of photoelectrons satisfies the relationship in equation 3.1.

Each photon must still act individually on one electron and can only impart $h\nu$ Joules of energy not enough to eject the electron. Very rarely do two photons strike the same electron in quick succession so that the electron absorbs a second dosage of energy before the first dosage is dissipated through the material [1].

The threshold frequency ν_0 of a photoemissive material is thus the frequency at which the quantify $h\nu$ is equal to the work function W_0. This leads to the equation

$$W_0 = h\nu_0 \tag{3.4}$$

a formula that is confirmed by the K_{max} versus ν graph for any photoemissive material (such as the graph in Figure 3.1). If we use the dotted portion of the graph between the x and y intercepts to calculate the slope, which we know is equal to h, Planck's constant, we get

$$slope = \frac{\Delta y}{\Delta x} = \frac{W_0}{\nu_0} = h \quad \text{or} \quad W_0 = h\nu_0 \tag{3.5}$$

Increasing the intensity of radiation increases the rate of emission of photoelectrons because more photons then strike the photoemissive material per second. If the photons

are energetic enough to eject electrons (above the threshold), the more of them that hit the material per second, the greater the number of electrons emitted per second [1].

3.2 Photomultiplier tubes

3.2.1 Principles of operation

A photomultiplier tube (PMT) converts light into an electrical signal, then amplifies that signal to a useful level by emission of secondary electrons [2]. Figure 3.2 shows the essential elements:

- a photocathode which converts a flux of photons into a flux of electrons;
- an electron-optical input system which focuses and accelerates the electron flux;
- an electron multiplier consisting of a series of secondary-emission electrodes (dynodes); and, finally
- an anode which collects the electron flux from the multiplier and supplies the output signal.

The two phenomena fundamental to the operation of a photomultiplier are photoemission and secondary emission.

Photoemission is due to a fraction of the incident photons that impart all their energy to bonded electrons of the photocathode material, giving some of them sufficient energy to escape. If the number of these photoelectrons that strike the first dynode is n_k, and the gain of the dynode is g_1, the number of resulting secondary electrons is $n_k g_1$. Then, if the second dynode has a gain g_2, it in turn emits $n_k g_1 g_2$ electrons. The process is repeated from dynode to dynode up to the anode where the electrons are finally collected. If N is the number of dynodes, the number of electrons collected is

$$n_a = n_k \prod_{i=1}^{N} g_i \tag{3.6}$$

The electrons are accelerated and focused by electric fields between the dynodes. The required potential gradients usually being obtained from a voltage divider across the

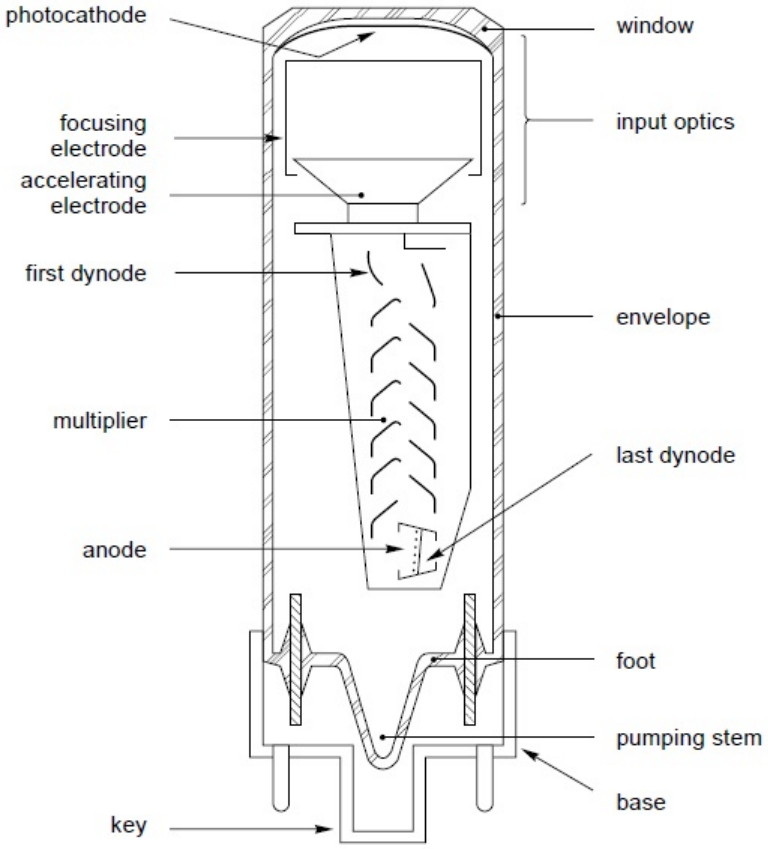

Figure 3.2: Elements of a photomultiplier based on the world's first PMT, the 56AVP, introduced by philips (photonis) in 1956 [2].

terminals of a high-voltage supply (Fig. 3.3).

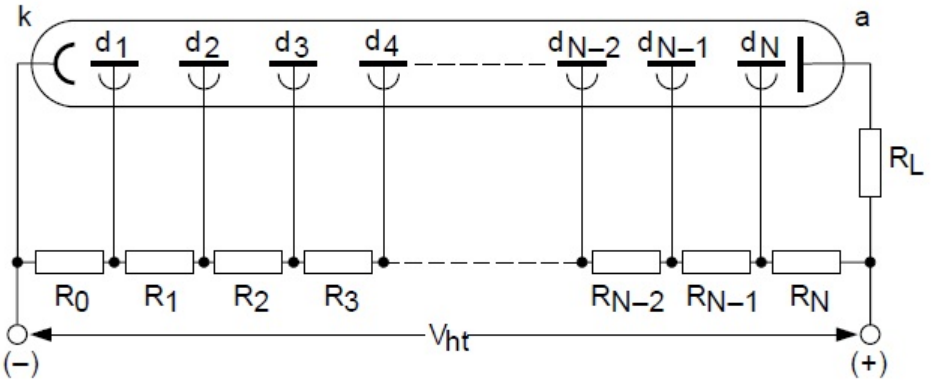

Figure 3.3: Voltage divider, high tension supply [2].

3.2.2 Main elements of PMTs

3.2.2.1 Photocathode

The cathodes normally used in photomultipliers are made of a deposited photoemissive semiconductor. There are two main kinds:

- Semi-transparent cathodes, the most widely used, are deposited on the inside of the input window; electrons are emitted from the side opposite to the incident light. The cathode can be large (from ten to a few hundred millimeters in diameter) and the window on which it is deposited can be flat or curved.
- Opaque cathodes, the most widely used, are deposited on the inside of the input window; electrons are emitted from the side opposite to the incident light. The cathode can be large (from ten to a few hundred millimeters in diameter) and the window on which it is deposited can be flat or curved.

Photoemissive materials used in PMTs are usually metal alloys that have extra electrons, usually bialkali antimonide compounds such as K_2CsSb and Na_2KSb. The Photomultiplier tube is an optical energy detector which has high enough internal gain to provide adequate output signal levels at low ligh levels. Electrons that are emitted at the cathode of a PMT are directed through a series of dynodes by an applied electric field. A single electron emitted at the cathode causes a number of secondary electrons to be emitted at the first dynode. These secondary electrons from the first dynode are in turn directed to a second dynode where this multiplication process is repeated for each impinging electron. This electron multiplication process is repeated through a series of dynodes until the electrons from the last dynode are collected at the PMT anode, with the resulting anode current being the PMT output [2, 3].

3.2.2.2 Dynode

A series of dynodes multiply the small number of electrons generated at the photocathode into a measurable electronic signal. They are made of metal alloys and are maintained at positive electrical potentials, each one higher than the last. They are curved or positioned

so as to direct the emitted electrons toward the next dynode. The absorption of one electron at a dynode causes emission of three to six electrons, depending on the potential difference from dynode to dynode. The electrons released at each dynode are accelerated, again because of the potential difference between dynodes.

The process continues for 9 to 12 dynodes, for a total multiplication factor of about a million, producing a small but measurable electronic signal. Finally the anode collects all the electrons produced from the final dynode and emits an output voltage signal [4].

3.2.2.3 Input Window

The material of the input window limits the spectral sensitivity in the short wavelength region. Figure 3.4 and Table 4.1 give the characteristics of some of the glasses used. These are mainly borosilicate glass (hard glass) and lime glass (soft glass), the cut-off wavelengths of which are between 250 and 300 nm, and UV-transparent glasses and fused silica, which have cut-off wavelengths below 250 nm. In some applications, the windows used with semi-transparent cathodes are frosted to reduce reflection.

Even with LiF or MgF_2, UV-radiation of less than 180 nm can be investigated only in vacuum because of the absorption of the air. For wavelengths less than 105 nm, there is no transparent material and windowless photomultipliers must be used in an evacuated system. (Alternatively, single-channel electron multipliers or microchannel plates may be used.)

Type of Window	**Cut-Off Wavelength (Decrease to 10%)** (nm)	**Refractive Index n** at λ (nm)
Lime glass	300	1.54 - 400
Borosilicate	200	1.50 - 400
UV-glass	190	1.49 - 400
Fused Silica	160	1.47 - 400 1.50 - 250
Sapphire(Al_2O_3)	145	1.80 - 400
MgF_2	115	1.40 - 400
LiF	105	1.40 - 400

Table 3.1: Characteristics of glasses used in PMT windows [2]

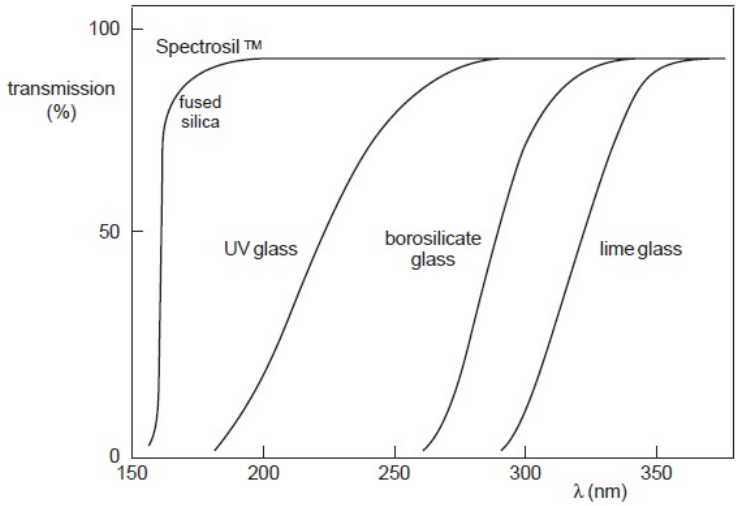

Figure 3.4: Transmission (%) as a function of wavelength λ for various glasses used in photomultiplier input windows (thickness 3mm) [2].

3.2.3 Similar elements

First of all, it is important to understand the basis of any of this elements we have considered before. Historically the vacuum tube is the beginning of electronics as we now it nowadays; its development has helped the mankind to build new electronic system; it has helped to reach the Moon, and it was the first approach into microelectronics as well. It was the beginning of computational science. Vacuum tubes were a starting point for Integrated Circuits (ICs) development and PMTs.

The principle of vacuum tubes was basically a device made of a sealed glass or ceramic enclosure used to control a flow of electrons. Its common applications were amplification of weak current, alternating electric current rectification to direct electric current, generations of radio frequency power for radio and radar, and creations of images on a television screen or computer monitor.

An IC consists of hundreds, thousands, or millions of microscopic electronic devices that have been fabricated and electrically interconnected on the surface of a silicon chip. A chip is a square or rectangular flat plate that is about 0.5 mm thick and typically 5 to 25 mm on a side. Each electronic device (e.g., transistor) on the chip surface consists of separate layers and regions with different electrical properties combined to perform the

particular electronic function of the device [5].

IC main functions are amplification, oscillation, timing, countering, computer memory and microprocessor. An IC can be categorized as either linear (analog) or digital, depending on its intended application.

3.2.3.1 Similarity and differences

A vacuum tube and a PMT show similarity, both are vacuum tubes, however, for different purposes. The PMT amplifies light and vacuum tube amplifies, rectifies and modifies weak currents. Also, their internal characteristics, composition, structure, and operating conditions are similar but different in principles of operation; i.e. different failure modes which, thus, a reliability analysis for PMT based on a vacuum tube is not the most appropriate or the most accurate for an instrument designed to be in Space .

ICs and PMTs in a reliability model are considered as system themself,however, according to this assumption, the IC is the closest element to the PMT in the current reliability standards. The Table 3.2 shows main differences between PMT, Vacuum Tubes and Integrated circuit.

Table 3.2. Similarity and differences among PMTs, VTs and ICs devices.

Element	Material	Feature Size	Physical Conditions	Operating Voltage (V)
PMT	Anode Cathode:(AgOCs,(SbKcS) Dynode:(AgMg),(CuBe)	mm	2"<Size≤30" Affected by Vibration Affected by Shock Affected by Light	500< V ≤3000
Vacuum Tube	Anode:Ni(Nickel) Cathode:W (Tungsten) Grid: Ni(Nickel)	mm	1.5"<Size≤25" Affected By Vibration Affected By Shock	10 < V ≤15000
Integrated Circuit	SiO_2(Silicon Dioxide)	nm	1.5"<Size≤25" Vibration Resistance Shocking Resistance Affected by temperature	2.3 < V ≤5

3.3 Photomultiplier tubes failure modes

3.3.1 Partial failure

Partial failures occurs in a system or part of a system from which recovery of part or all the system is possible. These kind of failures include temporal failures. Failures such as high dark current (noisy tube), gain drifts, decrease of cathode sensitivity, resulting in incorrect or degraded signals at the output are considered partial failures.

Due to long-term stability problem, an aging period has to be applied whenever tubes have not been operated for a long time. PMTs which do not reach a fairly constant gain after that period can be regarded as failing. This clearly indicates that the reliability of PMTs is closely connected to the mode of operation (voltage, mean anode current, etc.) and to the specifications which are expected from these tubes. It is also clear that photomultipliers are more like systems than components as far as reliability is concerned due the numerous characteristics affecting their operation (cathode sensitivity, noise, gain, etc.)

The reliability analysis of the PMT is a critical topic in ground-based experiments and space missions where the proper working condition of PMT's are crucial for the success of the experiment. The JEM-EUSO space telescope needs highly reliable PMTs since they are the most common components on the focal surface of the instrument. As usual, two types of failure must be determined [6].

As partial failure this work will consider:

- Failure caused by space radiation
- Quantum efficiency degradation
- Detectivity degradation
- Responsivity degradation

3.3.1.1 Radiation effects

The JEM-EUSO telescope, is being designed to operate for 5 years on board the ISS orbiting in a Low Earth Orbit (LEO) at an altitude of about 400 km. As for any mission

to be operated in space, the JEM-EUSO telescope must meet specific requirements, i.e. tolerate high radiation doses, unaccessible and remote controlled operations. Thus a reliability analysis and radiation hardness assurance is crucial in order to determine the tolerance and redundancy requirements within the system as previous studies show in case of Field Programmable Gate Array (FPGA) which applies to PMTs [7].

The design and the construction of the JEM-EUSO telescope is a real technical challenge as it involves the use of new technologies from the laboratories of both industrial and research centers in areas as diverse as large optical and accurate Fresnel lenses, a novel technique of photo detection highly sensitive with very accurate resolution, and very innovative analog and digital electronics as well.

Space is a hostile environment where radiation plays the main role as the most significant failure source due to the impact on the electronics devices. To gather evidence of radiation effect on the JEM-EUSO electronics, especially on the PMTs, is absolutely necessary as they are the main and most critical elements of the instrument.

Space radiation is made up of three components: particles trapped in the Earth's magnetic field, Solar Energetic Particle (SEP) events, and galactic cosmic rays, which are high-energy protons and heavy ions from outside our Solar System.

The ISS is placed at 51.6° orbit where half the exposure is from the highly penetrating galactic cosmic rays. This orbit is more susceptible to radiation from SEPs [8]. Moreover, space radiation can conveniently be placed into three main categories according to its effects: (a) Total Ionizing Dose (TID), (b) Displacement Damage, (c) Single Event Effect [9].

In terms of PMTs the kind of radiation that affect them the most are background events [10], they can be induced in a PMT by one of the following mechanism:

- Direct ionization in the cathode or dynode by a particle producing secondary electrons,
- Fluorescence, or more generally scintillation, in any optical components of the PMT induced as a result of the passage of an incident particle,
- Cherenkov radiation generated in any optical component of the PMT by fast charged particles.

3.3.1.1.1 Total Ionizing Dose

Total Ionizing Dose (TID) is defined as the amount of energy deposited by the radiation in their passage through a material per mass unit. In order to have a measure of radiation dose independently of the target material, TID is usually expressed in equivalent units of radiation dose in Silicon, rad(Si). The components with higher sensitivity to TID are active electronic devices such as transistors and ICs. Their sensitivity thresholds typically range from 1 krad(Si) to 1 Mrad(Si) depending on the technologies used. TID degradation in microelectronics results from the build up of charge in insulating layers, and has a cumulative effect on electronics, resulting in a gradual loss of performance and eventual failure.

Provided that the particle intensity and spectrum does not change significantly traveling through the material, TID can be determined from the charged particle fluence at the surface of the material, and the electronic stopping power of the particle based on [10]:

$$D = \frac{\Omega t_e}{\rho} \left(\frac{dE}{dx} \right)_{loss} \int_{E_1}^{E_2} \psi(E) \mathrm{dE} \tag{3.7}$$

where D is the Ionizing Dose, ρ is the mass density of the material, Ω is the solid angle of particle incidence, t_e is the exposure time, $\psi(E)$ is the differential energy spectrum, and $(\mathrm{dE/dx})_{loss}$ is the stopping power in units of energy loss per length unit.

3.3.1.1.2 Single Event Transient

A Single Event Transient (SET) is due to a strike by high-energy particle from cosmic radiation. The electron-hole pair produced by such a strike separates promptly in the presence of electric field and the temporary inversion layer created under the gate of a transistor produces a short voltage pulse, the Single Event Effect (SEE). If this generated SEE propagates and latches at a flip-flop, it causes Single Event Upset (SEU) or, otherwise called a soft error. Thus, a soft error is generated if the SET arrives within a given time period (called the latching window) and this requires time related calculations [11].

3.3.1.1.2.1 Basic mechanism of A SET

A charged particle moving through a semiconductor deposits a fraction of its energy in the medium by ionizing the atoms of the crystal along its path. The amount of energy received by the medium per unit path length is called Linear Energy Transfer (LET).

LET defines the efficiency of the energy transfer and is independent of both the electrical charge and the energy of the particle. It is usually expressed in units of MeV·cm^2/mg (energy loss divided by the material density). In Space most of heavy Ions from cosmic rays have LETs in Silicon ranging from 0.01 to 40 MeV cm^2/mg [12]. In Silicon devices, a LET corresponds to a charge deposition per unit length of 10 fC/μm. The typical range of deposited charge is from 0.1 to 400 fC/μm.

3.3.1.1.2.2 Single Event Transient Pulse

The statistical SET's width in logic circuits by applying the LET values to the commonly transient current double exponential model is shown below:

$$I(t) = \frac{Q_{coll}}{\tau_\alpha - \tau_\beta}(e^{-\frac{t}{\tau_\alpha}} - e^{-\frac{t}{\tau_\beta}}) \tag{3.8}$$

$$Q_{coll} = -10.8\frac{fC}{\mu m} \cdot \delta \cdot LET \tag{3.9}$$

where Q_{coll} is the collected charge in the sensitive region; τ_α is the collection time constant, which is a process dependent property of the junction and τ_β is the ion track establishment time constant, which is relatively independent of the technology. In Bulk-Silicon, a typical charge collection depth $\{\delta\}$ is 2 μm for every MeV·cm^2/mg, and an ionizing particle deposits about 10.8 fC charge along each micron on its track [13].

3.3.1.2 Quantum efficiency degradation

The quantum efficiency at wavelength λ is the average photoelectric yield per incident photon and is normally expressed as a percentage. It is the most fundamental unit concerning the performance of the PMT. Important practical considerations such as resolution, signal/noise and detectivity are all related to quantum efficiency [14].

The lifetime of the PMT depends on the working conditions when using it as well as for the charged applied on it. The following equations explains this situation

$$Q(t) = Q_{E_O} e^{t/\tau} \tag{3.10}$$

where τ is the lifetime of the cathode PMT under working conditions

$$Q(q) = Q_{E_O} e^{q/\tau_q} \tag{3.11}$$

where τ_q is the lifetime of the cathode PMT under charges applied on it. In most cases, this value is roughly 2-3 C/cm^2.

However, in case of evaluating the time dependent quantum efficiency, the next relation is assumed because of the linearity of both equations:

$$\frac{t}{\tau} = \frac{q}{\tau_q} \tag{3.12}$$

Therefore, in order to perform the analysis of the quantum efficiency -charge collected

dependent- (Q(q)), q is necessary to be evaluated, where q, is the charge collected at the cathode, expressed in C/cm^2 which is determined as follows:

$$q = \frac{e^- \cdot \phi_\gamma \cdot t \cdot E_\gamma \cdot Q_{E_O}}{Ei \cdot S_{PMT}} \tag{3.13}$$

Since q is the relation between the charge collected per unit area S_{PMT}, some considerations have been taken into account in order to express it including the intrinsic/physical parameters of the material. To express the charge (q) in terms of coulombs, for instance, it is necessary to consider the effect of the gain as the quality of the material to amplify the photo-current received. This photo current is basically the product of the electron's charge by the flux of photons (ϕ_γ) with its Energy (E_γ) received as well as by the product of the initial quantum efficiency of the material (Q_{E_O}), which is the amount of electrons produced per photon perceived. The division factor of the equation is related to the unit area necessary to express the charge collected. For instance, it is necessary to multiply the unit area by the Ionization Energy (E_i) since it is basically the energy necessary to remove an electron per unit area.

3.3.1.3 Detectivity degradation

Noise Equivalent Power (NEP) is the light power that gives a Signal-to-Noise Ratio (SNR) equal to 1 for an integration time of half a second [15]. The inverse value of NEP is the detectivity or detection capability. The detectivity is a measure of the least detectable radiant power or detector SNR. A higher detectivity indicates capability to detect lower levels of radiant power. Therefore, the NEP is calculated as follows [16]:

$$NEP = \frac{hc}{QE_0\lambda}\left(\frac{2I_D}{e}\right)^{1/2} e^{t/\tau} \tag{3.14}$$

where h is the Planck constant, c the speed of light, λ the wavelength and Dark Current Expressed by I_D and calculated as follows:

$$I_D = aAT^2 exp\left(-\frac{\phi_0}{kT}\right) \tag{3.15}$$

where a is the Richardson's constant, T is the Absolute temperature expressed in Kelvin, ϕ_0 is the Work function, k is the Boltzmann's constant and A is the Cathode Area respectively.

3.3.1.4 Responsivity degradation

The responsivity (R) expresses how much electrical signal is generated when a given amount of optical flux is incident on a detector. The electrical quantity can be current or voltage [17]:

$$R(t) = \frac{QE \times e}{hv} \tag{3.16}$$

3.3.2 Catastrophic failure

A catastrophic failure is a sudden and total failure of some system from which recovery is impossible. Catastrophic failures often leads to cascading systems failure. Failures such as cracks in the glass envelope, electrodes no longer connected or short-circuited, resulting in useless or non-existent signals at the output are considered catastrophic failures in PMTs [6, 18, 19].

3.3.2.1 Analysis

The analysis of catastrophic failures will be based on military, civil and space standards; it should be assessed according to the needs to be taken or the functional requirements. There are two standards that fit our needs, one is the 217 Plus [20] which is for military, ground and for Space applications as well and the MIL-HDBK-217-F [21] which is for the same applications than 217 Plus. The main difference lies in the fact that MIL-HDBK is obsolete and discontinued. Thus, it is not yet adapted to new components; however, it is yet useful and it is currently used by the space industry for reliability assessments.

On the other hand, 217 plus takes into account the new electronics component within Space and military industry as well as includes new characteristics that make it the most suitable and appropriate standard and prediction model for this work; anyway, the space industry does not consider it yet for their assessments as they do with its predecessor.

3.3.2.2 Evaluation using 217 Plus

Reliability analysis using 217 Plus prediction model is suitable for this work. It has been developed to be an updated and enhanced version of MIL-HDBK-217-F: the most extended method in reliability prediction. The 217 Plus has optional data used to enhance the predicted failure rate by adding more detailed and specific factors of pertaining to environmental stresses, operating profile factors and process grades. It contains default values for the environmental stresses and profile. It also includes many new more components like IC Encapsulated: elements proposed herein that can be used as equivalent to assess the PMTs. This elements are either missing or not upgraded in MIL-HDBK-217-F. The failure rate (λ_p) for plastic encapsulated (non-hermetic) integrated circuit applicable for the PMT is given by equation 5.8, where failure rate multipliers are shown in Table 3.3.

These failure rate multipliers considering their correspondent values, allows the estimation of the base failure rate for any environmental, operational or non operational conditions which the component is exposed to; having as result the analysis of catastrophic failure of PMTs.

$$\begin{aligned} \lambda_P = \pi_G(\lambda_{OB}\pi_{DCO}\pi_{TO} + \lambda_{EB}\pi_{DCN}\pi_{RHT} + \\ \lambda_{TCB}\pi_{CR}\pi_{DT}) + \lambda_{SJB}\pi_{SJDT} + \lambda_{EOS} \end{aligned} \tag{3.17}$$

The analysis that will be conducted herein on the JEM-EUSO PMT is in accordance with MIL-STD-756B [22]. It also follows the Method 1001 in order to determine subsystem and system reliability and Mean Time To Failures (MTTF). The failure rates of system and subsystem components (such as) resistors, capacitors, transformers, etc., will be calculated based on the Parts Stress Analysis Method given in MIL-HDBK-217-F [20, 21].

There are two ways that reliability is predicted under 217: Part Count and Part Stress Analysis Prediction [23].

Parts Count Prediction is generally used to predict the reliability of a product

Table 3.3: PMT failure rate multipliers for PMTs according to 217 Plus [20]

Failure Rate Multiplier(FRM)	**Symbol**
Reliability Growth FRM	π_G
Base failure rate, Operating	λ_{OB}
FRM for Duty Cycle Operating	π_{DCO}
FRM for Temperature Operating	π_{TO}
Base failure rate, Environmental	λ_{EB}
FRM, Duty Cycle, Non operating	π_{DCN}
FRM for Temperature environment	π_{RHT}
Base failure rate, Temp Cycling	λ_{TCB}
FRM, Cycling Rate	π_{CR}
FRM,Delta Temperature	π_{DT}
Base failure rate, Solder Joint	λ_{SJB}
FRM, Solder Joint Delta Temp	π_{SJDT}
Failure rate Electrical Overstress	λ_{EOS}

early in the product development cycle to obtain a rough reliability estimate relative to the reliability goal or specification. A failure rate is calculated by literally counting similar components of a product (i.e. Capacitor) and grouping them into the various component types (i.e. PMTs). The number of components in each group is then multiplied by a generic failure rate and quality factor found in 217. Lastly, the failure rates of all the different part groups are added together for the final failure rate. By definition, Parts Count assumes all components are in series and requires that failure rates for non-series components be calculated separately [23].

Parts Stress Analysis Prediction is usually used much later in the product development cycle, when the design of the actual circuits and hardware are nearing production. It is similar to Parts Count in the way the failure rates are summed together. However, with Parts Stress, the failure rate for each and every component is individually calculated based on the specific stress levels the component is subjected to (i.e. Quantum efficiency, Sensitivity ,temperature, vibration, voltage,). In order to assign the proper stress levels to each component, a product design and its expected environment must be well documented and understood. The Parts Stress Method usually yields a lower failure rate then

the Parts Count Method [23].

3.4 Mathematical models and methods

In this section, the mathematical methods used to model the reliability analysis in PMTs designed for Space applications are presented as well as basic notions and methods of the reliability theory used in this thesis. This dissertation is focused on the reliability of the PMT in terms of performance and other mechanism of failure in order to express new failure rates modeling and finally assessing statistical reliability of PMTs devoted to Space application.

3.4.1 Reliability theory

In this section the basic reliability measures used in the Space electronics components context are presented. Then, simple reliability assessment methods are given. The methods presented here are used in the remainder of the dissertation (see Chapter 4 and **??**). The basic definitions and concepts related to the reliability field with the application to electronics, optics, communication and computer sciences can be found for example in MIL-HDBK-217-F, 217-PLUS, JEDEC.

3.4.1.1 Reliability

Reliability, a design attribute, is a broad term that focuses on the ability of an asset (product) to perform its intended function. As defined in military standard MIL-STD-721-C, reliability is «the probability that an item will perform its intended function for a specific interval under stated conditions». An item or asset could be an electronic or mechanical hardware component or device, a software product, or a manufacturing system .

David L. Stringer, speaking at the Reliability Centered Maintenance Enterprise Asset Management conference (RCM/EAM), introduced a new definition of reliability. He said reliability is «the achievements of predictable results with as little variation as specific

circumstances permit» [24].

Reliability [25] is the probability of the product performing properly under typical operating conditions for the expected lifetime intended, and an expression to define reliability is:

$$R(t) = 1 - F(t) \tag{3.18}$$

Here, $R(t)$ is the reliability function, called the survivor function. This is defined as the probability of operating without failure to time t. $F(t)$ is the cumulative failure distribution function (CDF). In reliability, $F(t)$ is the probability that a randomly chosen part will fail by time t. A lifetime distribution model $f(t)$ is the probability density function (PDF) over the time range 0 to infinity. The relationship between the CDF and PDF is shown in 3.19 and 3.20.

$$\int_0^t f(\tau)\mathrm{d}\tau \tag{3.19}$$

$$f(t) = \frac{d}{\mathrm{d}t}\ F(t) \tag{3.20}$$

The hazard rate $h(t)$ is well known as the instantaneous failure rate. This is the probability that failure will occur in the next time interval divided by the reliability $R(t)$ (the probability of operating without failure up to that time interval) [26].

$$h(t) = \frac{f(t)}{1 - F(t)} = \frac{f(t)}{R(t)} \tag{3.21}$$

This can be written as:

$$h(t) = -\frac{1}{R(t)}\frac{dR(t)}{dt} \tag{3.22}$$

Which is equivalent to:

$$h(t) = -\frac{d}{d(t)}(lnR(t)) \tag{3.23}$$

The integral of the hazard rate is the cumulative failure rate (cumulative hazard rate)

$$\int_0^t h(\tau)\mathrm{d}\tau = -(lnR(t)) \tag{3.24}$$

The hazard rate $h(\tau)$ or instantaneous failure rate has dimensions of (t^{-1}), where t is in units of time. Since $R(0) = 1$ (no failures at time zero), the reliability rate over a time period t is the exponential of the cumulative hazard rate in that same time period t.

$$R(t) = e^{\int_0^t h(\tau)\mathrm{d}\tau} \tag{3.25}$$

An important quantitative reliability concept is how long the population will survive without a failure. This termed mean time to failure (MTTF), more specifically the mean-time to the first failure [27].

$$MTTF = \bar{t} \equiv \int_0^\infty t f(t)\mathrm{d}t \tag{3.26}$$

A basic measure of a system's reliability is the mean time between failure (MTBF). It is typically represented in units of hours. The higher the MTBF number is, the higher the reliability of the product [23].

3.4.2 Reliability function for data analysis

3.4.2.1 The exponential distribution

The exponential distribution is used to model the failure behavior of items having a constant failure rate. The exponential distribution is widely used in its own right as a model of the items to failure in some situations and is widely used as the standard to which other distributions are compared. It can be chosen for its constant hazard property or because it models the observed times.

An exponential distribution is used to define the probability of failure of electronic and electromechanical components [28]. The following holds:

$$F(t) = 1 - e^{-\lambda t} \tag{3.27}$$

where:

- $F(t)$ is the probability of failure

- λ is the failure rate in 1/time
- t is the time observed service life

This correlation applies only for the phase of constant failure rate in the tube curve, i.e. for λ = constant.

3.4.2.2 Poisson distribution

The Poisson distribution is quite frequently used in reliability analysis. The Poisson distribution is one of three discrete distributions (Binomial, Poisson, and Hypergeometric) that uses integers as random variables [29].

The Poisson equation for predicting the probability of a specific number of defects or failures (r) in time (t) is:

$$P(r) = \frac{(\lambda t)^r e^{-\lambda t}}{r!} \tag{3.28}$$

where:

- r = number of failures in time (t)
- λ = failure rate
- t = time
- $P(r)$ = probability of getting exactly r failures in time t

To calculate the probability of k or fewer failures occurring in time t, the probability of each failure occurring must be summed as follows:

$$P(r \leq k) = \sum_{0}^{k} P(r) \tag{3.29}$$

The Confidence Level (CL) that the population has a failure rate (λ) based on r $\leq k$ failures occurring in time t is :

$$CL = 1 - P(r \leq k) \tag{3.30}$$

3.4.2.3 Statistical independence

If two events are statistically independent of each other, the occurrence of one event has not influence on the occurrence of the other [30]. Therefore, events A and B are independent if and only if $P(A, B) = P(A)\ P(B)$. The probability of joint occurrence of K independent events can be generalized as

$$P\left(\bigcap_{k=1}^{K} A_k\right) = P(A_1) \times P(A_2) \times ... \times P(A_K) = \prod_{k=1}^{K} P(A_k) \tag{3.31}$$

It should be noted that the mutual exclusiveness of two events does not, in general, imply independence, and vice versa, unless one of the events is an impossible event. If the two events A and B are independent, then A, A', B, and B' all are independent, but not necessarily mutually exclusive, events.

3.4.2.4 Conditional probability

The conditional probability is the probability that a conditional event would occur [30]. The conditional probability $P(A|B)$ can be expressed as

$$P(A|B) = \frac{P(A, B)}{P(B)} \tag{3.32}$$

in which $P(A|B)$ is the occurrence probability of event A given that event B has occurred. It represents a reevaluation of the occurrence probability of event A in the light of the information that event B has occurred.

Intuitively, A and B are two independent events if and only if $P(A \mid B) = P(A)$. In many cases it is convenient to compute the joint probability $P(A, B)$ by

$$P(A, B) = P(B)P(A|B) \quad or \quad P(A, B) = P(A)P(B|A)$$

The probability of the joint occurrence of K dependent events can be generalized as

$$P\left(\bigcap_{k=1}^{K} A_k\right) = P(A_1) \times P(A_2|A_1) \times P(A_3|A_2, A_1) \times \cdots \times P(A_K|A_{K-1}, \cdots, A_2, A_1) \tag{3.33}$$

3.4.3 Other methods of Analysis

There are also many more methods to calculate reliability-based measures described in the literature. We do not characterize them here as they are not used in the calculations presented in the dissertation. Some of them are enumerated below:

- Repair-related metrics
- Availability
- Maintainability
- Parallel system
- Series-parallel systems
- k-out-of-n system
- Fault tree analysis
- Failure mode and effect analysis
- Failure mode, effects and criticality analysis
- Reliability Block Diagram method

Bibliography

[1] Judah Landa, David R. Kiefer, Reviewing Physics, The Physical Settings, Edition 3, January 2007, Chapter 5. , page 136 to 138.

[2] Photonis, Photomultiplier tubes, principles and applications, Chapter 1-3, Reedited September 2002.

[3] H.H.Tan, A Statistical model of the photomultiplier gain process with applications to optical pulse detection, TDA Progress report, January and February 1982.

[4] Jennifer Prekeges, Nuclear medicine instrumentation, Chapter 2, page 19-21, Second Edition, 2011.

[5] M. P. Groover, Fundamentals of Modern Manufacturing Fourth Edition, Chapter 34, pp.814. 2010 John Wiley & Sons, Inc. ISBN 978-0470-467002

[6] J.P. Boutot, J. Nussli, and D. Vallat, Recent trends in photomultipliers, page 270-297, 1983.

[7] Hector Prieto, Katsuhiko Tsuno, Marco Casolino,Luis del Peral, Toshikazu Ebisuzaki, J.A. Morales de los Ríos, G.S áez-Cano and M.D. Rodríguez Frías, for the JEM-EUSO Collaboration."FPGA Reliability Analysis for the JEM-EUSO Space Mission".ISBN: 84-616-2226-X.http://www.ramsinscience.es/posters/Prieto-ReliabilityWorkInJEMEUSO.pdf. (2012)

[8] G.D. Qualls et al. International Space Station Radiation Shielding Model Development. Paper number 01ICES-2370. (2001).

[9] Mark H. Holly. The effects of Space radiation flight film. NASA contractor report 188247.September (1995).

[10] European Cooperation For SPACE Standarization, Space Engineering, Calculation of Radiation and Its Effects and Margin Policy Handbook. December (2010).

[11] S.Gangadhar, S. Tragoudas, A novel Probabilistic SET Propagation Method, in proceedings og International Symposium on Quality Electronic Design, ISBN:978-1-4244-6455-5, (2010).

[12] P. Fouillat, V. Pouget, D. Lewis, S. Buchner, and D. McMorrow, Investigation of single-event transients in fast integrated circuits with a pulsed laser. Int. J. High Speed Comput. (Singapore), vol.14, no.2, pp.327-340. (June 2004).

[13] Fan Wang and V. Agrawal, "Soft Error Rate Determination for Nanometer CMOS VLSI Logic," Proc. Southeasthern Symp. System Theory, pp. 324-328, (2008).

[14] Electron tubes enterprises, understanding photomultipliers Handbook. Page 1-26.

[15] Hamamatsu. Technical Information SD-12. Characteristics and use of infrared detectors. 2004. Hamamatsu Web Page:https://www.hamamatsu.com/resources/pdf/ssd/infrared_techinfo_e.pdf

[16] J. Ready, Optical Detectors and Human Vision. Fundamentals of Photonics SPIE, Module 1.6. pp. 216-232. 2006.

[17] K.Laqua, B. Schrader, G. G. Hoffmann, D. S. Moore and T. Vo-Dinh. Detection of radiation. International union of pure and applied chemistry. Analytical chemistry division commission on spectrochemical and other procedures for analysis. Pure & Appl. chem, Vol 67, No, 10, pp. 1745-1760, 1995.

[18] Elmasri et al.,Fundamentals of database systems. 1st edition. Study guide. Cram101; 1 edition (September 13, 2012).

[19] K.K Aggarwal.Topics in safety, reliability and quality. Reliability Engineering.Chapter 1, pp. 9-10. 1993.Kluwer academic publishers. ISBN 0-7923-2524-9.

[20] United States of America Department of Defense, Handbook of 217 Plus, Reliability Prediction Models, (2006). 1-68.

[21] United States of America Department of Defense, Military Handbook, Reliability Prediction of Electronic Equipment, (1990). 22-127

[22] MIL-STD-756B, Reliability Modeling and Prediction.

[23] Wendy Torell and Victor Avelar, Mean Time Between Failure: Explanation and Standards. white Paper 78, Revision 1.Schneider electric's Data Center Science Center.

[24] Ramesh Gulati et al. (2009), Chapter 1, p. 4-5

[25] A.L. Hartzell et al., MEMS Reliability, MEMS Reference Shelf, DOI 10.1007/978−1−4419−6081−4−2, © Springer Science + Business Media, LLC 2011.

[26] Guttman, I., Wilks, S.S., Hunter, J.S. (1982) Introductory Engineering Statistics. New York: John Wiley and Sons.

[27] Nash, F.R. (1993) Estimating Device Reliability: Assessment of Credibility. Dordrecht: Kluwer Academic Publishers, p. 64, Springer Publishing, now copyright holder.

[28] SIEMENS. Background information on MTBF. 03/01/2011.

[29] Edward R. Sherwin, START-Selected Topics in Assurance Related Technologies, Volume 9, Number 1. Reliability Analysis Center, 2002.

[30] T.T. Soong, Fundamentals of Probability and Statistics for Engineers. John Wiley and Sons, Ltd. 2004. Chapter 2, page 20.

Chapter 4

PMT radiation hardness assurance as reliability analysis

4.1 Considerations and assumptions

The focal surface of JEM-EUSO has a curved surface of about 2.5 m in diameter, and it is covered with 4932 multi anode photomultiplier tubes (Hamamatsu R11265-03-M64 MOD: MAPMT), one PMT can be observed in Figure 4.1. The focal surface detector consists of Photo-Detector Modules (PDMs), each of which consists of 9 Elementary Cells (ECs). Each of the EC contains 4 units of MAPMTs. Therefore, about 1500 ECs or about 137 PDMs are arranged on the whole focal surface [1, 2].

So far, standards that technically describe PMTs reliability have not been formally developed. In this work, it is intended to develop such a model and technic with which to assess the reliability and performance of the PMTs. vacuum tube and integrated circuits (ICs) are going to be considered as equivalents thanks to the multiple similarity between vacuum tubes, ICs and PMTs have and share. Such a consideration is done so to develop a model for the PMT taking as reference the most similar element in terms of functionality.

The organization of the analysis consists of three main sections:

- Definition the overall purpose, scope , nomenclature, and general reference material for the reminder of the reliability analysis.

Figure 4.1: The MAPMT for the JEM-EUSO photodetector (R11265-113-M64 MOD2) [3]

- Reliability analysis of the PMT partial failure (including radiation effects).
- Conclusions

4.2 Technical specifications of the JEM-EUSO PMTs

The PMTs used in JEM-EUSO have been specially designed and manufactured by Hamamatsu in collaboration with the RIKEN research institute (Wako-Japan). They are «exclusively» intended for this space mission. With the aim to improve the technical specification of the PMT for the JEM-EUSO space telescope, Hamamatsu, the Japanese PMT manufacturer, has developed a special PMT according to the JEM-EUSO space requirements. Tables 4.1 and 4.2 show the technical characteristics of the PMT with a spectral window in the UV enough broad to observe both the fluorescence as Cherenkov light generated by the EAS.

A gain ratio of 10^6 added to a cathode sensitivity of 90 μA/lm allows the detection of low light levels with a very low dark current of 0.4 nA. The PMT is operative in a wide temperature range. Table 4.3 lists nominal voltage ratios for the dynodes of the PMTs [3].

Table 4.1. Electronic characteristics of the JEM-EUSO PMT at 25°C [3]

Parameter		Min	Typ.	Max.	Unit
Cathode Sensitivity	Luminous (2856K)	70	90	-	μA/lm
Anode Sensitivity	Luminous (2856K)	-	90	-	A/lm
Gain (Current Amplification)		-	1×10^6	-	-
Anode Dark Current (Each Anode) (After 30 min. storage in darkness)		-	0.4	4	nA
Cathode Sensitivity	Anode Pulse Rise Time	-	0.6	-	ns
	Anode Transit Time	-	5.1	-	ns
Uniformity Ratio Between Anodes		N/A	1:3	1:5	N/A
Pulse Linearity (Each Anode)	±2% Deviation	-	0.2	-	mA
	±5% Deviation	-	0.4	-	mA

Table 4.2. Nominal voltage distribution ratios for JEM-EUSO PMTs where Dynodes from 3 to 10 have voltage distribution ratio [3]

Electrodes	K	Dy_1	Dy_2	Dy_3	Dy_{10}	Dy_{11}	Dy_{12}	G.R	P
Ratio	2.3	1.2	1.2	1	1	1	1	1	0.5

Table 4.3. Technical specifications of the JEM-EUSO PMT [3]

Parameter	Description
Spectral Response Range	185 to 650 nm
Window material/Thickness	Ultra Violet glass/0.8 mm
Photocathode Material	Bialkali
Photocathode minimun effective area	23×23 mm^2
Dynode structure	Metal channel Dynode
Number of stages	12
Weight	27 g
Operating ambient temperature	-30 to +50°C
Storage temperature	-30 to +50°C
Voltage Supply (anode-cathode)	1100 VDC
Average anode current	0.1 mA

4.3 Reliability analysis objectives

This study of the reliability of the PMT is referred to the radiation hardness assurance as a part of reliability study. It is intended to assess the affection of the Total Ionizing Dose, Single Event Transients while in space and according to the ESA standard ECSS-E-HB-10-12A [4]. And last but not least devoted to study the degradation of the performance during the operation of the PMT background events.

The objective of the reliability analysis is to test the validity of concepts and technical

choices made today for the JEM-EUSO space mission or any subsequent project aimed at achieving an observatory of giant air showers induced by energetic cosmic rays from space.

The main aim of this work is to determine the failure rate, Mean Time To Failures (MTTF), reliability analysis of the JEM-EUSO PMT as well as radiation hardness assurance of PMTs to evaluate its present and potential reliability, taking into account those failures caused by space radiation. This work will focus on the development of reliability, estimation of the JEM-EUSO PMT implemented on the focal surface of the space telescope. The PMTs is an essential part of the instrumentation of the telescope, that is why it is crucial conducting a reliability analysis because PMTs failure would be catastrophic for JEM-EUSO.

4.4 PMT partial failure evaluation

The radiation hardness assurance of PMTs for their qualification requires meeting stringent radiation tolerance levels. Currently the focus of the radiation hardness assurance has mainly been focused on laboratory tests. Therefore, it is of importance to ascertain a probabilistic model to predict the reliability of the PMTs when exposed to the space environment.

4.4.1 Total Ionizing Dose Radiation Hardness Assurance Model

TID for the JEM-EUSO mission was calculated using the Space Environment Information System (SPENVIS) [5] taking into account the orbital parameters of the ISS, shown in Table 4.4 [6]. Appropriate parameter values for JEM-EUSO were used as input for SPENVIS simulation. The basic parameters for the mission were; the trajectory path, mission duration, and mission Space Segments. According SPENVIS, and taking a 3 mm shielding for JEM-EUSO into account, the main contribution to the dose rate will be due to trapped protons and electrons, for a total dose estimation of 1 krad (Fig. 4.2), which leads to conclude that given this type of radiation the shielding is adequate.

Table 4.4: the international Space station in orbit (ISS) [6]

Specs	**Value**
Brightness	Approximately -4 (less than Venus)
Launch Window	5-10 min
Orbital Altitude	409 km at Perigee 416 km at apogee
Mass	419455 kg
Dimensions	108.5 × 72.8 × 20 m
Average speed	approx. 7.66 km/s
Orbital Inclination	51.65°
Orbital Period	approx. 92.69 min
Observational Visibility	60 N & 60 S
Orbital Type	Elliptical

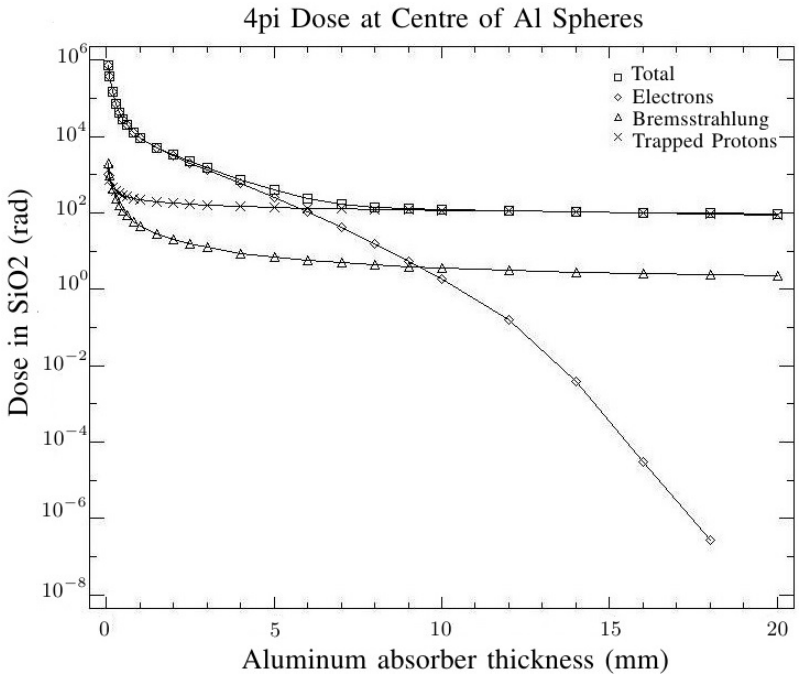

Figure 4.2: Total Dose as a function of shielding that JEM-EUSO will receive during 5 years mission [5]

The reliability of a PMT under TID may be evaluated, taking into account that the probability of failure is equal to the probability that its TID exceeds its hardness [7]. Then, when a component with a radiation hardness H, received a TID x_D the time-

dependent reliability $R(t)$ of the component may be calculated by the joint distribution function as:

$$R(t) = \int_0^\infty \int_{x_D}^\infty f(x_D, x_H, t)\ \mathrm{dx}_H \mathrm{dx}_D \tag{4.1}$$

where x_D is the TID received by the PMT in one year; x_H is the hardness of PMT (relative to TID); t is the exposure time to the radiation in years; and, $f(x_D, x_H, t)$ is the joint probability distribution function for x_D and x_H at time t.

Low Earth Orbit (LEO) refers to orbits in the 100-1,000 km altitude range, which includes Earth-Observing Satellites (EOS). The International Space Station (ISS), is located at this orbit, specifically at $\sim$ 400 km. The environment in LEO is fairly benign, with a typical dose rate of $x_D = 0.1$ krad/year. For a mission with a typical duration of 3-5 years, the total dose is < 0.5 krad [8].

A lognormal probability density function is an approximation of the uncertainty of TID at the ISS $\pi_D(x_D, t)$ given by:

$$\pi_D(x_D, t) = \frac{1}{\sqrt{2\pi}\sigma_D x_D} \exp\left\{ -\frac{\left[\ln(x_D) - \mu_D\right]^2}{2\sigma_D^2} \right\} \tag{4.2}$$

where $\sigma_D \sim 0.4$ is the standard deviation of the log-normal distribution in the vicinity of the ISS and μ_D is the mean of the distribution, given by:

$$\mu_D = \ln\left[D_0(0.2t + 1)\right] - \frac{\sigma_D^2}{2} \tag{4.3}$$

Here μ_D is a function of TID mean value, $D_0 \sim 0.1$ krad/year and t is the time in years, which is multiplied by the Duty Cycle of the instrument, in our case 20%.

A lognormal distribution also provides a reasonable approximation to the uncertainty in the hardness. Taking the probability density function for PMT hardness as:

$$\pi_H(x_H) = \frac{1}{\sqrt{2\pi}\sigma_H x_H} \exp\left\{ -\frac{\left[\ln(x_H) - \mu_H\right]^2}{2\sigma_H^2} \right\} \tag{4.4}$$

with σ_H expressed as a function of the coefficient of variation and μ_H representing the

mean value of the PMT log-hardness with respect to TIDs.

$$\mu_H = \ln(H_R) - \frac{\sigma_H^2}{2} \tag{4.5}$$

$$\sigma_H = \sqrt{\ln(COV^2 + 1)} \tag{4.6}$$

Hence, taking into account a radiation hardness for JEM-EUSO of $H_R = 10$ krad [1] and a coefficient of variation $COV \sim 0.5$, the time dependent joint probability distribution function is given by the products of Eq (4.3) and (4.4) given a PMT time-dependent reliability as follows:

$$R(t) = \int_0^\infty \int_{x_D}^\infty \pi_D(x_D, t)\pi_H(x_H)\mathrm{dx}_H\mathrm{dx}_D \tag{4.7}$$

integrating with respect to x_H

$$R(t) = \frac{1}{2}\int_0^\infty \pi_D(x_D, t)\left\{1 + \mathrm{erf}\left[\frac{\mu_H - \ln(x_D)}{\sqrt{2}\sigma_H}\right]\right\}\mathrm{dx}_D \tag{4.8}$$

R(t), the reliability of the PMTs as a function of time is shown in Figure 4.3. Since the JEM-EUSO mission time is intended to be 5 years Eq (4.8) indicates the PMTs reliability is around 99.86%.

If we assume higher TIDs radiation levels, obviously, the reliability of the PMTs will exhibit a considerable decrease. Taking a look at Figure 4.4, assuming that the radiation is $H = 6$ krad total dose, the reliability range would roughly fall between a maximum of 50% and a minimum of 40% during the first year and the last year of operation respectively.

The estimation obtained by applying the total ionizing dose radiation hardness assurance model provides the reliability for a single PMT. Hence, to determine the reliability of all PMTs that will be used in the JEM-EUSO telescope focal surface, it is necessary to apply the Poisson distribution. This is shown in Figure 4.5. In this case, for a total

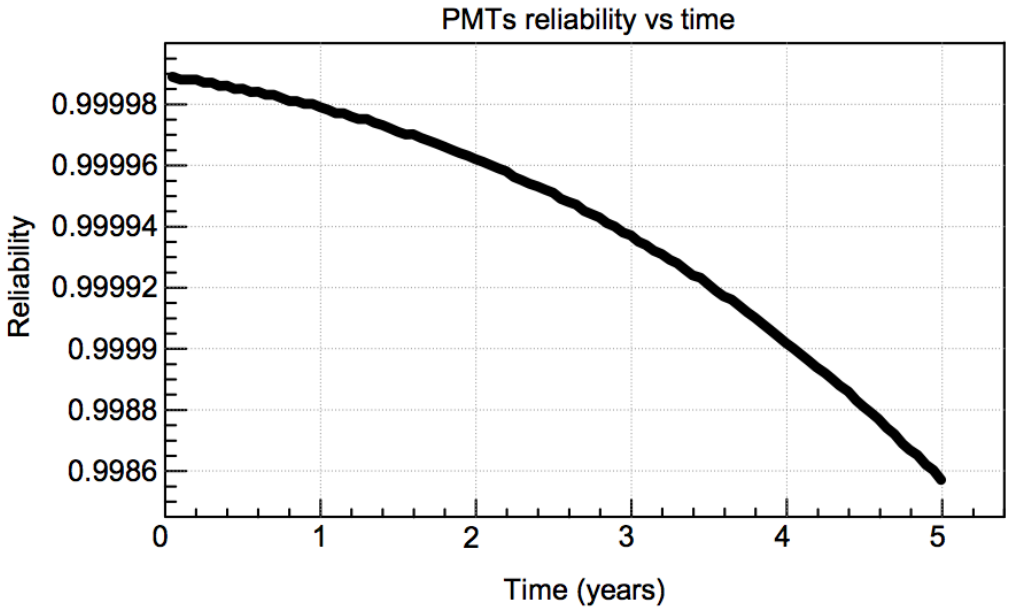

Figure 4.3: Reliability vs time of JEM-EUSO PMTs due to TIDs according to the TID radiation hardness assurance model.

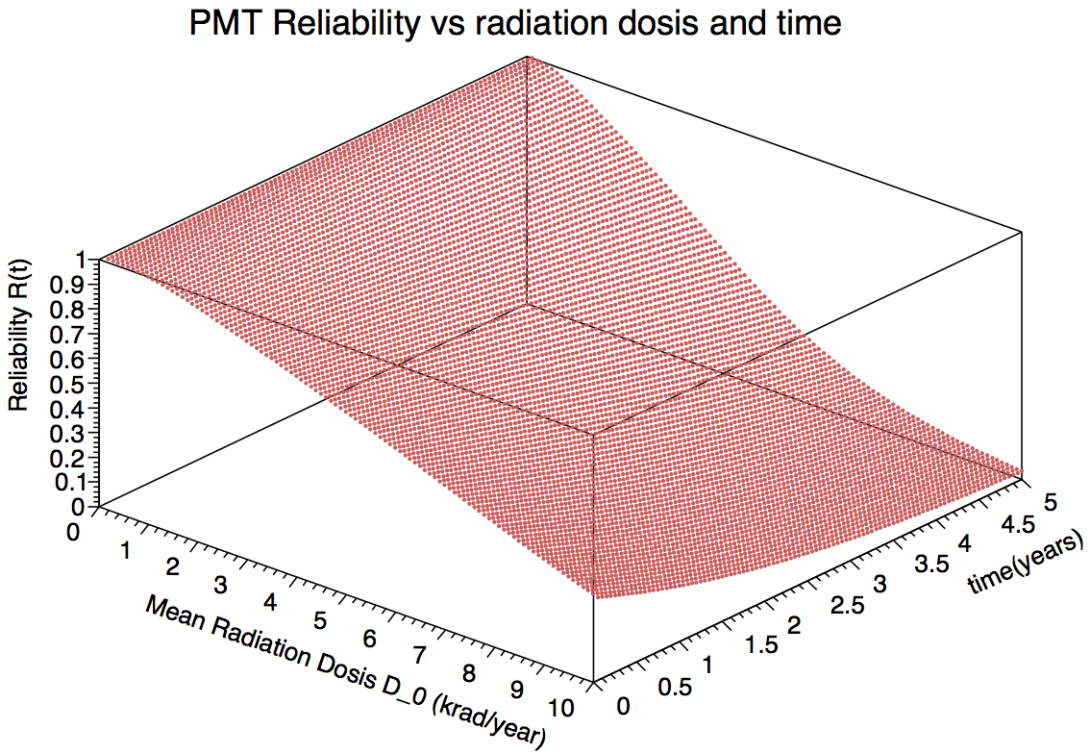

Figure 4.4: 3D view of the obtained reliability vs time due to TIDs of JEM-EUSO PMTs

of 4932 PMTs, 7 ± 2.5 are expected to fail. It does suggest that the PMT designed for JEM-EUSO is robust and highly reliable against the influence of TIDs.

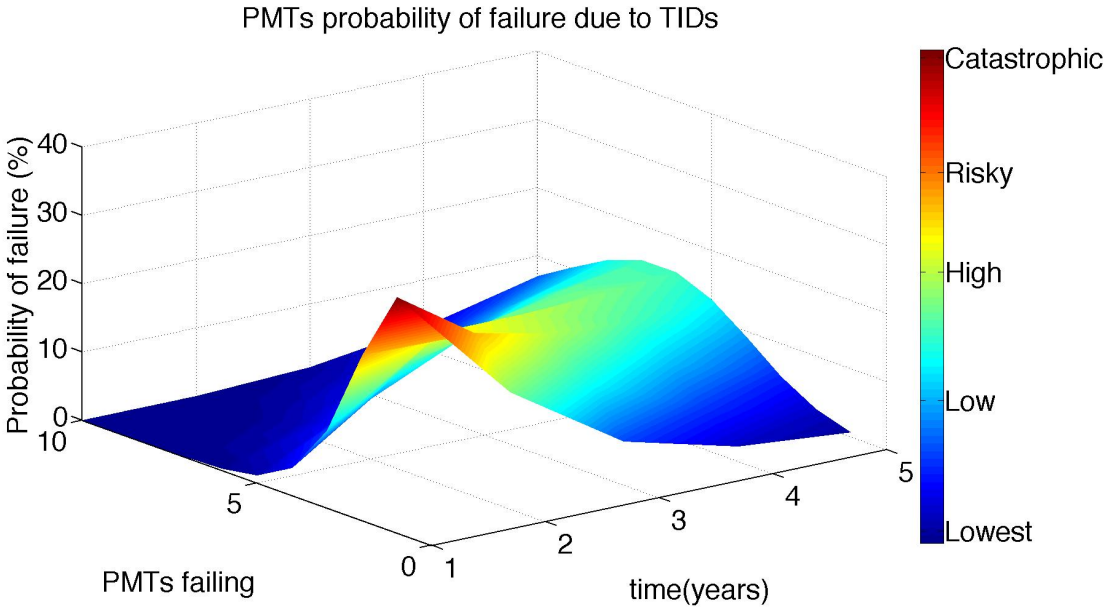

Figure 4.5: 3D view of reliability vs time due to TIDs according to the Total Ionizing Dose Radiation hardness assurance model

4.4.2 Single Event Effect Radiation Hardness Assurance Model

A Single Event Transient (SET) or single event disturb is a momentary voltage spike at a node in semiconductors. The voltage spike is originally formed by the electric field separation of the charge generated by an ion passing through or near a circuit junction [4].

Depending the node where it appeares, the spike propagates inside the circuit resulting in several consequences at the component level:

- The spike can be absorbed by local RC elements of the circuit and have no impact on the component behavior.
- The spike can be propagated up to at least one output of the component.
- It can be converted to a Single Event Upset (SEU) when the signal reaches a latch.

4.4.2.1 Basic Mechanism of A SET

A charged particle moving through a semiconductor deposits a fraction of its energy in the medium by ionizing the atoms of the crystal along its path. The amount of energy received by the medium per unit path length is called Linear Energy Transfer (LET).

LET defines the efficiency of the energy transfer and is independent of both the electrical charge and the energy of the particle. It is usually expressed in units of MeV·cm^2/mg (energy loss divided by the material density). In space most of heavy ions from cosmic rays produce LETs in Si ranging from 0.01 to 40 MeV cm^2/mg [9]. In Si devices, a LET corresponds to a charge deposition per unit length of 10 fC/μm. The typical range of deposited charge is from 0.1 to 400 fC/μm.

4.4.2.2 Single Event Transient Pulse

The statistical SET's width in logic circuits by applying the LET values to the commonly transient current double exponential model is shown below:

$$I(t) = \frac{Q_{coll}}{\tau_\alpha - \tau_\beta}(e^{-\frac{t}{\tau_\alpha}} - e^{-\frac{t}{\tau_\beta}}) \tag{4.9}$$

$$Q_{coll} = -10.8\frac{fC}{\mu m} \cdot \delta \cdot LET \tag{4.10}$$

where Q_{coll} is the charge in the sensitive region; τ_α is the collection time constant, which is a process-dependent property of the junction and τ_β is the ion-track establishment time constant, which is relatively independent of the technology. In bulk Si, a typical charge collection depth, δ, is 2 μm for every MeV·cm^2/mg and an ionizing particle deposits about 10.8 fC along each micron on its track [10]. Typical values are approximately 1.64×10^{-10}s for τ_α and 5×10^{-11}s for τ_β.These parameters are summarized in Table 4.5.

Table 4.5: SET Pulse Calculations Parameters Values Used [9, 10]

Parameter	**Description**	**Value**
LET	Linear Energy Transfer	0.01 - 37MeV·cm^2/mg
δ	Depth	2μm · MeV^{-1}·cm^{-2} ·mg
τ_α	Collection time constant	$1.64\times10^{-10}s$
τ_β	Ion Track Establishment Time	$5\times10^{-11}s$

The SET pulse produced by heavy ions in CMOS devices, calculated using transient current double exponential model is shown in Figure 4.6. As can be seen, the highest intensity value is 3 mA and its Full Width Half Maximum (FWHM) $\sim$ 0.2 ns. This is not a negligible current pulse since average anode current is around 0.1 mA. Moreover it could create electromigration effects at the output of the PMT.

4.4.2.3 Analysis of SET's

The distribution that best describes the event cross-section as a function of LET is the Weibull function. The Weibull function is widely used to fit direct ionization (heavy-ions) Single Event Effect (SEE) cross-section data, since it provides great flexibility in fitting the turn-on in the cross section and naturally levels to a plateau or limiting values [11,12].

The Weibull function is given by:

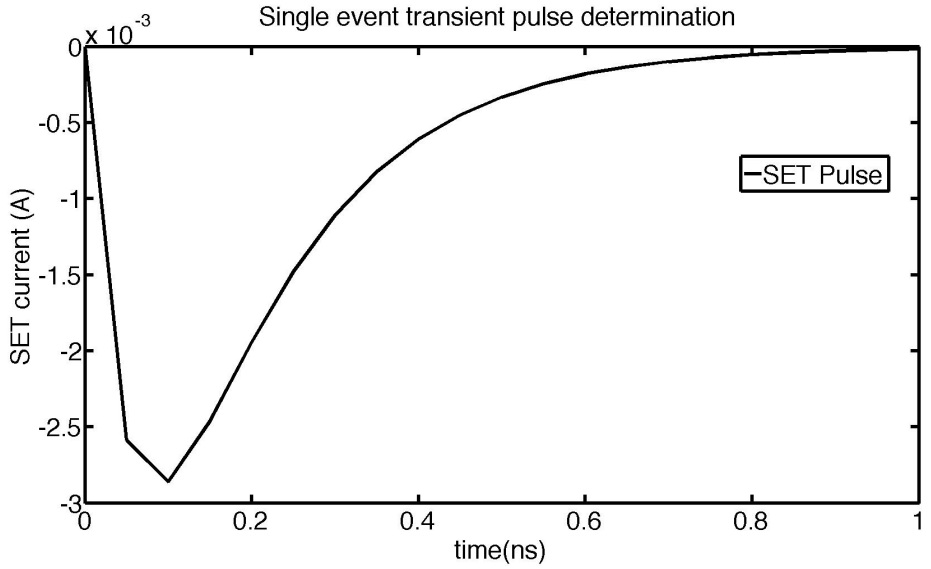

Figure 4.6: Temporal profile of a Single Event Transient.

$$\begin{aligned} F(L) &= \sigma_{HL} \cdot \left\{ 1 - exp\left[-\left(\frac{L - L_0}{W} \right)^S \right] \right\}; L > L_0 \\ &= 0; L < L_0 \end{aligned} \tag{4.11}$$

where all these parameters needed for the cross-section calculation are described in Table 4.6.

Table 4.6: Event Cross-Section parameters for a particular LET [13]

Parameter	**Description**	**Value**
F(L)	Event Cross-Section/LET	
σ_{HL}	Limiting Cross-Section	220 μm^2
W	Width of the distribution	12,4MeV $\cdot cm^2/mg$
L_0	Threshold of LET	4MeV $\cdot cm^2/mg$
S	Shape parameter	2,7

These parameters were taken from a calculation by E.L.Petersen [13] when trying to

re-examine the use of the SEU Figure Of Merit for heavy ion upset rate predictions. Moreover, if SET pulse has enough amplitude and duration and coincides with a clock, then an incorrect value is registered and the SET becomes a SEU [14]. These values belong to the device "Bulk CMOS". The reason for specifying this device is the fact that it does cover all CMOS devices taking into account that this approximation is based on the principle that PMT's are similar to ICs, CMOS or FPGAs components. Figure 4.7 shows the event cross-section vs LET from 4 to 40 MeV·mg^{-1} ·cm^2, which is the surface affected by the particle when it crosses the component.

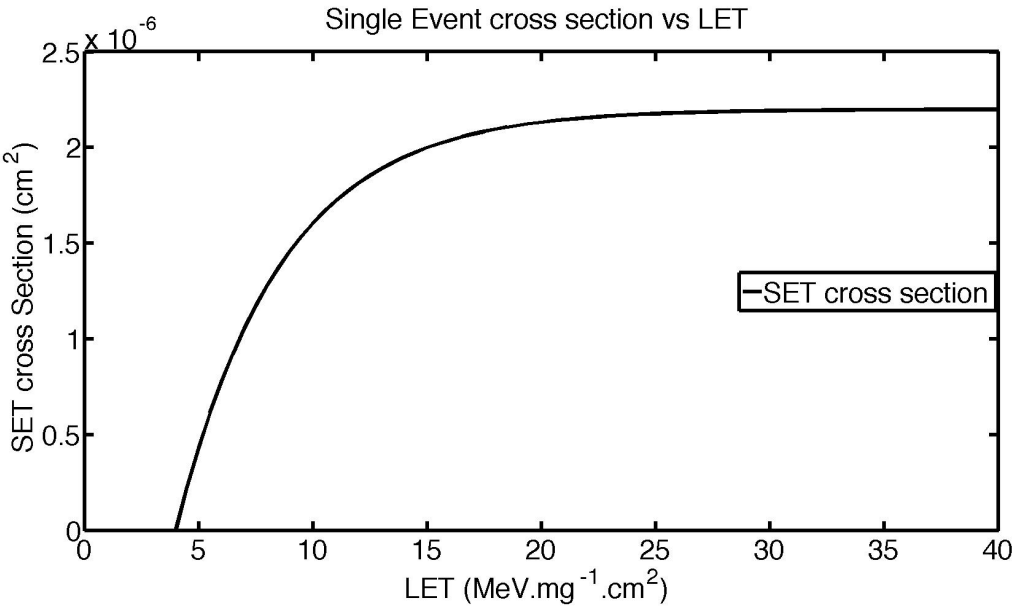

Figure 4.7: Total SET cross section as a function of effective LET

4.4.2.4 Single Event Transient Rate definition

4.4.2.4.1 Heavy-Ion Figure of Merit According to E.L.Petersen [13], the total upset rate for a part in a particular orbit can be calculated using its characteristic Figure of Merit (FOM) and a single orbit specific rate coefficient, the sum of the heavy ion and proton rate coefficients.

FOM was introduced in 1983 as a useful parameter for describing part upset sensitivity and for approximating upset rates in geosynchronous orbit [15]. FOM for heavy ions is defined as:

$$FOM_H = \frac{\sigma_{HL}}{L_{0.25}^2} \left[\frac{(MeV/mg/cm^2)^2}{cm^2} \right] \tag{4.12}$$

where σ_{HL} is the limiting heavy ion cross section per bit at large LET and $L_{0.25}$ is the LET at 25% of the limiting cross section which is calculated as follows:

$$L_{0.25} = L_0 + W \times 0.288^{(\frac{1}{S})} \tag{4.13}$$

Since it is common to describe the heavy ion cross section curve using the cumulative Weibull distribution, the calculation of FOM will implement the same parameters, and the calculation result is presented in Table 4.6.

4.4.2.4.2 Protons Figure of Merit E.L Petersen [15] realised that there is a simple relationship by examining the limiting proton cross section (σ_{PL}) as a function of the FOM for parts, for which both proton and heavy ion data are available. In that case, FOM can be determined directly from the limiting proton cross section as follows:

$$FOM_p = 4.5 \times 10^4 \sigma_{PL} \tag{4.14}$$

4.4.2.4.3 Rates The upset rate R in a particular orbit is calculated by introducing an orbit specific rate coefficient C with units of (upsets/bit-day), which stands as follows:

$$R = C \times FOM \tag{4.15}$$

4.4.2.4.4 Orbit Specific Rate Coefficient If we define CO as the rate coefficient with 100 mils of shielding [15] , a very approximate equation for the change of the rate coefficient with depth is:

$$C = 2 \cdot CO - 0.45 \cdot CO \cdot log(n) \tag{4.16}$$

where n is the shielding thickness in mils and according to E.C Smith [16], typical satellite shielding corresponds to 0.3 inch to 1 inch of Aluminum. The accompanying rate factors would be 75% to 50% of CO.

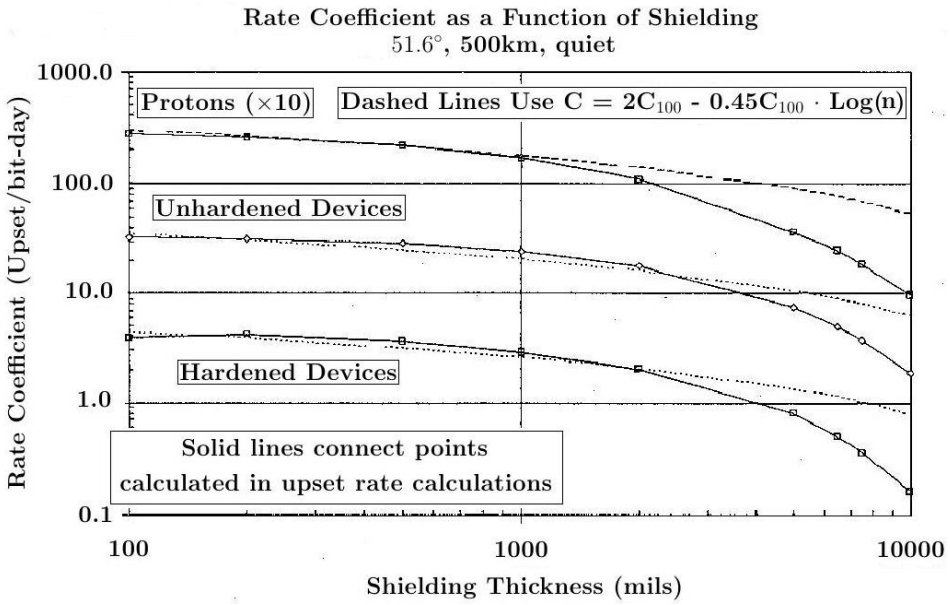

Figure 4.8: Orbit Specific Rate Coefficient for heavy ions. Similar rates coefficients for protons should be obtained by multiplying heavy ions curves by a factor of ten. [15]

According to Figure 4.8, the best fitted parameter CO given in upsets/bit-day for JEM-EUSO instrument are CO = 10 for heavy ions and CO = 100 for protons. Since electronics equipment has a shielding of 3 mm (118.11 mils) C = 10.7 for heavy ions and C = 107 for protons are obtained.

4.4.2.5 PMT Reliability Concerning Single Event Transient

4.4.2.5.1 Rates calculation Previously, in the calculation of SET cross-section (Figure 4.7), the parameters considered were those corresponding to the ones estimated by Petersen [13], considering PMTs as Bulk CMOS devices. These parameters have also been used to estimate protons and heavy ions SETs, which are shown below in Table 4.7.

Table 4.7: Device Parameters [13]

Device	Type	FOM	C Heavy Ions	C Protons
6516	Bulk CMOS	1.575×10^{-8}	10.7 upsets-bit/day	107 upsets-bit/day

The estimation of SETs caused by heavy ions and protons using the methods and models explained before by Equation 4.15, are summarized in Table 4.8. To find the Rate (number of events) per year, it was necessary to multiply the result of Equation 4.15 by 30 days and by 12 months.

Table 4.8: SET Rates [13]

SET Type	Rate Value Per Year
Heavy Ion	60.7×10^{-6}
Proton	607×10^{-6}

This radiation hardness assurance aims to encompass the possible behaviour of the JEM-EUSO PMTs. However, considering that these components have a constant failure during the mission in case of single event effects, the best characteristic failure distribution is an exponential. The values obtained from this estimation, considering the rates for heavy ions and protons, are shown in Figure 4.9.

In case of heavy ions, the reliability is around 99.98% during 5 years of operation and 99.7% in case of protons. These results mean that the probability of being affected by a SET is in either of these two types minimal, which also highlights the good performance of the

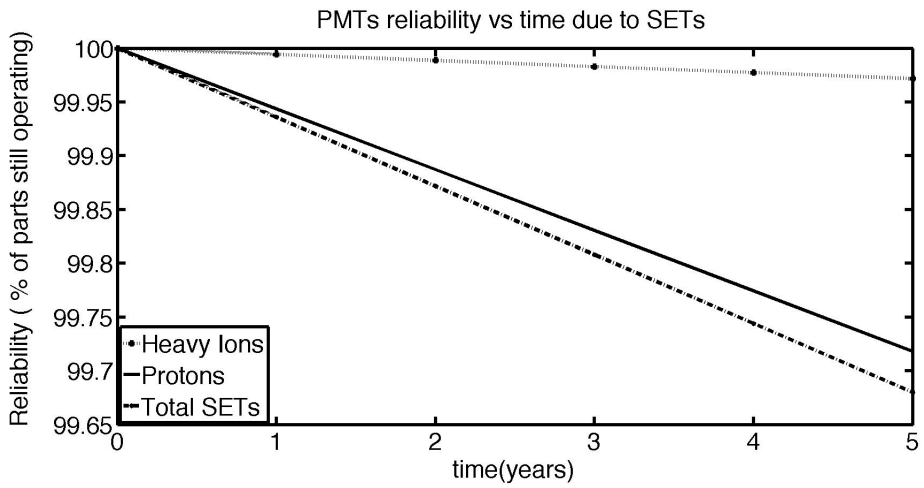

Figure 4.9: Reliability of JEM-EUSO PMTs vs time, whose value reflects the "absence" of SETs events in the LEO orbit where JEM-EUSO is going to be placed.

PMTs under the influence of SETs; however, the combination of the affected population of PMTs by different types of SETs reveals a reliability of 99.68%, which corresponds to around 16 PMTs failures during the JEM-EUSO mission time.

As a result of the previous study, we can state that only a small fraction of PMTs is lost due to SETs. In fact, we calculated the number of failing PMTs to be around 14.79 for protons, 1 for heavy ions and 16 for the combination of both populations. Furthermore, we estimated the probability distribution of the number of failing PMTs after five years. We assumed this function to be a Poissonian. The results are shown below in Figure 4.10 and Figure 4.11. As can be seen, the effect of SET radiation on the JEM-EUSO PMTs reliability can be neglected.

Finally, Figure 4.12, shows that the total number of PMT losses associated with SET radiation is less than 25 PMTs during the five year operation of the JEM-EUSO mission. The critical loss threshold of PMTs is not reached, thus demonstrating the quality of PMTs and therefore ensuring the success of the mission.

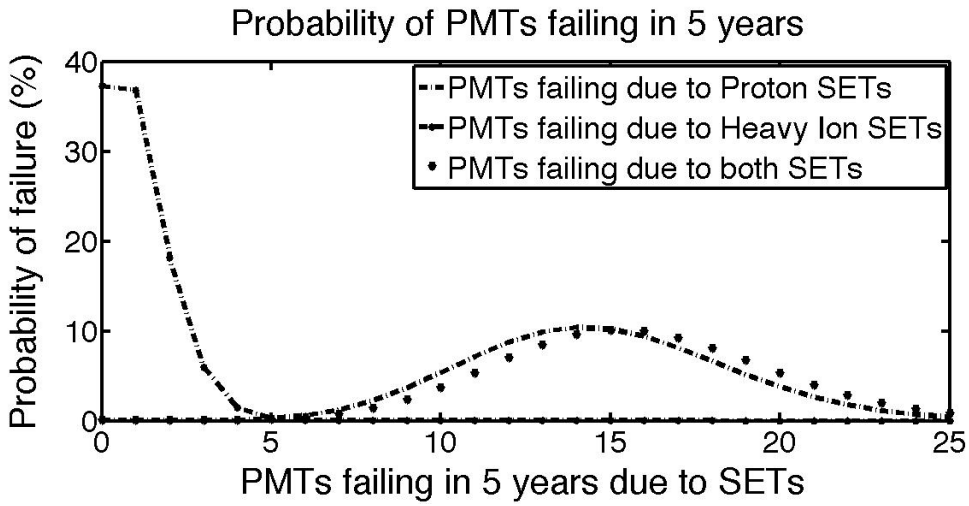

Figure 4.10: Reliability Distribution due to SETs, shows the level of robustness of the PMTs.

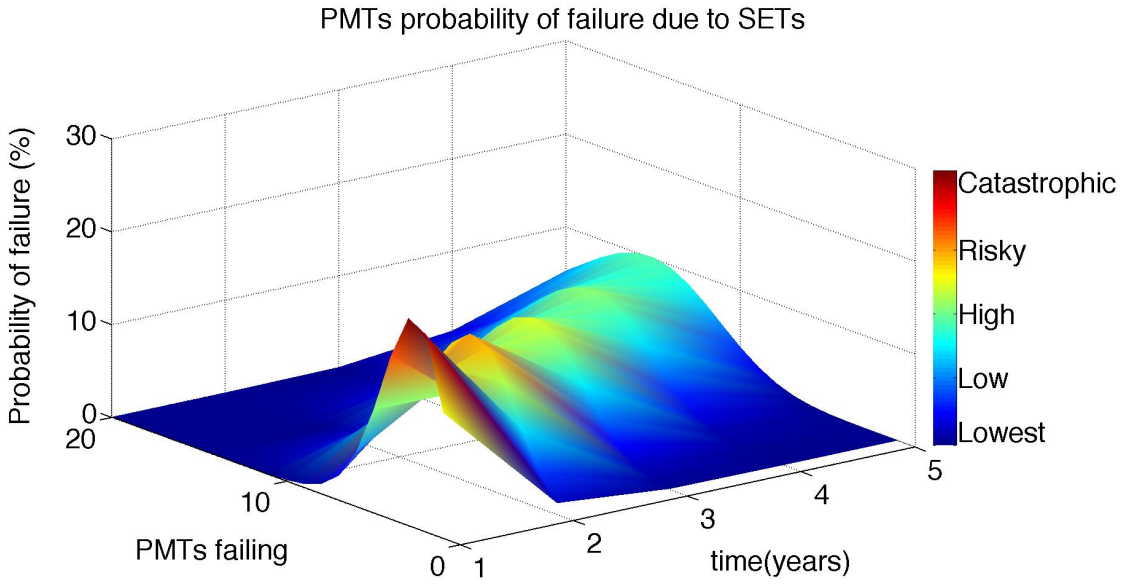

Figure 4.11: 3D Reliability Distribution Due to SETs during the JEM-EUSO time mission, where the degradation measure is less than the critical threshold value.

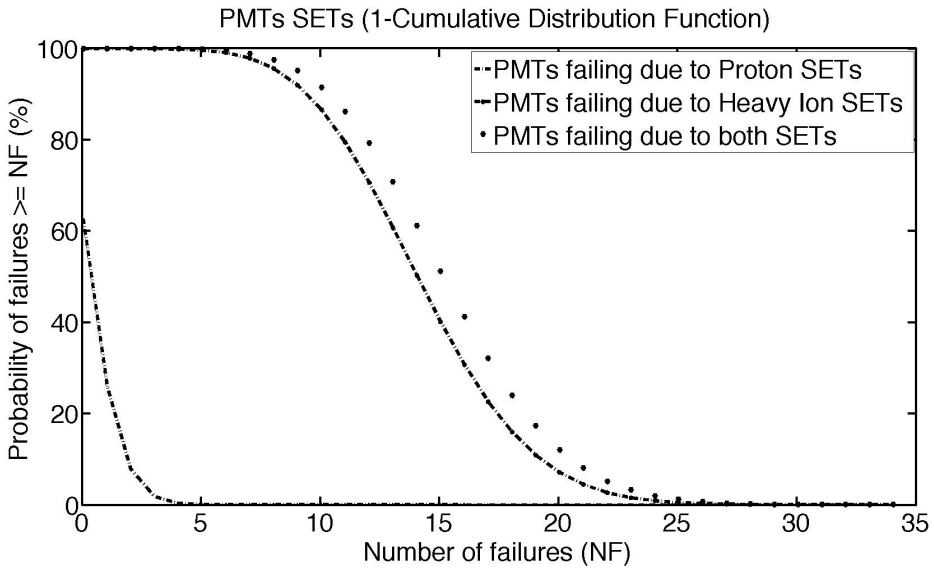

Figure 4.12: Inverse of cumulative distribution function for a certain number of PMTs failures.

4.5 PMT performance degradation

4.5.1 PMTs "browning" of the glass window

Among the effects that can degrade the performance of a PMT, in space the most relevant is background radiation. This type of radiation can darken the glass of a PMT reducing its light transmission capacity, which directly reduces the PMT quantum efficiency. Since JEM-EUSO is a space telescope aboard the ISS, such effects directly affect measurements of fluorescence radiation, Cherenkov, Transient Luminous Events (TLE) such as Elves, Sprites, Lightning and finally others associated with light pollution due to the cities, Moonlight and Sidereal light.

In terms of reliability of the electronic components, as well as in case of the PMTs, the maximum allowed value of loss (loss threshold) is approximately 10%, i.e., if JEM-EUSO has around 5000 PMTs in the focal surface, we can assume as tolerable value a loss of 500 PMTs. Therefore, if loss threshold value previously stated is expressed in Quantum Efficiency (QE) degradation, which is initially 20% for JEM-EUSO PMTs, a maximum reduction of 10% of this value could be accepted. Since the QE is linearly associated with

the absorption of photons in the PMT, where the UV crystal designed for JEM-EUSO has an initial transmittance of 90%, we can consider as a failure if the transmittance of crystals is reduced in 10%.

The JEM-EUSO observation principle affects directly the performance of the PMTs since ultraviolet radiation as ionizing causes darkening in the PMT window glass as stated previously.

To estimate the degradation of the entrance window, it is necessary to evaluate the probability of interaction of UV photons with the PMT glass [17]. The probabilty of interaction of an UV photon in the PMT glass can be expressed as follows

$$f = 1 - e^{-\mu x} \tag{4.17}$$

where $\mu = 10^{-5}$ cm^{-1} is the photoelectric mass attenuation coefficient and $x = 0.08$ cm is the thickness of the PMT input window.

An estimation of the UV photon flux from different sources is needed in order to calculate its effect on the PMT window transmittance at the time the PMT is operational.

4.5.2 PMT UV photon flux

The average background of UV photons in the 300-430 nm range reaching the focal surface of JEM-EUSO after filter has been evaluated by J.H Adams et al. [18]. The background flux average value obtained of $\phi_{\gamma UV,bk}$= 550 m^{-2}ns^{-1}sr^{-1} yields for the whole telescope focal surface ϕ_{bk}^{Tel}= 2.75×10^{12} s^{-1} UV photon flux.

Besides the continuous background, PMTs will be affected by atmospheric transients as lightning, elves, sprites, blue jets, etc. We estimate their contribution based on the values obtained by the satellite Universitetsky-Tatiana-2 [19]. According to this study, the number of TLE in the most active areas is approximately 6×10^{-4} events/km ^{2} hr. This value can be assumed for the worst case scenario in order to evaluate the most critical side effect that can affect the operation of the PMTs.

Considering the values obtained by the satellite Tatiana, events with larger number of photons are associated with effects of lightning, which generate $\sim 1 \times 10^{26}$ ph/event,

while those associated with TLE have a emission of $>1\times10^{23}$ ph/event, with a wavelength of 300-400 nm and a duration of between 1-123 ms at altitudes above 50 km. However, because this study aims to consider the most critical effects we have to take into account all events having a release of 10^{26} ph/event in order to not understimate the photon flux. Therefore, the photon flux received by the focal surface is of 2.5×10^{14} ph/event.

Taking into account that the minimum observational area of JEM-EUSO is 140000 km^2, and the average rate of occurrence of these transient events is 6×10^{-4} events/km^2 hr, the average number of events per hour affecting the focal surface is 84. In other words, the total flux of photons per second reaching the focal surface of the telescope due to the occurrence of these transient events, is $\phi^{Tel}_{TLE} \simeq 6 \times 10^{12}$ ph/s.

In order to determine the total contribution of luminous events in the darkening of the glass of the PMTs, the radiation values of TLE, Moon light, lights from the cities, lightening were taken into account. Their total contribution will be equal to the sum of the fluence of photons per second reaching the focal surface, which have already been determined. Hence, a total flux is obtained $\phi^{Tel}_{TLE,bk} \sim 10^{13}$ ph/s.

However the total number of photons arriving to the surface, is affected by the losses associated to the JEM-EUSO optics, which consists of three Fresnel lenses whose efficiency is lower than 60% when the angle of incidence is 0°, the angle at which the maximum concentration of photons reach the center of the focal surface. Because this study includes the reliability analysis of the whole PMTs on the focal surface, we will take this value as a reference, to estimate the overall degree of damage to the entire surface. This value of efficiency can be seen in the Figure 4.13.

Hence, considering photon losses in the lenses, the value of the total flux reaching the focal surface is $\phi^{FS}_{TLE,bk} \sim 6\times10^{12}$ ph/s. Assuming that photons are uniformly distributed among the 5000 PMTs of the focal surface the PMT flux is $\phi^{PMT}_{TLE,bk} \sim 1.2 \times 10^9$ s^{-1}.

Therefore, the rate of γ_{UV} accumulated in the PMT glass will be estimated as:

$$\phi^{glass}_{TLE,bk} = \left(\phi^{PMT}_{\gamma_{TLE,bk}} \cdot f\right) = 960ph\ s^{-1}. \tag{4.18}$$

Figure 4.13: Total Efficiency Optics of JEM-EUSO telescope for $\phi = 0°$ [20]

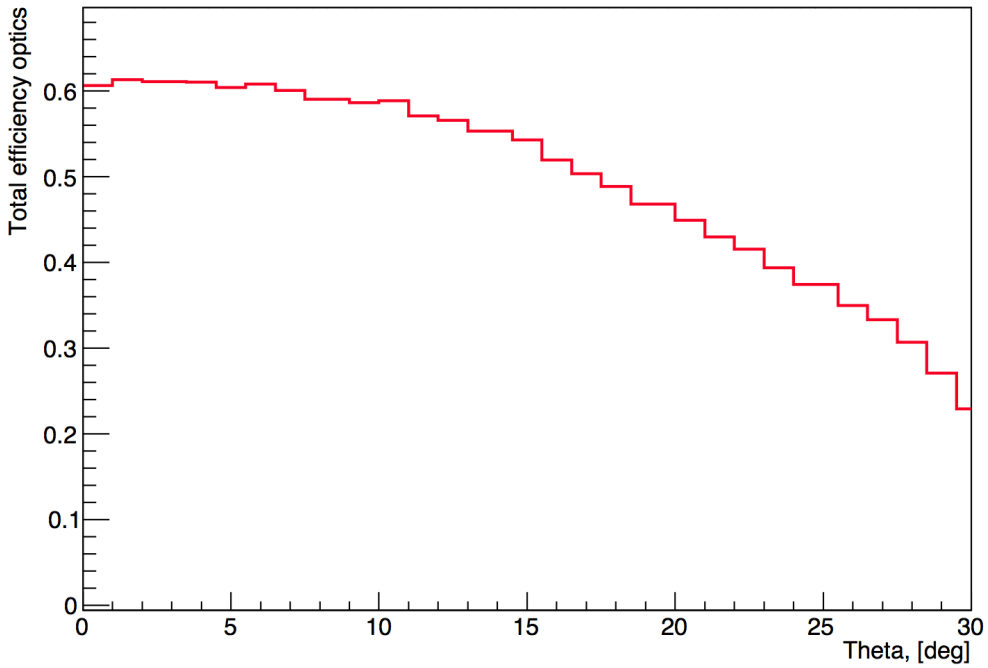

Hence, the total deposition energy rate per year in the glass of the PMTs E_{glass}^{PMTs} is 2×10^{-8} J/yr taking into account the glass density of 2.203 g cm^{-3} and a volume of 4.232×10^2 mm^3 gives us an equivalent radiation dose $D_{TLE,bk} \sim 1$ mrad/yr.

In conclusion, in terms of UV radiation, the performance of the PMTs is not degraded, since the dose received is negligible compared with the effects of particle radiation of 100 rad/yr for the ISS orbit. It does not affect anyway the PMT QE since the browning effect is absolutely negligible.

4.5.3 Total transmittance degradation

Optical materials may darken when exposed to ionizing radiation. This darkening is attributed to electrons (or holes) that are trapped in inherent defect sites and also to the creation of new defect sites by the ionizing radiation [21]. The window transmittance has been modeled as follows:

$$T(\lambda, D, x) = T_0 e^{-\alpha_D x} \tag{4.19}$$

where T is the transmission at wavelength λ through an optical path lenght x of material that has received an accumulated radiation dose D, T_0 is the transmission before irradiation (0.9) [22], and α_D is the radiation induced absorption coefficient.

In section 1.4.1, the estimation of the dose rate received by JEM-EUSO was assumed to be of 100 rad/year. As the radiation dose from UV photon is negligible, though will contribute to the browning of the PMT glass window.

Irradiating the UV glass of the PMTs windows with a ^{60}Co gamma rays source, Hamamatsu determined the effect of the different radiation levels (R) on the transmittance of the UV glass windows of their manufactured PMTs. This measurement was performed for a wide wavelength range. The result of this evaluation can be seen in Figure 4.14. Selecting data for 300 nm shown in table 4.9, an exponential function

$$T(R) = T_0 e^{-\alpha R} \tag{4.20}$$

has been fitted to data in order to obtain the dependence of UV glass transmittance on radiation dose. T_0 has been fixed to the transmittance of the non irradiated UV glass ($T_0 = 0.9$) and a value of $\alpha = 2\times\ 10^{-7}$ rad^{-1} has been obtained (Figure 4.15).

Making use of Equation (4.20) and introducing the radiation dependence on time $R = D_y[rad/yr]t[yr]$ we can obtain the dependence of the PMT glass transmittance on time as follows:

$$T(R) = T_0 e^{-\alpha D_y t} \tag{4.21}$$

Figure 4.16 shows the degradation of the PMT glass transmittance for the JEM EUSO experiment versus time. Analyzing the obtained results, it is possible to conclude that, due to the lower value of the reduction of the transmittance of the UV glass window of MAPMT designed for JEM-EUSO, the degradation of the transmittance caused by TIDs in the glass is absolutely negligible.

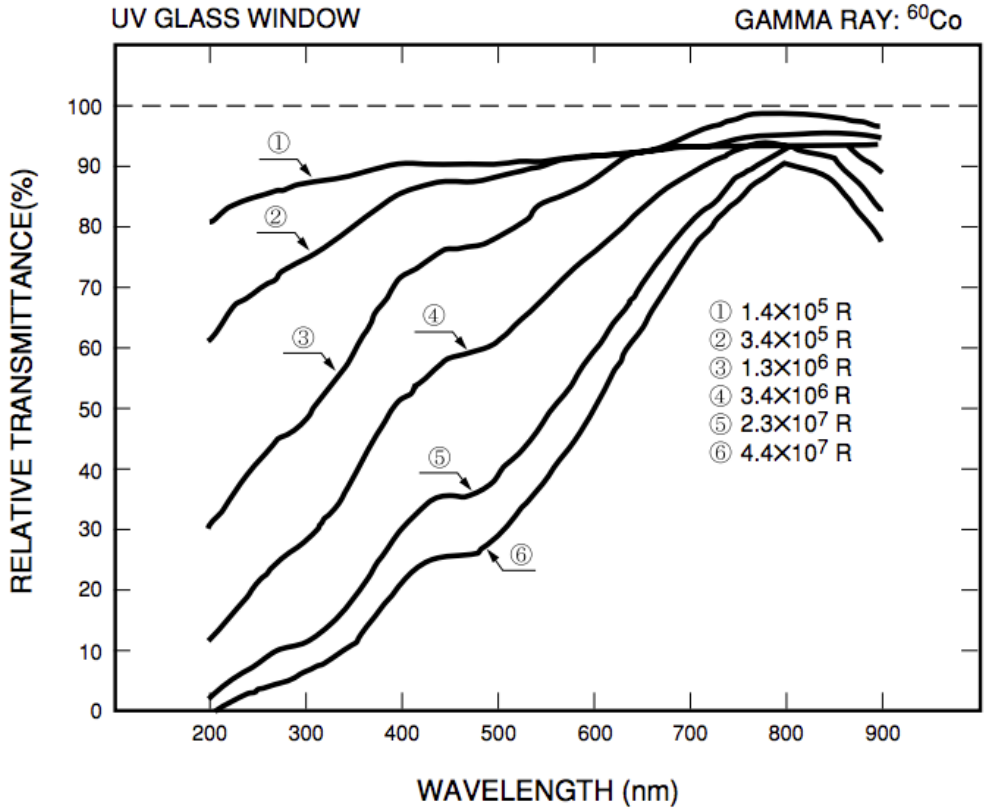

Figure 4.14: Transmittance change of UV glass window irradiated by gamma rays/neutrons [22]

Table 4.9: JEM-EUSO PMTs glass windows transmittance vs radiation dose for 300 nm

Dose (R) in rad	Transmittance of the PMT glass (%)
1.4×10^5	88
3.4×10^5	74
1.3×10^6	48
3.4×10^6	28
2.3×10^7	11
4.4×10^7	8

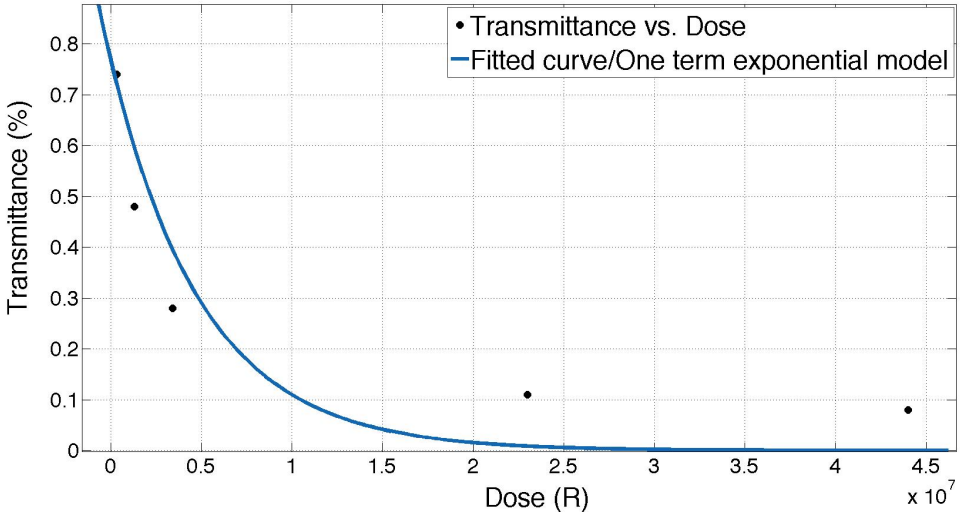

Figure 4.15: Transmittance vs. TID [22]

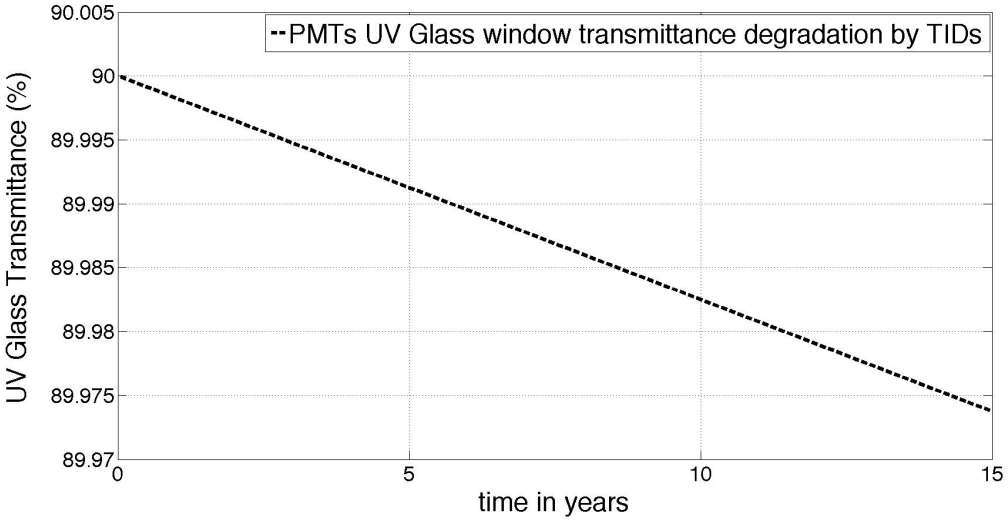

Figure 4.16: PMT UV Glass Transmittance degradation vs time in years

Bibliography

[1] H.Prieto-Alfonso, K. Tsuno,L. del Peral, M. Casolino, T. Ebisuzaki, J.A. Morales de los Ríos, G.Sáez-Cano and M.D. Rodríguez Frías for the JEM-EUSO collaboration. Multi-Anode Photomultiplier Tube reliability analysis and radiation hardness assurance for the JEM-EUSO Space mission, in: Proceedings of the 33rd International Cosmic Ray Conference , 2013, p.95,(ID 0343), arXiv:1307.7071.

[2] H.Prieto-Alfonso, L.Del Peral, M. Casolino, T. Ebisuzaki and M.D Rodríguez Frías. Radiation Hardness Assurance for the JEM-EUSO Space Mission. Reliability Engineering & System Safety, Vol 133, pp.137-145. Published (January 2015).

[3] Y. Kawasaki et al., The focal surface of the JEM-EUSO Instrument. Proceedings of 32nd ICRC Beijing 2011.(ID0472).

[4] European Cooperation For SPACE Standarization, Space Engineering, Calculation of Radiation and Its Effects and Margin Policy Handbook. December (2010).

[5] SPENVIS Home Page http://www.spenvis.oma.be/

[6] Canadian Space Agency Home Page http://www.asc-csa.gc.ca/eng/iss/Default.asp

[7] C. Everline, K. Clark, G.Man, R. Rasmussen, A. Johnston, C. Kohlhase, T. Paulo,"Estimating the Reliability of Electronic Parts in High Radiation Fields", Proceedings of the International Conference on Probabilistic Safety Assessment and Management, PSAM 9, 2008.

[8] Petkov, M.P., The Effects of Space Environment on Electronic Components, BEACON eSpace at Jet Propulsion Laboratory, 2014/7913, 2003

[9] P. Fouillat, V. Pouget, D. Lewis, S. Buchner, and D. McMorrow, Investigation of single-event transients in fast integrated circuits with a pulsed laser. Int. J. High Speed Comput. (Singapore), vol.14, no.2, pp.327-340. (June 2004)

[10] Fan Wang and V. Agrawal, "Soft Error Rate Determination for Nanometer CMOS VLSI Logic," Proc. Southeasthern Symp. System Theory, pp. 324-328, (2008).

[11] Texas Instrument, Single Event Effect Report. SNAA155. August 9, (2010).

[12] Chumakov, A.I.; Nikiforov, A.T.; Telets, V.A.; Gerasimov, V.F.; Yanenko, A.V.; Sogoyan, A.V. IC space radiation effects experimental simulation and estimation methods, Radiation Measurements vol.30 issue 5 October,pp. 547-552, (1999).

[13] E. L. Petersen, "The SEU figure of merit and proton upset rate calculations," IEEE Trans. Nucl. Sci., vol. 45, pp.2550, (1998).

[14] Jameel Hussein and Gary Swift, Mitigating Single-Event Upsets. Xilinx White Paper: 7 Series FPGAs. WP395 (v1.0). (2010).

[15] E.L Petersen,Suggested Single Event Upset Figure of Merit.IEEE Trans. Nuc. Sci., NS-30, 2396, (1983).

[16] E.C Smith. Effects of realistic satellite shielding on SEE rates. IEEE Trans. Nuc. Sci., NS-41, 2396, (1994).

[17] R.D. Evans "Gamma Rays" Chap. 8e in "American Institute of Physics Handbook", 3rd Ed., McGraw–Hill, (1972).

[18] J. H. Adams Jr et al. JEM-EUSO Collaboration, Astrop.Phys. 44 (2013), 76.

[19] P. A. Klimov et al., Analysis of UV flashes measured by Universitetsky-Tatiana-2 satellite as significant factor of TUS detector operation, in Proceedings of the 33rd International Cosmic Ray Conference (ICRC 2013), Rio de Janeiro, Brazil, 2-9 July 2013, (id 406) .

[20] Fenu, F. A simulation study of the JEM-EUSO Mission for the detection of Ultra-High Energy Cosmic Rays, Doctoral thesis. Tubingen sept. 2013.

[21] G. Richard Wirtenson, and Richard H. White. Effects of ionising radiation on selected optical materials: An overview. Tech. Report LLNL, UCRL-ID-111453, (1992).

[22] Hamamatsu. Photomultiplier tubes, Basics and Applications, Page 251. Third Edition. (2006).

Chapter 5

Reliability analysis of JEM-EUSO PMTs Performance

Performance degradation of an electronic component is an intrinsic characteristic that eventually can cause a failure. When the degradation is possible to be measure, it provides the data necessary with which improving the equipment reliability.

It is considered that a component failure is related to degradation when one of its main functional parameters (power,current, etc.) undergoes a variation out of its permitted limits from which it will not perform its intended functionality anymore.

With regards to JEM-EUSO PMTs as for any other PMT model the functional parameters evaluated to analyze reliability in terms of degradation where as follows:

- Quantum efficiency
- Detectivity
- Responsivity
- Performance according to 217 Plus prediction model

5.1 Partial failure evaluation of JEM-EUSO PMTs

5.1.1 Quantum Efficiency degradation

The lifetime of the PMT is related to its working conditions and the electrical charge applied on it. The following equations give a proper description of this situation

$$QE(t) = QE_0 e^{-t/\tau} \tag{5.1}$$

where QE_0 is the quantum efficiency of a new PMT; τ is the lifetime of the PMT cathode under working conditions and t is the working time of the PMT.

$$QE(q) = QE_0 e^{-q/\tau_q} \tag{5.2}$$

where τ_q is the quantum efficiency scale factor of the PMT cathode when electric charge is received. In this particular case, this value is roughly 2-3 C/cm^2. Finally q is the charge collected at the cathode, expressed in C/cm^2.

In order to perform the analysis of $QE(q)$, q, should be determined as follows:

$$q = \frac{e \cdot \phi_\gamma \cdot t \cdot E_\gamma \cdot QE_0}{E_i \cdot S_{Pk}} \tag{5.3}$$

where ϕ_γ is the photon flux; t is the working time; E_γ is the photon energy; E_i is the ionization energy of the PMT cathode; and S_{Pk} is the photo-cathode active surface. The values considered to calculate the collected charge, are provided in Table 5.1

Anyway, considering Eqs. (5.1-5.3), the lifetime can be calculated as follows:

$$\tau = \frac{\tau_q \cdot E_i \cdot S_{Pk}}{e\phi_\gamma \cdot E_\gamma \cdot QE_O} \tag{5.4}$$

The obtained lifetime is 1.69$\times$ 10^{11}s. Therefore, the Quantum Efficiency as a function of time of operation of JEM-EUSO is 19.98%.

In other words, a loss of 0.1% of the quantum efficiency in 5 years per PMT as seen in Figure 5.1 where the first 5 years of degradation are expressed by the red line over the

Table 5.1: JEM-EUSO PMTs QE parameters

Parameter	**Value**
Initial Quantum Efficiency (QE_O)	20 %
Electron's Charge (e^-)	1.6×10^{-19}C
Photon Flux (ϕ_γ)	1.2×10^{9}ph/s
Time (t)	5 Years
Photons Energy (E_γ)	3.10 eV
Charge collection (τ_q)	2-3 C/cm^2
Ionization Energy (E_i)	1.9 eV
Photocathode Active Surface (S_{Pk})	5.29 cm^2

blue line. According to this study, the Quantum Efficiency degradation is inconsequential. It can be also said that this degradation is related to the low level of light intensity the PMTs are going to be exposed to during the time of the mission.

Therefore we consider the failure rate of the PMT due to the degradation of the quantum efficiency as the inverse of its lifetime, as $\lambda_{QE} = 2.12\times 10^{-2}$ Failures/10^6 h. Hence, the MTTF is 47×10^6 h.

Since the Quantum Efficiency affects some performance characteristics of the PMT as responsivity and detectivity, their affection and contribution to failure has been evaluated in the following subsections.

5.1.2 PMTs detectivity degradation

The Noise Equivalent Power (NEP) is a measure of the sensitivity of a photodetector. It is defined a the signal power that gives a signal-to-noise ratio of one in one Hertz output bandwidth (equivalent to half a second of integration time). [1].

The inverse value of NEP is the detectivity (detection capability). The detectivity is a measure of the least detectable radiant power or detector signal to noise ratio. A higher detectivity indicates capability to detect lower levels of radiant power [2].

Therefore, the NEP is calculated as follows:

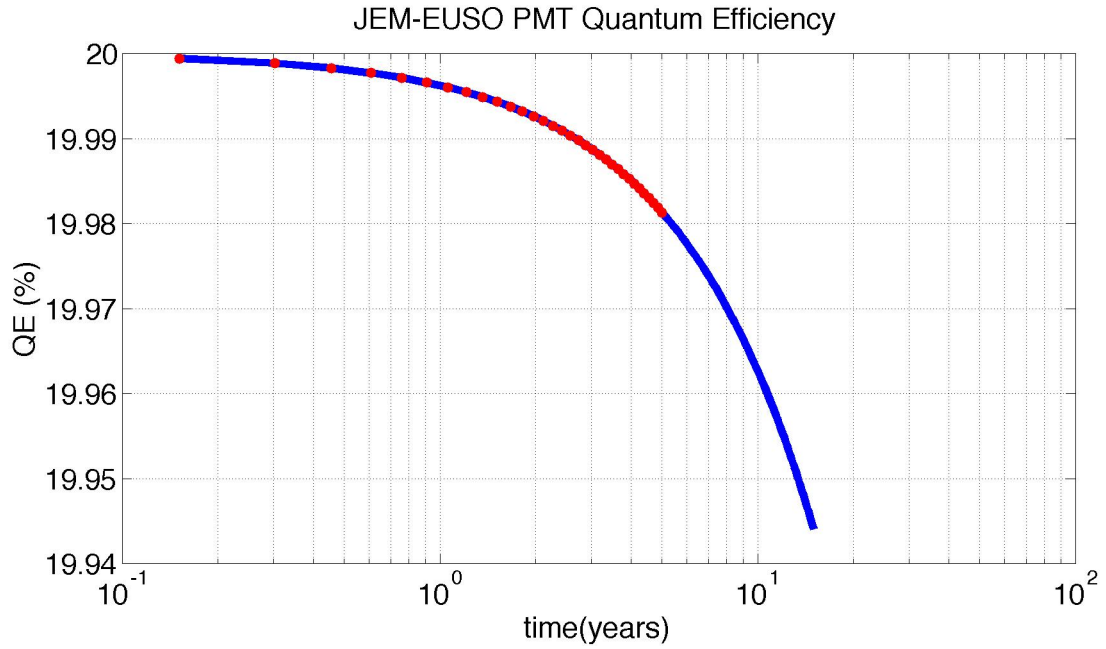

Figure 5.1: JEM-EUSO PMTs Quantum Efficiency degradation expressed at different time periods. According to this results, the QE degradation in five years operation is of 0.1%

$$NEP = \frac{hc}{QE\lambda}\left(\frac{2I_D}{q}\right)^{1/2} e^{t/\tau} = 3.78 \times 10^{-14} e^{t/\tau} \mathrm{WHz}^{-1/2} \tag{5.5}$$

The parameters given in Table 5.2 were used to estimate dark current (I_D) considering following expression:

$$I_D = aAT^2 exp\left(\frac{-\phi_0}{kT}\right) = 2.970 \times 10^{-13} A \tag{5.6}$$

Finally, in order to obtain NEP and therefore detectivity, parameter values are provided in Table 5.3.

Previously we mentioned that the reduction of a PMT quantum efficiency is a parameter that directly affects its performance. Hence this can be seen not only as a percentage of the ratio of photons entering the number of subsequently emitted electron. The quantum efficiency degradation can be also express in terms of loss of detectivity of the detector, ie as soon as it has reduced the ability of photons that can be detected throughout the

Table 5.2: JEM-EUSO PMTs I_D characteristics

Parameter	**Value**
Richardson's constant (a)	$1.2\times\ 10^6$ A/(m^2 K^2)
Absolute temperature (T) in K	300 K
Work function (ϕ_0)	2.24 eV
Boltzmann's constant (k)	$8.62\times\ 10^{-5} eV/K$
Cathode Area (A)	$5.29\ \times\ 10^{-4}$m^2

Table 5.3: JEM-EUSO PMTs NEP characteristics

Parameter	**Value**
Planck constant (h)	$6.62\times\ 10^{-34}$ J·s
Speed of light (c)	$3\times\ 10^8$ms^{-1}
Dark Current (I_D)	$2.97\times\ 10^{-13}$A
Elementary charge of the electron (q)	1.62×10^{-19} C
Wavelength (λ)	400nm

lifespan and therefore the number of photons produced. This effect is shown by Figure 5.2, which clearly shows the linearity between the QE and detectivity. In the end, the reduction of the detectivity is as low as the QE. However its reduction is not considerable enough during the period of the mission since 0.1% of loss is acceptable considering that 10% of threshold loss is accepted by the JEM-EUSO scientific requirements.

5.1.3 Responsivity degradation

The responsivity (R) expresses how much electrical signal is generated when a given amount of optical flux is incident on a detector, and it can be also consider as the sensitivity of the detector. The electrical quantity can be current or voltage [3].

$$R(t) = QE(t)\frac{e}{h\nu} \tag{5.7}$$

where $\nu = 7.5 \times 10^{14}$ Hz.

As for detectivity, responsivity is a parameter related to the quantum efficiency. Its

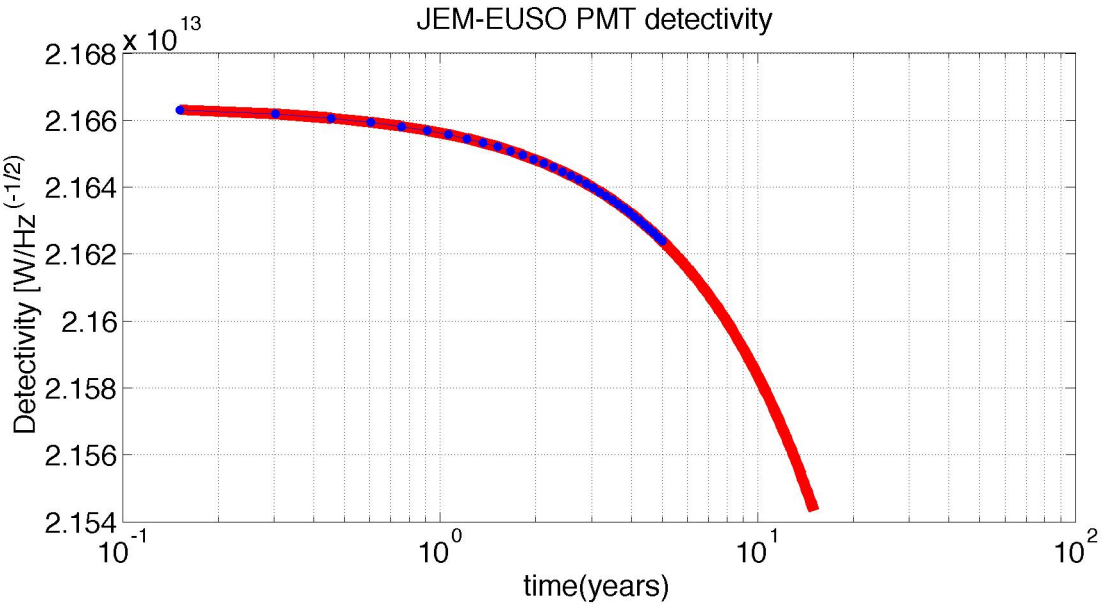

Figure 5.2: JEM-EUSO PMTs detectivity degradation expressed for different time periods

behavior allows to predict the performance of the PMTs. Its understanding also contributes to calibrate the instrument in order to guarantee the success of the mission as well. However, the responsivity shown by this study, is within the parameters of the manufacturer, with a value of about 2.542 mA/W over the first 5 years and a reduction of up to 0.1% of its value during the same period of time.

5.1.4 PMTs performance degradation due to radiation

According to [4], the amount of PMTs that will fail during the JEM-EUSO operating time is about 23 including all Space radiation contributions. Thus, the failure rate in terms of radiation is $\lambda_{RAD} = 0.12$ Failures/ 10^6 h, whereas, the MTTF of about 8.74×10^6h. These values will be explained in detail in the next subsections when whole sources of failure are considered in order to stablish the total Failure Rate of the JEM-EUSO PMTs.

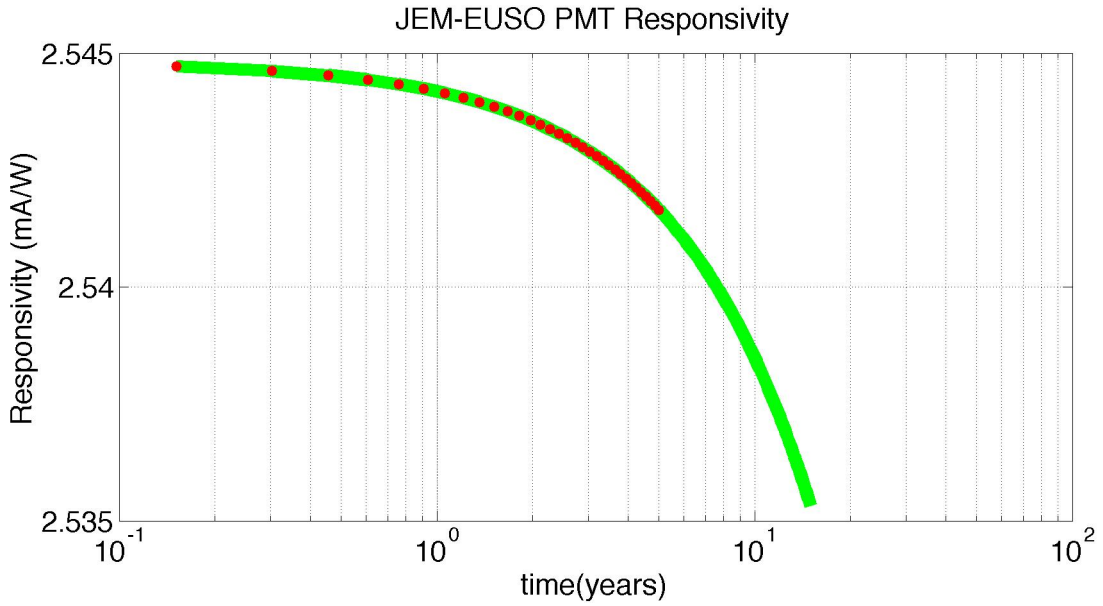

Figure 5.3: JEM-EUSO PMTs Responsivity degradation versus operation time

5.2 Catastrophic failure evaluation of JEM-EUSO PMTs using 217 Plus prediction method

Reliability analysis using standard 217 Plus is quite useful since it is basically the latest version of MIL-HDBK-217-F. Also, the 217 Plus has optional data included in order to enhance the predicted failure rate by adding more detailed parameters pertaining to environmental stress, operating profile factors and process grades. It also contains default values for the environmental stress and environmental profile as well as many more and new components missing in MIL-HDBK-217-F. The failure rate (λ_p) for plastic encapsulated (non-hermetic) integrated circuit applicable for the PMT is given by Eq (5.8), and the conditions and values according to the 217 Plus method are shown in Table 5.4. These values allow us to estimate the base failure rate and failure rate multipliers for any environmental, with operational as well as non operational conditions which the component is exposed to. The calculations results from the failure rate evaluation made to PMT are shown in Table 5.5.

$$\lambda_P = \pi_G(\lambda_{OB}\pi_{DCO}\pi_{TO} + \lambda_{EB}\pi_{DCN}\pi_{RHT} + \lambda_{TCB}\pi_{CR}\pi_{DT}) + \lambda_{SJB}\pi_{SJDT} + \lambda_{EOS} \tag{5.8}$$

The key factor in failure rate evaluation for PMT according to 217 Plus is: failure rate multiplier, solder joint delta temperature (π_{SJDT}), this value reflects that the most important aspect to consider when assembling our electronics system in case of PMT is soldering: a well known critical parameter due to vibration effects. A parameter now confirmed and reflected by this evaluation.

Table 5.4: PMT Condition Values according to 217 Plus

Condition	**Value**
Integrated Circuit, Plastic Encapsulated	PMT
Year of Manufacture	2010
Growth constant (β)	0.293
Duty Cycle	20%
Cycling Rate	5840 y^{-1}
Activation Energy Operating (Eaop)	0.8 eV
Activation Energy nonoperating (Eanonop)	0.3 eV
Ambient temperature, operating in °C (TAO)	26°C
Ambient temperature, non operating in °C (TAE)	15°C
Duty Cycle Operating (DC1op)	0.28%
Duty Cycle non Operating (DC1nonop)	0.72%
Default temperature rise ($TR_{default}$) in °C	25°C
Delta Temperature (DT_1) in °C	26.5°C
Cycling Rate (CR_1)	482.46 y^{-1}

Table 5.5: PMT Failure Rate Calculations according to 217 Plus

Failure Rate Multiplier (FRM) or Base failure rate	**Symbol**	**Result**
Reliability Growth FRM	π_G	6.867×10^{-3}
Base failure rate, Operating	λ_{OB}	1.3×10^{-5} F/10^6h
FRM for Duty Cycle Operating	π_{DCO}	0.714
FRM for Temperature Operating	π_{TO}	12.18
Base failure rate, Environmental	λ_{EB}	1.997×10^{-3} F/10^6h
FRM, Duty Cycle, Non operating	π_{DCN}	1.11
FRM for Temperature environment	π_{RHT}	0
Base failure rate, Temp Cycling	λ_{TCB}	8.9×10^{-5} F/10^6h
FRM, Cycling Rate	π_{CR}	12.10
FRM,Delta Temperature	π_{DT}	3.405
Base failure rate, Solder Joint	λ_{SJB}	4.850×10^{-3} F/10^6h
FRM, Solder Joint Delta Temp	π_{SJDT}	0.635
Failure rate Electrical Overstress	λ_{EOS}	1.562×10^{-3} F/10^6h
	Failure Rate = 4.658×10^{-3} F/10^6h	

5.3 Estimation of PMTs reliability and Discussions

Reliability has many connotations. In general, it refers to an item's ability to successfully perform an intended function during a Space mission. The longer the item performs its intended function, the more reliable it is.

Some systems, such as spacecrafts, cannot be repaired after a major failure, which is obviously the case of JEM-EUSO PMTs. In other cases, even though maintenance tasks can be performed offline, they cannot be performed during a mission. For all of these types of non-repairable systems, the time to system failure is an important reliability characteristic. The expected value is known as mean time to failure (MTTF). [5].

Table 5.6. PMT Failure Rates values

Study / Reliability Expression	Radiation	Quantum Efficiency	217 Plus
Failure Rate	0.11F/10^6h	2.12×10^{-2}F/10^6h	4.658×10^{-3}F/10^6h

The failure rates calculated before yield the MTTF Values are listed in Table 5.6. A MTTF of 7.36 million hours (7.36×10^6 hours) according to the addition of every PMT

failure source. Certainly they do not mean we can expect a PMT to operate for 840 years before failing. MTTF is a statistical measure, and as such, it cannot predict anything for a single unit. Assuming that during the useful operating life period the PMT have constant failure rates, and part failure rates (λ_{parts}) follow a Poisson distribution. In this case, the MTTF of the product can be calculated as:

$$MTTF = \frac{1}{\sum \lambda_{PMT}} \tag{5.9}$$

and the probability that the component will work for some time t without failure is given by:

$$P(t) = e^{-\frac{t}{MTTF}} \tag{5.10}$$

Thus, in case of JEM-EUSO PMT with an MTTF of 6.85×10^6 h (All failure sources included) and a mission duration of 5 years (43,800 h) of continuous operation, with 99.4% of reliability for five years without a failure. Figure 5.4 illustrates this situation. In other words, an estimated lost of 0.6% of the JEM-EUSO telescope focal surface in 5 years of operation period according to 217 Plus, radiation failure sources and Quantum efficiency degradation.

We can use MTTF rating more accurately, however, in JEM-EUSO focal surface we have 4,932 PMT operating continuously, so, we can expect about 30 PMTs to fail in five operation years according to this study. This gives a $\lambda = 6.85 \times 10^{-4}$ PMTs failing per hour.

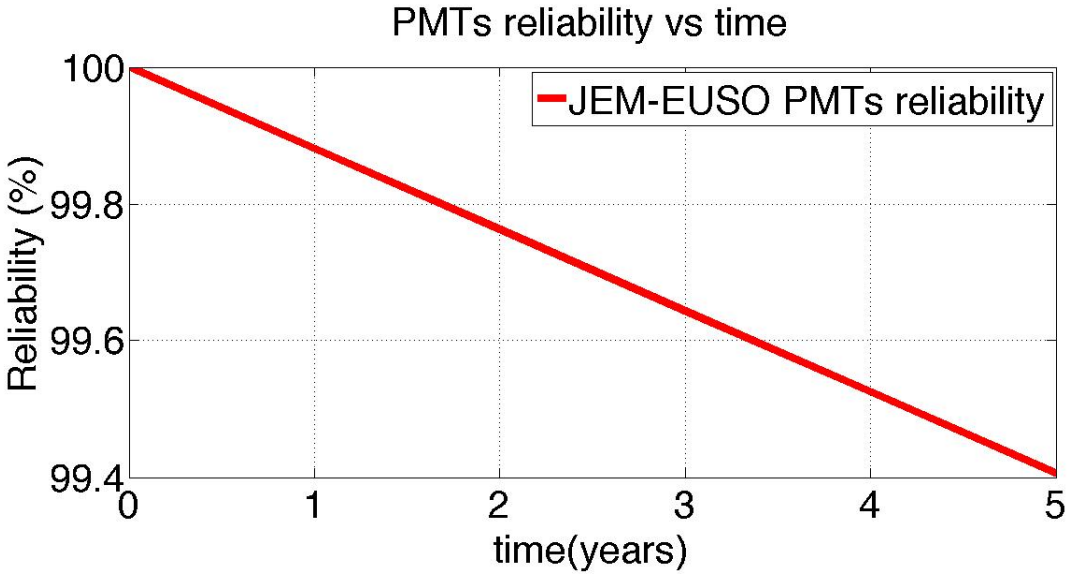

Figure 5.4: JEM-EUSO PMTs reliability vs time including multiple failure sources

5.4 Estimation of PMTs failures during JEM-EUSO mission

In order to estimate the failing JEM-EUSO PMTs during the time of the mission, the Poisson distribution has been used.

The Poisson equation for predicting the probability of a specific number of failures (r) in time (t) is as follows [6] :

$$P(r,t) = \frac{(\lambda t)^r e^{-\lambda t}}{r!} \tag{5.11}$$

where:

- r = number of failures in time (t)
- λ = failure rate per hour
- t = time expressed in hours
- $P(r,t)$ = probability of getting specific r failures in time t

Assuming that the population of the PMTs that JEM-EUSO telescope focal surface will use has a failure rate (per year) of 6 failures or roughly 30 PMTs are going to fail during

the mission due to the quantum efficiency degradation and it is expected to operate during 43800 hours, it is necessary to estimate the specific number of failures during mission time. The values from the estimation were calculated using Eq (5.11), and the results are shown in Figure 5.5.

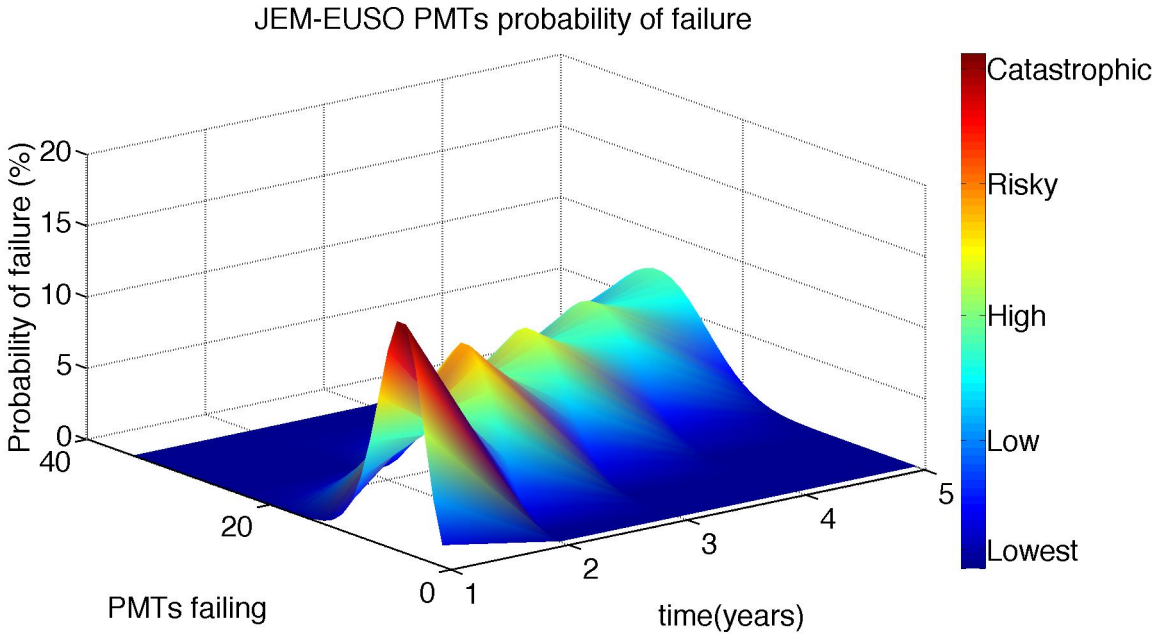

Figure 5.5: Approximate number of PMT's Failing

Bibliography

[1] Hamamatsu. Technical Information SD-12. Characteristics and use of infrared detectors. 2004. Hamamatsu Web Page:https://www.hamamatsu.com/resources/pdf/ssd/infrared_techinfo_e.pdf

[2] J. Ready, Optical Detectors and Human Vision. Fundamentals of Photonics SPIE, Module 1.6. pp. 216-232. 2006.

[3] K.Laqua, B. Schrader, G. G. Hoffmann, D. S. Moore and T. Vo-Dinh. Detection of radiation. International union of pure and applied chemistry. Analytical chemistry division commission on spectrochemical and other procedures for analysis. Pure & Appl. chem, Vol 67, No, 10, pp. 1745-1760, 1995.

[4] H.Prieto-Alfonso, L.Del Peral, M. Casolino, T. Ebisuzaki and M.D Rodríguez Frías. Radiation Hardness Assurance for the JEM-EUSO Space Mission. Reliability Engineering & System Safety, Vol 133, pp.137-145. Published (January 2015).

[5] European Power Supply Manufacturers Association. Reliability, Guidelines to understanding reliability prediction, EPSMA web page: https://www.epsma.org, 2005.

[6] Mohammad Modarres,Reliability Engineering and Risk Analysis, A Practical Guide,Chapter 1. Page 15-21 Second Edition, 2010.

Chapter 6

The Sakura code development

6.1 Introduction

Sakura has been created based on the importance of having a deep understanding of the reliability of any equipment dedicated to operate in space.

Currently, during the development of this work, it is possible to find models as Spenvis used to study the impact of space radiation (radiation hardness assurance) in any material devoted to space applications. There is also programs as Windchill (formerly Relex), which intention is to provide the user with a system to perform a reliability assessment of any device devoted for ground or space applications. However, there is no programs -at least during the completion of this work- which combine both the reliability (related to the equipment performace) and radiation hardness. Sakura is "Born" based on this premise. Finally pretending to be a computational tool that lead the user to understand the functionality and reliability of equipment devoted to operate in outer space.

Sakura can be useful at any space orbit, however, in this study, it has been made and special emphasis on LEO: the Orbit where the ISS (Space Telescope platform for JEM-EUSO support) is located at.

Employment and use of a reliability analysis tool may significantly increase the knowledge and behavior of components implemented in JEM-EUSO Space telescope. This tool should be able to provide basic reliability data applying prediction models developed by

RIAC in 2008. This tool also leads the user to perform radiation hardness assurance of electronic components designed to be working in Space. The radiation sources included in this tool are related to Total Ionizing Dose and Single Event Effects. Particularly, Single Event Transients.

Finally, in order to have a better comprehension of mechanism of failures, one of the characteristics of this software is the incorporation of those intrinsic failures sources associated to the performance of the component not included in most of prediction models devoted for either Space or military applications.

So far, with regards to the analysis of degradation of performance, the model developed in this work is refereed exclusively to PMTs. Any other element, is not yet included.

6.2 Analysis

Predicting the behavior of any mechanism whether electronics, mechanic or optic is the fundamental objective in reliability engineering. Scientist and Engineers have always been aware of developing last longer and successful components. After aviation industry started, the interest in reliability engineering has increased exponentially since human life was involved as part of collateral damage in case of catastrophic failure.

JEM-EUSO, a technical and challenging instrument, will be built considering reliability engineering as a mandatory procedure. Assessing and therefore ensuring its success during its time mission is not trivial. Many failure sources are involved, they could be either mechanical, optical (if applicable) and degradation of the equipment performance. The reliability analysis tool described in this thesis, pretends to evaluate, assess and therefore ensure the success of the mission since it entails the majority of failure contribution sources the instrument could face during its time mission in Space.

Among the characteristics the reliability analysis tool, there are:

- Ability to perform a reliability analysis of any components using 217 plus prediction model;
- Ability to perform a radiation hardness assurance of any electronic components considering TID and SEE radiation sources (LEO orbit);

- Special ability to perform a reliability analysis of the intrinsic characteristics and parameters that make the PMT prone to fail;
- Ability to export the data obtained from any assessment performed.

Following subsections will explain in detail the concepts considered while developing this reliability analysis tool, such as:

- Use case diagram;
- Requirements of JEM-EUSO mission;
- Brief description of Graphical User Interface designed as a part of reliability analysis tool;

6.3 UML use case diagram

Use case diagrams describe what a system does from the standpoint of an external observer. The emphasis is on what a system does rather than how. They are closely connected to scenarios, an example of what happens when someone or something interacts with the system. An use case is a summary of scenarios for a single task of goal. An actor is who or what initiates the events involved in that task. The connection between actor and use case is called a communication association. An use case diagram can be viewed as a collection of actors, use cases and their communications [1].

According to the theory described above, Sakura, could be illustrated as a Graphical User Interface (GUI) that leads the user interacts with the application; thereby the possibility to estimate a reliability analysis of different electronic components. The user can either input its own data associated to the specific component or using the data available within the GUI; having as result multiple and different reliability assessment as a final goal for diver purposes.

6.3.1 Actors

An Actor models a type of role played by an entity that interacts with the subject (e.g., by exchanging signals and data), but which is external to the subject (i.e., in the sense

that an instance of an actor is not a part of the instance of its corresponding subject). Actors may represent roles played by human users, external hardware, or other subjects. Note that an actor does not necessarily represent a specific physical entity but merely a particular facet (i.e., "role") of some entity that is relevant to the specification of its associated use cases [2].

Sakura is a standalone desktop tool without data transferred among networks or databases. It is therefore controlled and manipulated by the end-user. User who will be able to work with the application with no modification capabilities.

In UML, the use case actor of Sakura reliability analysis tool, is devoted to one user, the end user, which is represented by Figure 6.1.

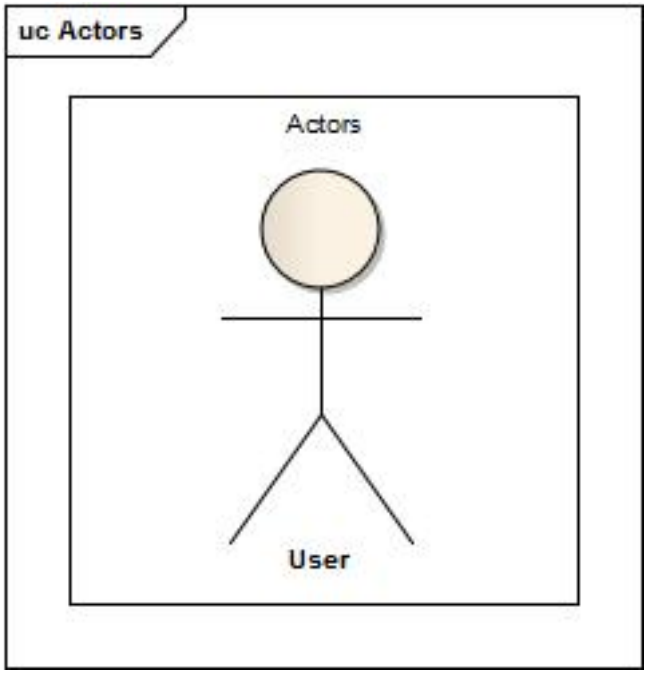

Figure 6.1: Sakura's actors diagram

6.3.2 Use case model of Sakura system

Figure 6.2 refers to Sakura system **use case**. It is referred to all use cases within Sakura System (i.e., "Authentication","Login/Enter" and "Menu"). Further sections will describe in detail all factors with regards to this use case.

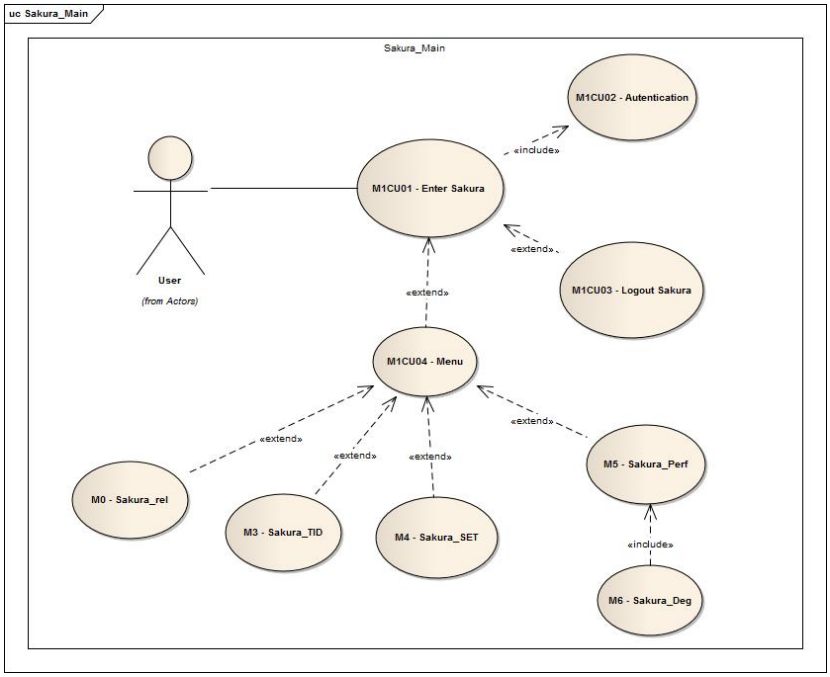

Figure 6.2: Sakura main diagram

6.3.3 M1CU01 - Enter Sakura

Figure 6.3 shows all steps performed by the user when working with SAKURA Reliability analysis tool. In principle, when entering Sakura, the user will find a screen prompting its password and login: user validation step. If validated, the user will be able to access to those models within Sakura analysis tool, otherwise, the user will be prompted again for login and password. Anyway, the user has 3 chances to access the system. After three failing attempts, the system will be locked and the user may start the program again.

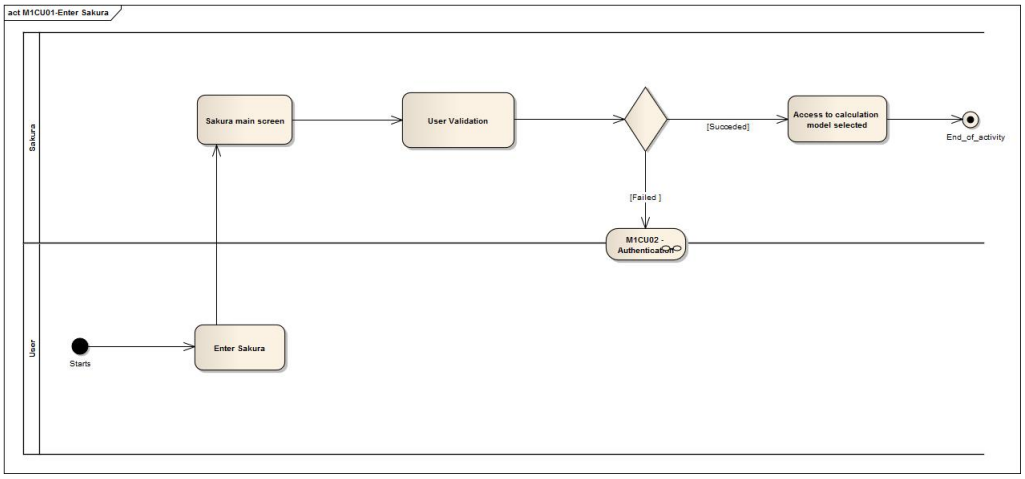

Figure 6.3: Enter Sakura activity diagram

6.3.4 M1CU02 - Authentication

Figure 6.4 describes the process realized by the user when entering Sakura reliability analysis tool. As seen, the process starts when users is prompted by a username and password. If successful when authenticating, user is able to select any of the four models available at the Sakura reliability analysis tool.

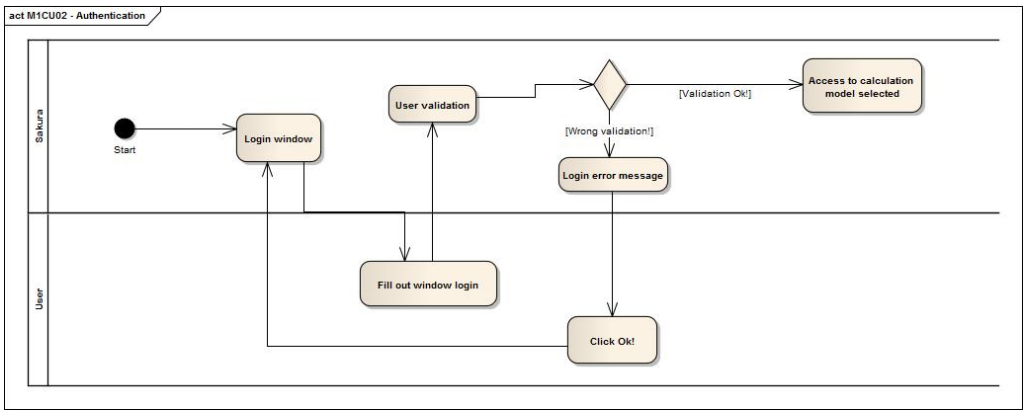

Figure 6.4: Sakura Authentication activity diagram

6.3.5 M0 - Sakura_rel

This model uses 217 Plus data (RIAC 2008) to perform the reliability assessment of any electronic, optical, mechanical component devoted for Space applications. The additional

information included in this works, relies on the fact that PMT elements (dynode and cathode) are considered semiconductor. Therefore, the PMT is evaluated as IC encapsulated element. The demonstration of this assumption can be found in previous chapters of this work. Figure 6.5 describes the use case for the first model of Sakura system:

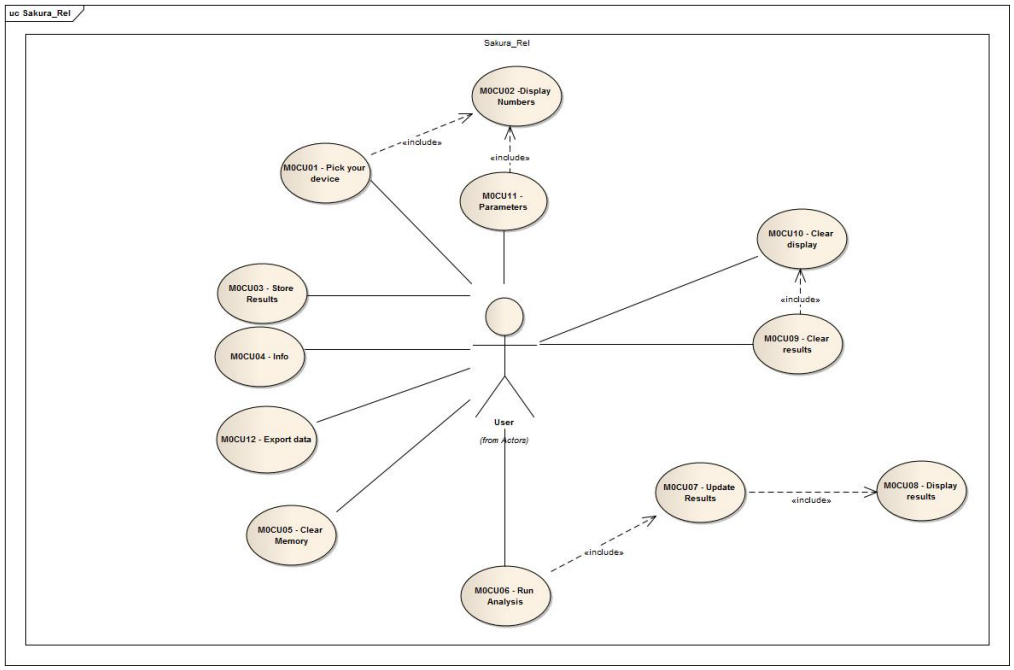

Figure 6.5: Sakura reliability analysis model related to based on 217 Plus prediction model – Use Case

Description

- User can perform a reliability analysis of any electronic component selected from the drop-down list created for this purpose. There is neither any ability from the user standpoint to create a new component nor changing or modifying any characteristics related to whatever the component is selected.

Actors

- There is only one actor in this tool: the final user.

Precondition

- User shall be previously logged in.

Basic flow of events

- User can select the component to be evaluated, as well as the environmental conditions the component under study may be subjected to.
- The intrinsic parameters corresponding to the element will be displayed by the system.
- User proceed with performing the reliability analysis by clicking the RUN button -created for this purpose- which results are displayed immediately by the system.
- User may export and plot the results obtained from the reliability analysis.

6.3.6 M3 - Sakura_TID

Figure 6.6 describes the use case of Sakura Radiation Hardness assurance model. This model was developed in order to assess electronics components devoted for Space. The electronics are supposed to be exposed to Ionizing dose sources. It was mainly designed for photomultiplier tubes. However, since ionizing dose exposure "creates" similar effects in any semiconductor family, It is applicable to any member of these families considering their own characteristics during their assessment.

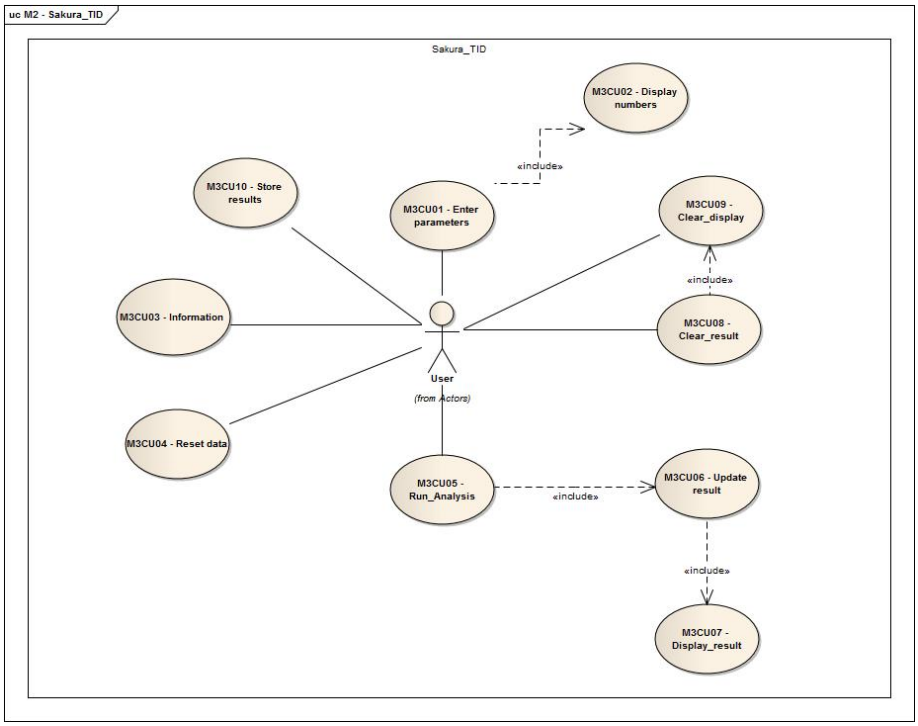

Figure 6.6: Sakura reliability analysis model related to TID − Use Case

Description

- With TID model, users are able to perform a Total Ionizing Dose (TID) radiation hardness assurance of any semiconductor or electronic component after entering the intrinsic parameters of the element into the text boxes -designed for this purposes- which are presented at the graphical user interface. These parameters are: radiation hardness of the component and its shielding. It is important to highlight that, this model is designed for elements that are supposed to operate in LEO orbit.

Actors

- There is only one actor in this tool, the final user.

Precondition

- User shall be previously logged in.

Basic flow of events

- User enters radiation hardness of the element; its shielding and coefficient of variation.
- User select performing analysis and results are displayed by system.
- User may export and plot the results obtained.

6.3.7 M4 - Sakura_SET

Figure 6.7 describes the use case for Sakura reliability analysis tool radiation hardness assurance section for electronic components devoted for space exposed to Single Event Transient radiation sources. As in case of TID, SET model was developed for PMTs, however, this model is applicable to FPGAs, ASICs boards, as well as for any microprocessor family and semiconductor elements that can be affected by Single Event Transient.

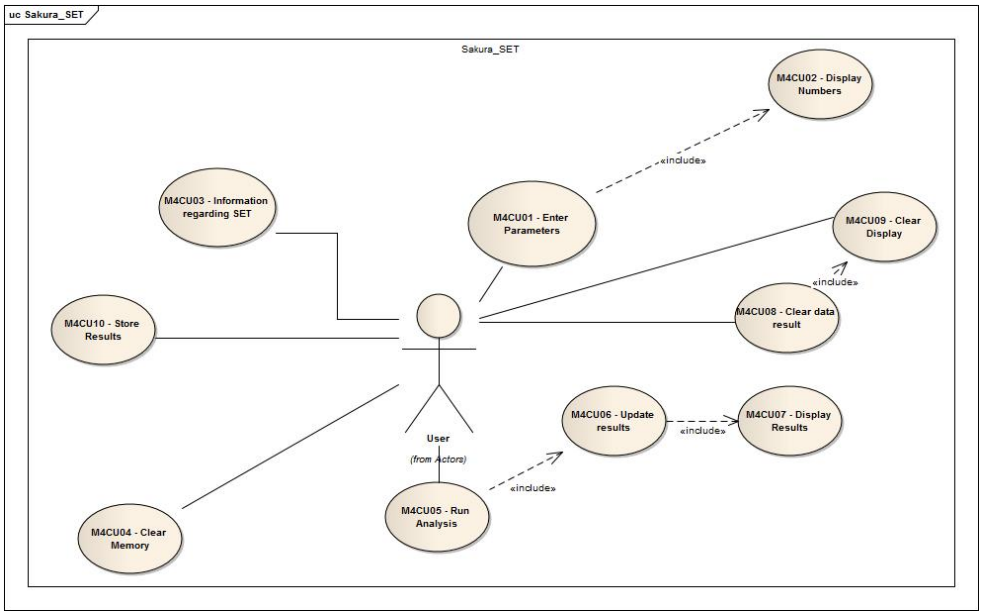

Figure 6.7: Sakura reliability analysis model related to SET − Use Case

Description

- User can perform a Single Event Transient radiation hardness assurance of any semiconductor or electronic component devoted to be operating in LEO orbits.

Actors

- There is only one actor in this tool, the final user.

Precondition

- User shall be previously logged in.

Basic flow of events

- User shall evaluate single event transient pulse in order to have a better understanding of the magnitude of the pulse received by the element produced by SETs radiation.
- Single event cross section is studied to analyze the surface being affected by charged particle when it crosses the component.
- Once SET cross section and SET pulse are analyzed, set rate evaluation is the next step towards to analyze the radiation effects on the electronic component subjected to the evaluation.
- User select to perform the radiation hardness assurance and reliability analysis. The results of these assessment are displayed on screen by Sakura system as well as the statistics plots corresponding to the analysis.
- User may export and plot the results obtained.

6.3.8 M5 - Sakura_Perf

Figure 6.8 describes the use case of Sakura reliability analysis tool reliability model section devoted to study the degradation of the performance of the photomultiplier tubes. It contemplates optical windows degradation and browning effect by outer space radiation. It also considers the quantum efficiency and responsivity degradation during PMTs operation. This model can be used for to assess the degradation of any optical component as well.

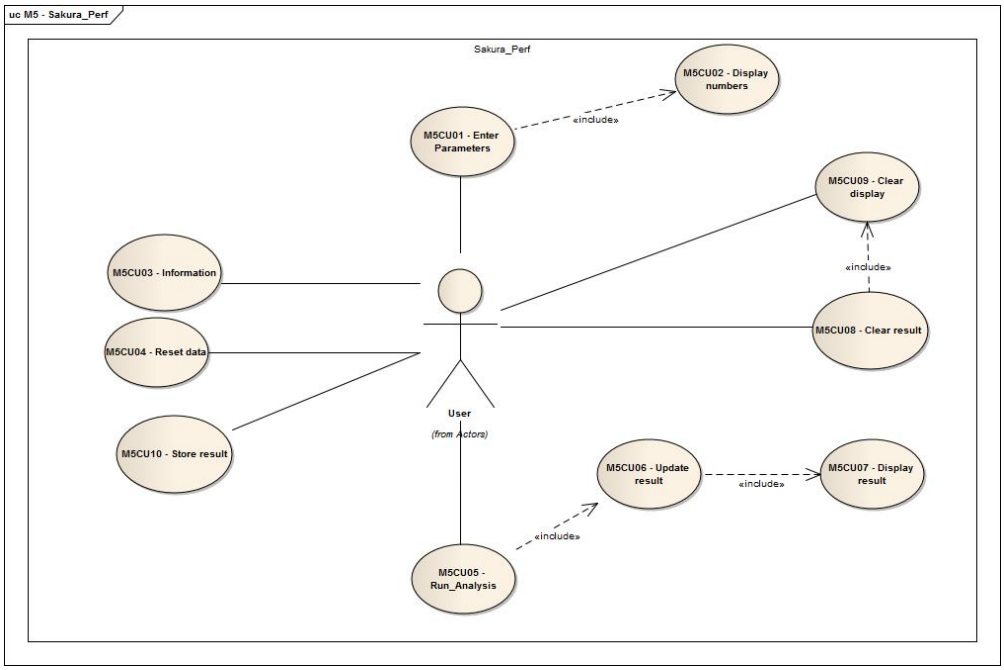

Figure 6.8: Sakura reliability analysis model related to Performance degradation − Use Case

Description

- User can perform a reliability analysis of photomultiplier tubes based on its quantum efficiency degradation. A "condition" which mostly affect Lifetime, response and detectivity of this type of elements.

Actors

- There is only one actor in this tool, the final user.

Precondition

- User shall be previously logged in.

Basic flow of events

- Users should input the initial parameters related to the quantum efficiency of the PMT, such as:

  - Initial quantum efficiency,
  - Cathode active area,
  - Photon flux received
  - Charge collection
  - Absolute temperature.
- Once initial parameters are set by the user, as an additional step, metal compound of photo-cathode should be selected.
- If photo-cathode metal compound is selected, and intrinsic parameters are set, Energy GAP and Electron affinity is obtained; finally the system will determine the Ionization energy the photo cathode would withstand.
- Photon energy, work function and Dark Current are calculated when wavelength is selected from the drop-down list of the application (Sakura, Reliability vs. Performance Model).Naturally, previously determined the Ionization energy.
- Quantum efficiency degradation can be analyzed by clicking on Q.E Simulation button.
- Quantum efficiency over years is plotted.
- Users can load "save" the data obtained on a table -Final Results- shown on the application. As seen, many different parameters in term of Detectivity, Quantum efficiency, Response, Failure rate and many other appears in order to express the degradation in terms of Reliability analysis.
- Statistical plots related to the data obtained with regards to reliability analysis are also shown.
- Users may also want to export the data obtained on a `.CSV` file by clicking on Export Data button shown at the bottom of the Final Result Table.

6.3.9 M6 - Sakura_Deg

Figure 6.9 describes the use case for Sakura reliability analysis tool intended to analyze the crystal degradation of Photomultiplier tubes. However, it can be applicable to any kind of crystal affected by ionizing radiation.

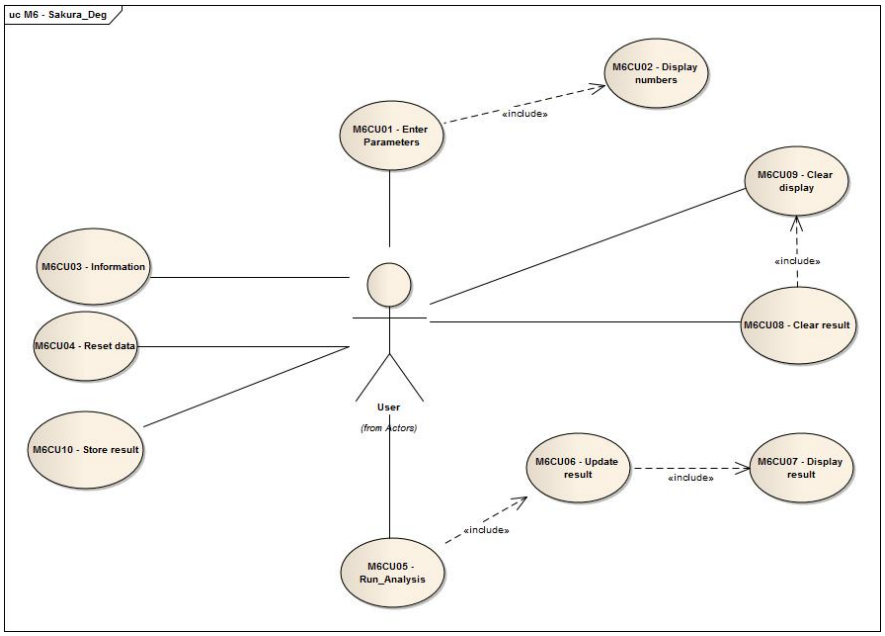

Figure 6.9: Sakura reliability analysis model related to Crystal Degradation − Use Case

Description

- User can perform a Single Event Transient radiation hardness assurance of any semiconductor or electronic component devoted to be operating in LEO orbits.

Actors

- There is only one actor in this tool, the final user.

Precondition

- User shall be previously logged in. Access to this model is possible by opening `Sakura_Perf`.

Basic flow of events

- User must open `Sakura_perf` model
- Many intrinsic parameters of the crystal window of the PMT and initial conditions shall be introduced or selected (by the user) from the different drop-down list.
- When parameters and initial conditions are selected and introduced, the user must click on the run button to perform the calculation of the browning effect: analysis based on the impact of the ionizing dose on the glass of the photomultiplier tube.
- Results may be displayed.
- Plot regarding glass transmittance degradation of the PMT is shown.
- Reliability analysis according to the degradation of the crystal windows is automatically performed. Data is expressed as Failure rate, MTTF and many other well known reliability parameters.
- Data can be stored.
- Different assessment can be performed and data obtained be saved.
- Statistical plots regarding to reliability analysis is shown.
- Assessment can be exported to an external .CSV file.

6.4 Requirements

User requirements most typically describe the relative needs, tasks, and goals of the user of a computational tool. There is therefore a need to define, document, and describe the requirements of the end-user of this computational tool. It is important to note that needs and requirements change over time and a computational tool must be initially designed to accommodate these changes through updates and further additions.

The first step considered when developing Sakura reliability analysis tool was related to end-user requirements, which are summarized as follows:

- Intuitive.
- Flexible.
- Light.

- Entails all electronics components currently used in Space industry.
- Encompass multiple ways to perform reliability analysis of electronic components.
- Up to date to newest standard and old-standard as a background in terms of methodology.
- Cross-Platform.
- Able to export to Excel data from analysis performed by the user.
- Suited to export plots derived from calculations.

6.4.1 Graphical User Interface

Since the reliability analysis tool presented in this work was developed using Matlab as a Integrated Development Environment (IDE), we would like to consider the definition of GUI Mathworks has.

A graphical user interface (GUI) is a graphical display in one or more windows containing controls, called components, that enable a user to perform interactive tasks. The user of the GUI does not have to create a script or type commands at the command line to accomplish the tasks. Unlike coding programs to accomplish tasks, the user of a GUI need not understand the details of how the tasks are performed [3].

GUI components can include menus, toolbars, push buttons, radio buttons, list boxes, and sliders⁻ just to name a few. GUIs created using MATLAB tools can perform any type of computation, read and write data files, communicate with other GUIs, and display data as tables or as plots.

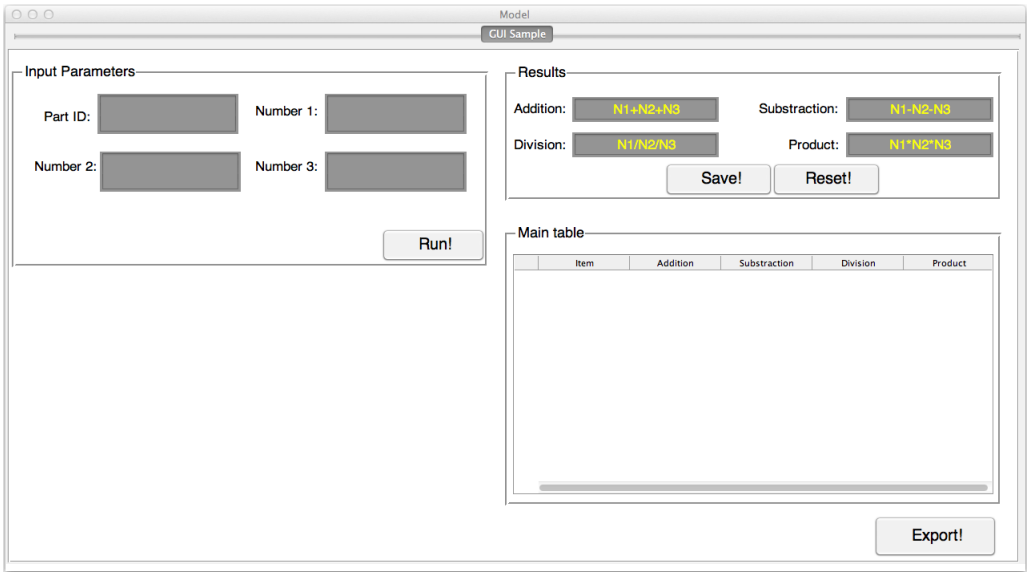

Figure 6.10: Example of a GUI designed in MATLAB

The GUI contains:

- A tab panel to show a variety of "screens" within GUI;
- Static text used to set different values to perform multiple calculations.
- Static text used to display those results from calculations performed;
- Uitable to summarize those values related to calculation made by the user;
- Push buttons to "run" activities within the GUI such as: Calculations, reset, save and export data from assessments;
- Among multiple options that can be created within a GUI, there is axes, to plot figures in 2-D and 3-D.

6.5 Design

Sakura, reliability analysis tool allows users to perform reliability analysis and radiation hardness assurance of electronics components designed for Space and military applications. Users can store an intermediate result in a memory cell. The stored result can be erased or recalled when needed.

6.5.1 UML component diagram

A component diagram is devoted to show interdependence of various software components the system involves. Sakura reliability analysis tool has 4 main components. These components are:

- A component designed to perform reliability analysis of electronics components designed for military and Space applications using 217 Plus prediction model as background: `cmp Sakura_Rel`.
- A component designed to perform reliability analysis of electronic components designed for military and Space applications which are exposed to Total Ionizing Dose (TID): `cmp Sakura_TID`.
- A component designed to perform reliability analysis of electronic components designed for military and Space applications which are exposed to Single Event Transient (SET): `cmp Sakura_SET`.
- A component designed to perform reliability analysis of photomultiplier tubes regarding to various failure sources while operating: `cmp Sakura_Perf`.

6.5.1.1 cmp Sakura_Rel

`Sakura_Rel` component, as part of **Sakura reliability analysis tool**, is an application designed to perform a reliability assessment of electronic components designed for military and Space applications using a prediction (statistical) model designed by RIAC - 217 Plus. However, the original contribution of this model represented by **"cmp Sakura_Rel"** component, Figure 6.11, lies in the fact that it includes new elements such as Photomultiplier tubes as well as new environment such as Outer Space.

The **"cmp Sakura_Rel"** component is based on multiple component, such as follows:

- **Rel_Selection:** responsible for displaying all drop-down lists. Letting the user select the component to be studied, and the year of manufacture of the element.
- **Rel_Parameters:** responsible for invoking and displaying parameters for evaluation such as : Ambient Temperature Operating(TAO), Ambient Temperature nonoperating (TAE),Cycling Rate(CR) and Relative Humidity(RH); These param-

eters are not possible for being modified; This component needs to make use of the `Rel_Selection` component to obtain this data.

- **Rel_Estimation Component:** responsible for calculating the failure rate of the element selected; this component needs to make use of `Rel_Parameters` and `Rel_Selection` data to perform the failure rate estimation.
- **Mission:** responsible for collecting the number of years the component will be operating under the conditions previously mentioned.
- **Rel_Result:** responsible for calculating the reliability of the element previously selected; this component needs to make use of `Rel_Estimation` and Mission Component data to perform this analysis.
- **Summary_Rel:** Responsible for invoking the data of `Rel_Result` component and to displaying in a summary table; this component needs to make use of `Rel_Result` component data.
- **Reliability:** Responsible for letting its subcomponent perform its own operations.

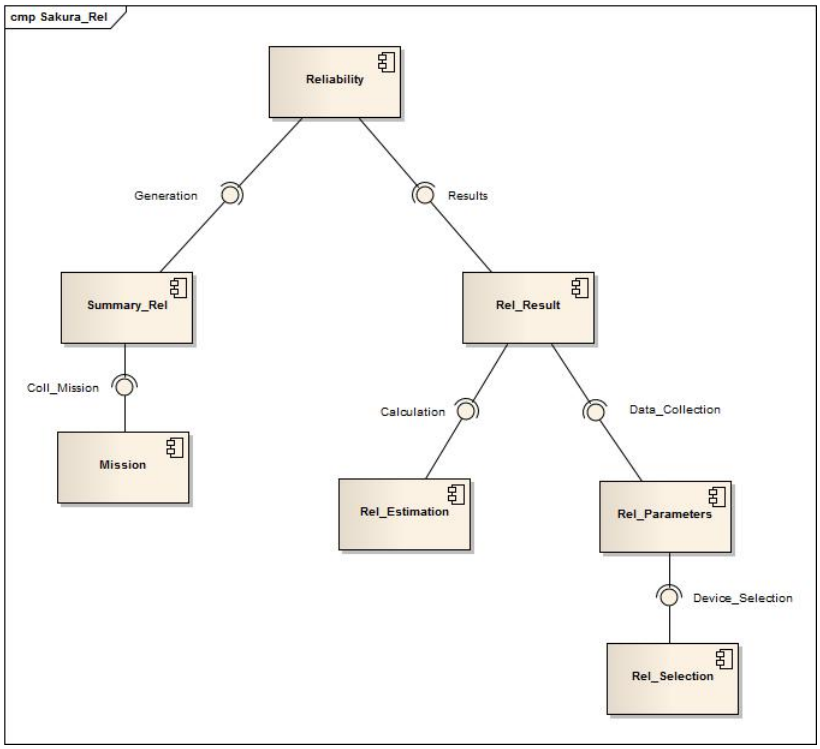

Figure 6.11: Component in Sakura related to Reliability analysis using 217 Plus prediction model adapted to new electronics designed for Space applications

6.5.1.2 cmp Sakura_TID

Figure 6.12 refers to the component dedicated to predict the impact of Ionizing dose of electronics and optical elements when facing Ionizing space radiation at LEO orbits. It can also helps to predict the shielding necessary to be implemented on the electronics elements to avoid serious damage inflicted by ionizing radiation. This component was built considered following 4 parts:

- **TID_Parameters:** Responsible for collecting the operational details of the component, such as: mission time; date of manufacture and so many other parameters.
- **TID_Estimation** Responsible for calculating the reliability of the electronic component when affected by ionizing dose when in LEO Orbit. It is done considering the operational details of the element, such as: radiation hardness, radiation received, exposure time to the radiation in years, etc.
- **TID_Results:** Responsible for displaying the reliability of the element when facing TID; It needs to make use of the TID Parameters component to obtain input from the user and TID Results which to calculate the TID with.
- **TID:** Responsible for letting its own subcomponents perform their own operations.

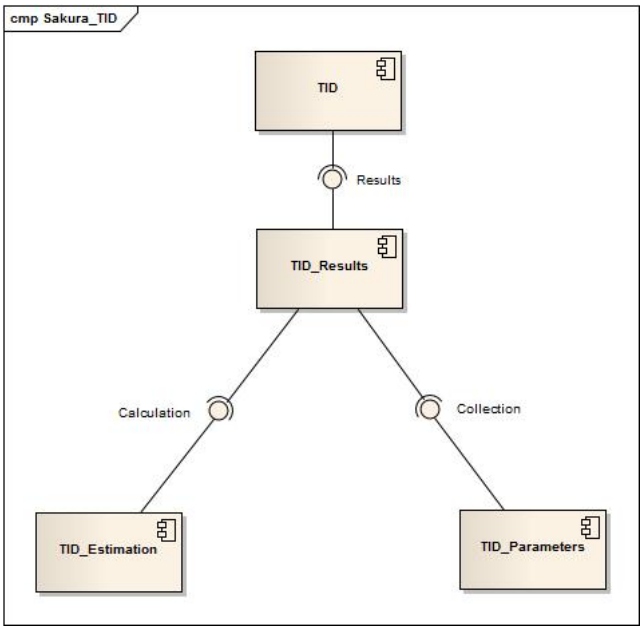

Figure 6.12: Component in Sakura related to estimate reliability of electronic components designed for Space applications which are exposed to Total Ionizing Dose radiation sources

6.5.1.3 cmp Sakura_SET

Figure 6.13 express everything related to SET model developed in this work. This component is responsible for implementing the reliability estimation and radiation hardness assurance of electronics equipments affected by Single Event Transients (SET affection of protons and heavy ions as radiation particles).

- **Pulse_Parameters:** responsible for collecting the parameters necessary to predict and determine SET Pulse. Those parameters are: Linear energy Transfer; Charge Coll Depth; Charge deposited and Time in ns the assessment is required to be performed.
- **Pulse_Estimation:** In charge of estimate the main parameters of SET pulse,such as: Current and Charge collected at the element by considering parameters previously collected by **Pulse_Parameters** component.
- **SET_Pulse:** devoted to display SET pulse in terms of Current and Charge collected at the element by considering parameters previously collected by **Pulse_Parameters** component.

- **Cross_Section_Parameters:** responsible for collecting statistical parameters of SET pulse such as: width of the distribution (Weibull distribution); threshold of LET and Shape parameters which to predict the set cross section.
- **Cross_Section_Estimation:** In charge of estimate the main parameters of SET cross section,such as: EventCross-Section/LET by considering parameters previously collected by **Cross_Section_Parameters** component.
- **SET_Cross_Section:** responsible for displaying Event Cross-Section results.
- **SET_FOM_Parameters:** responsible for analyzing, calculating and displaying Figure of Merit (FOM) Event values, considering **SET_Pulse** and **SET_Cross_Section** components.
- **SET_Rate:** responsible for collecting and analyzing Heavy Ions and Protons C Rates received with regards to FOM, SET Pulse and SET Cross section calculated previously.
- **SET_Result:** responsible for displaying Heavy Ions and Protons C Rates received with regards to FOM, SET Pulse and SET Cross section calculated previously, as well as radiation hardness assurance with regards to Single Event Transient expressed in reliability terms such as MTTF and R(t).
- **SET:** responsible for letting its subcomponents perform their own operations.

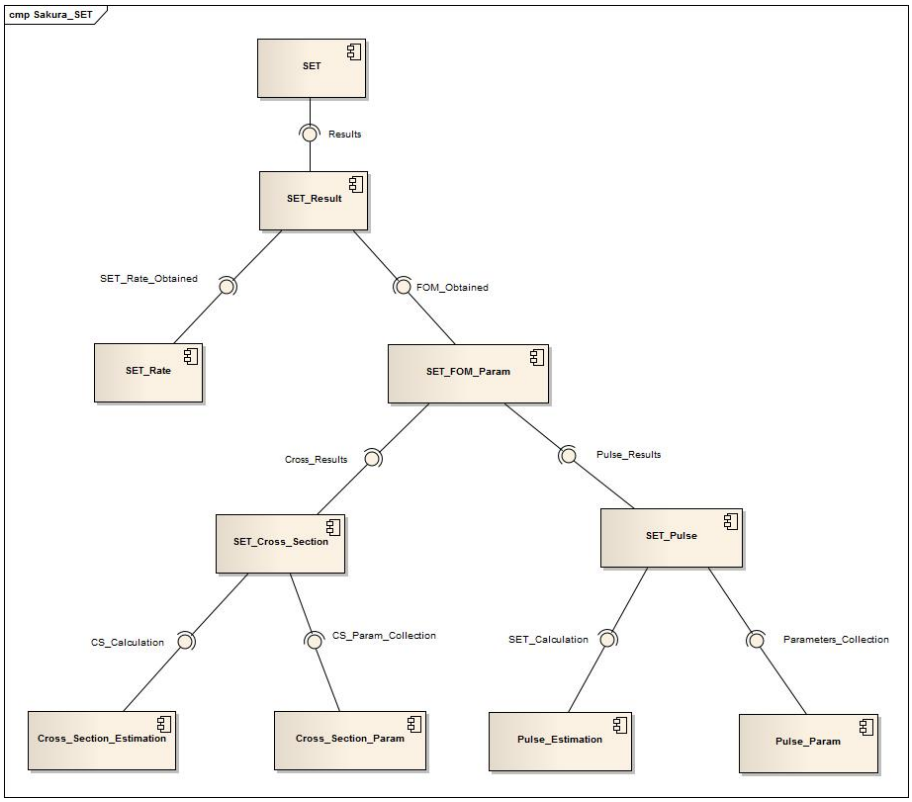

Figure 6.13: Component in Sakura related to estimate reliability of electronic components designed for Space applications which are exposed to Single Event Transient radiation sources

6.5.1.4 cmp Sakura_Perf

Figure 6.14 is responsible for assessing the reliability analysis of photomultiplier tubes when affected by multiple sources of degradation, such as: browning effect of the crystal windows, lighting effects and so on. It is an standalone component; not necessary at all to perform any other assessment throughout this tool.

- **Parameters:** Responsible for collecting quantum efficiency parameters that may affect the photomultiplier tubes during its lifetime. These parameters are: Initial quantum efficiency, Cathode active area; Time in years, Photon flux, charge collection and temperature.
- **Estimation:** In charge of estimating Photon energy, work function and dark current, partially responsible for quantum degradation of PMTs, considering quantum

efficiency parameters previously mentioned.

- **Results:** Responsible for displaying Photon energy, work function and dark current taking into account parameters and Estimation components.
- **Summary:** Responsible for analyzing and determine reliability analysis of PMTs by using as a main failure source quantum efficiency degradation.
- **Performance:** Responsible for letting its subcomponents perform its own operations..

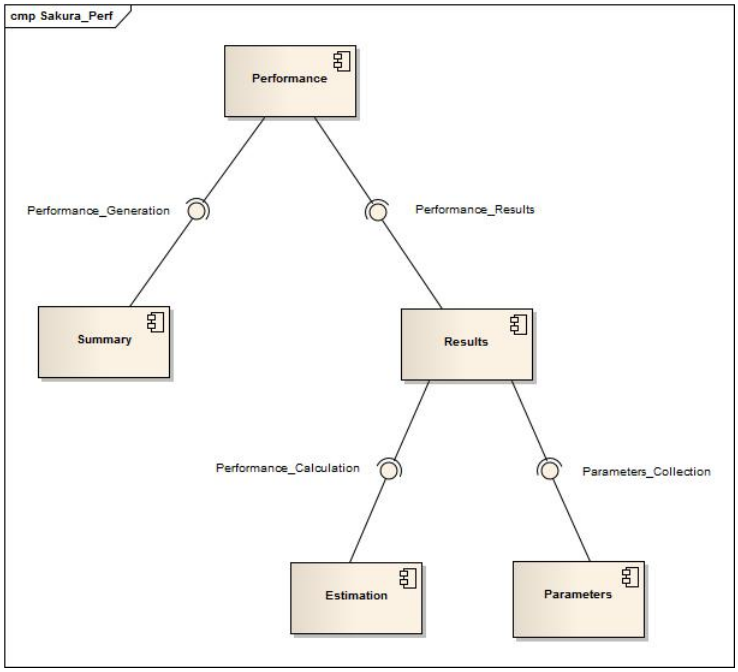

Figure 6.14: Component in Sakura related to estimate reliability of photomultiplier tubes (PMTs) designed for Space applications

6.5.1.5 cmp Sakura_Deg

Figure 6.15 is responsible for assessing the reliability analysis of photomultiplier tubes when affected by multiple sources of degradation, such as: browning effect of the crystal windows, lighting effects and so forth. It is an standalone component; it is not necessary in any case to perform any other assessment within this tool.

- **Parameters:** Responsible for collecting intrinsic parameters of the glass of photomultiplier tubes and providing multiple drop down list which to select the environ-

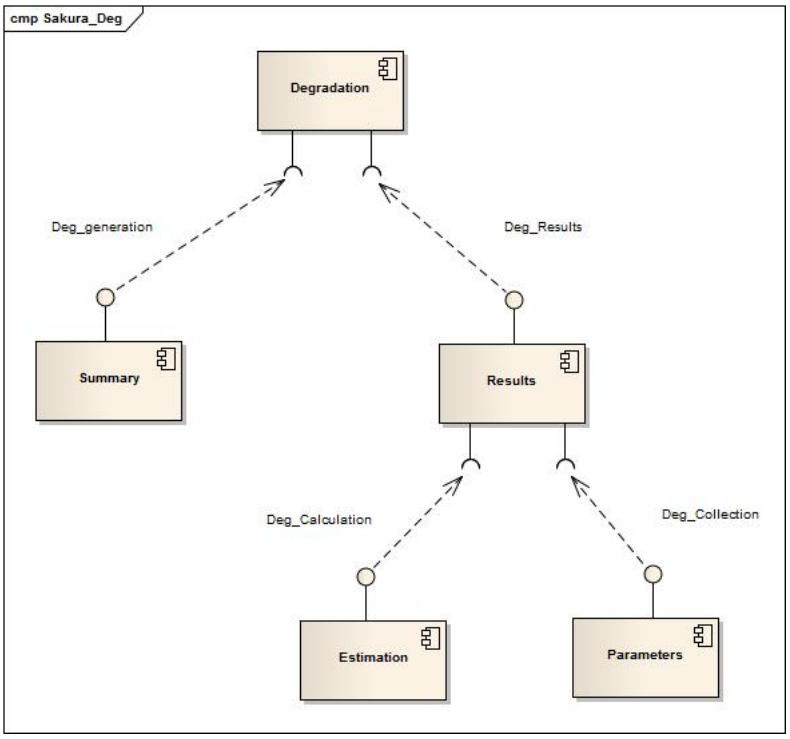

Figure 6.15: Component in Sakura related to estimate reliability of photomultiplier tubes (PMTs) crystal windows prone to be affected by Space radiation

mental conditions it is going to be subjected to.

- **Estimation** In charge of estimating Browning effect, total dose and transmittance degradation of Photomultiplier tube crystal window considering the parameters and environmental conditions previously mentioned.
- **Results:** Responsible for displaying Browning effect, total dose and transmittance degradation of Photomultiplier tube crystal window taking into account parameters and Estimation components.
- **Summary:** Responsible for analyzing and determine reliability analysis of PMTs by using as a main failure source windows transmittance degradation.
- **Degradation:** Responsible for letting its subcomponents perform their own operations.

6.6 Programming

At early stages throughout the design process of Sakura reliability analysis tool, multiple IDE candidates such as Python, Access and Matlab were used. However, when the performance of Matlab was tested, it was selected as the ideal IDE for creating this tool. Its attributes and options for developing computational tools were as needed. The comprehension and logic when programming with matlab were the main feature considered when selecting the IDE.

Among the programming code, five different models intended to perform a reliability analysis and radiation hardness assurance, can be found. These models are:

- Enhancement of 217 plus prediction model.
- TID Model.
- SET Model.
- Model of PMT performance degradation.
- Model of PMT crystal window degradation.

6.6.1 Enhancement of 217 plus prediction model

To improve the 217 prediction model, in this project, new ways of performing reliability analysis and radiation hardness assurance of electronics components have been included. These ways lie in the fact of considering the PMTs as Linear circuits, since their main aim is to amplify light current after transforming photons into photo electrons by using dynodes as multiplication chain when High voltage is applied. In other words, photo-emission effect process. PMTs are not "singular-special" devices, certainly, they are being used by many Space experiments mostly devoted for astronomy and cosmic rays research. We did include space environment to comprehend radiation impact on electronic devices. Figure 6.11 shows the GUI "module" related to 217 Plus where many of the internal model are exposed.

Therefore, this model includes following parts:

- PMT as linear circuits.

- Photocathode and Dynodes as semiconductor components.
- Space as new environment.

6.6.2 TID Model

This model is designed to analyze the reliability of any electronic component designed for Space application. Electronics certainly affected by Total Ionizing Dose (TID) at LEO orbits. A crucial source of failure for JEM-EUSO telescope when considering it will operate on-board the International Space Station in this orbit.

6.6.2.1 TID Parameters

The fundamental variables related and adapted to any orbit where TID is intended to be estimated can be observed. These variables are:

- Coefficient of variation related to the hardness of the component.
- Radiation Hardness of the component in krads.
- Shielding thickness expressed in mm.
- μ_D and μ_H represent the function of TID mean value and the radiation hardness of the equipment respectively;
- Dose received by the component expressed in krads.

Note that in case of TID model, most of the parameters stated before are entered by the user at GUI. The part of the code dedicated to prompt for this parameters is shown at Listing 6.1.

```
1 H_R = str2double(get(hRadTIDInput,'string'));%Rad Hard
```

Listing 6.1: Line of the code written in Matlab for Sakura reliability analysis tool dedicated to prompt for the radiation hardness of the component exposed to TID at LEO orbit.

In terms of programming, it is define so as to the user can enter the level of radiation the element is exposed to; it is also applicable to subsequent lines of the code where str2double(get('parameterX')) is shown.

There are also other parameters previously defined by the system. These parameters along those requested, are used by the system to determine the TID level. Condition shown by Listing 6.2.

```
function TIDMainPushButton_Callback(varargin)
H_R = str2double(get(hRadTIDInput,'string')); %Rad Hard
D_0  = str2double(get(hDoTIDIn,'string'));% Dose received
time_initial = 0:0.5:str2double(get(hTimTIDIn,'string'));
time_final = str2double(get(hTimTIDIn,'string'));
COV = str2double(get(hCOVTIDIn,'string'));%COV
sigma_D = str2double(get(hSigTIDIn,'string'));%Sigma
format long;
iter=50000; % iterations within the integration
sigma_H =sqrt(log(COV.^2+1));
mu_H=log(H_R)   (sigma_H.^2 ./ 2);
mu_D0 = log(D_0)   (sigma_D.^2 ./ 2); %rel is normalized
mu_D=log(D_0.*(time_final.* 0.2 + 1))   (sigma_D.^2 ./ 2);
mu_D2=log(D_0.*(time_initial.* 0.2 + 1)) (sigma_D.^2 ./ 2);

```

Listing 6.2: Capture of script of TID model where the definition of variables and constants associated to estimate total ionizing dose affection on electronic and optical devices are shown.

6.6.2.2 Analysis of TID model

Listing 6.3 is a part of the TID function shown at Listing 6.2. It shows the equations adapted to any electronic element when considering its own fundamentals variables. Feature necessary to estimate TID affection. In this case, by using the graphical user interface (GUI), the responsible of performing the radiation hardness assurance, can therefore, enter the associated parameters related to the environment where the equipment is going to be operating in. Thereby, this model can be adapted to any orbit where TID radiation can affect the device.

```
1  par1=sqrt(2 .* sigma_H.^2);
2  par2=mu_H; par3=sqrt(2 .* sigma_D.^2);
3  par4=mu_D; par5=mu_D2;
4  par6=mu_D0;
5  rel_nor= double(0.);
6  rel=double(0.); rel2=double(0.); %disp(rel);
7  dx_D=double(1000. ./ iter);
8  for ii=1:iter
9  x_D = ii .* dx_D;
10 Var= (1 + erf ((par2  log(x_D)) ./ par1));
11 rel_nor = rel_nor + dx_D ./ x_D .* Var.* exp( (log(x_D)   par6).^2 ./ (
    par3.^2));
12 rel= rel + dx_D ./ x_D .* Var.* exp( (log(x_D)   par4).^2./ (par3.^2));%
    real
13 rel2= rel2 + dx_D ./ x_D .*Var.* exp( (log(x_D)   par5).^2./ (par3.^2));
    %over time
14 end
15 rel = ((rel ./ (2 .* sqrt(pi) .* par3))./rel_nor);
16 rel2 =(rel2 ./ (2 .* sqrt(pi) .* par3)./rel_nor);
17 end
18
```

Listing 6.3: Screen capture of TID model script code where the definition of variables and constants associated to estimate total ionizing dose affection on electronic and optical devices are shown.

6.6.3 SET Model

SET model as previous sections explained in detail: It analytically represents the affections that electronic devices face when exposed to Single Event Transient radiation. With this model the materials used when designing, building and developing the electronic component can be selected -modeling process-. When the component is modeled under the influence of SETs, the user will be able to reduce SET affection to its minimum level. In other words, SET model it is not only intended to assess the electronic element already constructed, it can be used to select its materials during its development phase.

In reference to the programming code, SET model is represented by 4 modules:

- Single Event Transient Pulse (SET pulse)
- Single Event Cross Section
- Figure of Merit
- Single Event Rate Definition

6.6.3.1 SET Pulse

SET pulse module is based on the Linear Energy Transfer mechanism: the amount of energy received by the medium per unit path length. The pulse observed, depends on the type of element (silicon in this case) as well as the orbit the element, will be operating in. The importance of this module lies in the fact that it can give the user an idea of the current pulse received by the electronic component due to SET. A critical parameter to consider during the engineering design process. Listing 6.4 shows a statistical representation of SET pulse.

```
1 it =((Qc./(ta tb)).*(exp( t.*10.$^9$./ta) exp( t.*10.$^{9}$./tb)))./1e 3
```

Listing 6.4: Statistical representation of SET Pulse.

Where:

- it is the transient current expected to be received.
- Qc is the collected charge in the sensitive region.

- ta is the collection time constant.
- tb is the ion track establishment time constant.

Anyway, as in case of TID, most of the parameters needed to estimate SET pulse are prompted by the system. Thereby, letting the user to enter its own equipment requirements. Situation shown at Listing 6.5: the screen capture of the code written in Matlab.

```
function SETMainPushButton_Callback(varargin)
LET = str2double(get(hLetSETInput,'string')); %LET Stands for Linear
   Energy Transfer
Depth = str2double(get(hDepthSETInput,'string')); %2um.MeV^ 1
time_initial = 0.001:0.005:str2double(get(hTimeSETInput,'string'));
time_final = str2double(get(hTimeSETInput,'string'));
Ch = str2double(get(hCdepoSETInput,'string')).*( 1.*10.^15); %Ch stands
   for charge deposited
ta = 1.64e 10;%Collection time constant; % Time in ns
tb = 5e 11;%Ion track establishment time; % Time in ns
Qc =(Ch.*Depth.*LET);
it_final =((Qc./(ta tb)).*(exp( (time_final).*10.^9./ta) exp( (time_final
   ).*10.^9./tb))./1e 3;
it =((Qc./(ta tb)).*(exp( time_initial.*10.^9./ta) exp( time_initial
   .*10.^9./tb))./1e 3;
end
```

Listing 6.5: Screen capture of the script to perform the SET transient pulse estimation.

6.6.3.2 SET Cross Section

SET cross section is implemented in order to comprehend the nature of the pulse received by the electronic component. It is also included in order to understand the possible damage the component may have after SET pulse is received.

At Listing 6.6, event cross-section, is represented by:

```
FL = (limit).*(1 exp( ((LET2 Thresh)./width)).$^{shape}$)
```

Listing 6.6: Screen capture of the script that represent the event cross section/LET at Sakura reliability analysis tool. It is based on the Weibull function which is the distribution that best describes the event cross section.

At Listing 6.7, the representation of the function to calculate SET cross section as a function of effective LET is found:

```
function CrossSET_Callback(varargin)
LET = str2double(get(hCrSECSETInput,'string')); %LET Stands for Linear
    Energy Transfer
LET2 = 0:0.05:str2double(get(hCrSECSETInput,'string'));
limit = str2double(get(hCrsecSETInput,'string')).*(1e 8 ); %Limit regards
    to limiting cross section
width = str2double(get(hWidthSETInput,'string')); %width refers to the
    width of the distribution
Thresh = str2double(get(hThreshSETInput,'string')); %Thresh refers to
    threshold of LET
shape = str2double(get(hShapeSETInput,'string')); %Shape
FL1 = (limit).*(1 exp( ((LET Thresh)./width)).^shape);
FL = (limit).*(1 exp( ((LET2 Thresh)./width)).^shape);
LET25 = limit + (width.*0.288.^shape);
set(hFLSETOutput,'string',num2str(FL1));
end
```

Listing 6.7: Screen capture of SET transient pulse cross section estimation for SET model

Where:

- Limit is the asymptotic upper section of the linear-energy-transfer (LET) vs cross-section curve.
- Width, pulse width of the distribution.

- Shape and duration of single-event current pulses are strong functions of the incident heavy-ion strikeś linear energy transfer (LET).
- LET corresponds to the most sensitive region being hit in its most sensitive location.

6.6.3.3 Figure of merit and SET rates

Figure of merit has been used to predict the upset rate of electronic devices, by using Weibull distribution in order to characterize the failure behavior of the device. At Listing 6.8, which is part of the script shown at Listing 6.7. It has been evaluated using different particles, Protons and Heavy ions. Feature expressed by:

```
FOMHI = (limit./LET25) ;
RpL = 2.22.*10.^5.*(limit./LET25);
set(hLET25Out,'string',num2str(LET25));
set(hFOMHeavyOut,'string',num2str(FOMHI));
set(hRLOut,'string',num2str(RpL));
FOMPro =(4.5.*10.^4).*RpL;
set(hFOMProOut,'string',num2str(FOMPro));
axes(hSETG2);
```

Listing 6.8: Screen capture of the script showing Single event transient rates ecuations. Formulae intended to analyze SET from heavy Ions and Protons

Where RpL is the limiting proton cross section as a function of the FOM for electronics, and semiconductor family, for which, both proton and heavy ion data, are available. In terms of Protons, FOM at at Listing 6.9 is expressed by:

```
FOMPro =(4.5.*10.$^4$).*RpL
```

Listing 6.9: Screen capture of the script dedicated to analyze Single Event Transient due to Protons. Designed for Sakura Reliability Analysis tool

In terms of Heavy Ions, FOM at at Listing 6.10, is expressed by:

```
FOMHI = (limit./LET25)
```

Listing 6.10: Screen capture of the script dedicated to analyze Single Event Transient due to Heavy Ions. Designed for Sakura Reliability Analysis tool.

Where Limit is related to the cross section and LET25 is The linear Energy Transfer at 25% of the limit cross section.

Rates can be expressed as the association of events or number of particles received by the device per unit of time.

An association of SET rate of protons and heavy ion was realized. A technique described in Chapter III using the well known method of assessing reliability: Failure rate estimation. This is done in order to comprehend the reliability and radiation hardness assurance of any designed and built electronics devoted for Space applications. The function implemented in Sakura reliability analysis tool to analyze this situation is shown at Listing 6.11.

```
function SETHI_Callback(varargin)
%               Heavy Ions                      %
TIME_INITIAL = 0:0.5:str2double(get(hTimeSETIn,'string')); % Time is
 expressed in Years
TIME_FINAL = str2double(get(hTimeSETIn,'string')); % Time is expressed
 in Years
CHI = str2double(get(hCRHiOut,'string'));
FOM_HI = str2double(get(hFOMHeavyOut,'string'));
V_CHI =(CHI.*FOM_HI.*365);% Failure Rate/year
mttf_chi=(1./V_CHI);
pp1 = exp(( TIME_FINAL)./(mttf_chi)).*100;% Fixed value
p1=exp(( TIME_INITIAL)./(mttf_chi)).*100;% Plot
%            Number of components               %
Comp = str2double(get(hEleSETIn,'string'));
xComp = 0:0.5:Comp;
%             Failing units               %
FUnitsHi = Comp((pp1.*Comp)./100);
%           FWHM Heavy Ions           %
AverageHi = (FUnitsHi./TIME_FINAL);
sigmaHi = (AverageHi.^0.5);
FWHM_Hi = (2.35482.*sigmaHi);
set(hFWHMhiOut,'string',FWHM_Hi);
%           Protons                 %
CPRO = str2double(get(hCRProOut,'string'));
```

```
23   FOM_PRO = str2double(get(hFOMProOut,'string'));
24   V_CPRO =(CPRO.*FOM_PRO.*365);% Failure rate/year
25   mttf_cpro=(1./V_CPRO);
26   pp2 = exp(( TIME_FINAL)./(mttf_cpro)).*100;%fixed valed
27   p2=exp(( TIME_INITIAL)./(mttf_cpro)).*100;%plot
28   %           Failing units              %
29   FUnitsPro = Comp ((pp2.*Comp)./100);
30   %          FWHM Protons         %
31   AveragePro = (FUnitsPro./TIME_FINAL);
32   sigmaPro = (AveragePro.^0.5);
33   FWHM_Pro = (2.35482.*sigmaPro);
34 end
```

Listing 6.11: Screen capture of function written for Sakura Reliability Analysis tool to express reliability and radiation hardness in terms of proton and heavy ion rate.

Procedure developed to predict proton rate estimation shown at 6.11, is summarized at Listing 6.12 by:

```
1 V_CPRO =(CPRO.*FOM_PRO.*365)
```

Listing 6.12: Screen capture of proton rate estimation for Sakura reliability analysis tool

Where:

- CPRO is the orbit specific rate coefficient expressed in mils (2.54×10^{-2} mm).
- FOM_PRO is the figure of merit of protons (way of estimation previously shown).

In terms of heavy Ions, its rate estimation is shown at Listing 6.13:

```
1 V_CHI =(CHI.*FOM_HI.*365)
```

Listing 6.13: Screen capture of heavy ion estimation for Sakura reliability analysis tool

After FOM, Proton and Iron Rates are determining, reliability analysis in terms of MTTF as well as failure rate is expressed by using the Exponential distribution (shown

at Listing 6.14): A distribution which to predict the reliability of the component for a period of time.

```
1 Heavy Ions R(t): pp1 = exp(( TIME_FINAL)./(mttf_chi)).*100
2 Protons R(t): pp2 = exp(( TIME_FINAL)./(mttf_cpro)).*100
```

Listing 6.14: Exponential function used to determine reliability of electronics devices affected by protons and heavy ions.

Where MTTF prediction is given at Listing 6.15:

```
1 Heavy Ions MTTF : mttf_chi=(1./V_CHI)
2 Protons MTTF: mttf_cpro=(1./V_CPRO)
```

Listing 6.15: Mean Time To failure prediction formulae for Heavy Ions and Protons affections.

6.6.4 Performance degradation model

The Performance degradation model of PMTs is one of the main contributions in this project. Therefore, establish and predict analytically and mathematically the degradation of the intrinsic characteristics of PMT is intended. Fundamental affections of PMTs performance are:

- Quantum Efficiency degradation
- Detectivity
- Responsivity

6.6.4.1 Quantum efficiency degradation

Quantum efficiency is the number of photoelectrons emitted from the photocathode divided by the number of incident photons. Therefore, its degradation refers to the lifetime reduction of the PMT Cathode when electric charge is received. The ability to convert electron from incident photon is reduced. In terms of programming, Sakura, express this ability reduction at Listing 6.16:

```
1 lifetime = ((Charge.*Ionization.*Area)./((1.6.*10.^19).*Photon.*PEnergy.*
    Qeff))./ys;
```

Listing 6.16: Part of the script dedicated to express the Equation that shows quantum effficiency degradation at Sakura reliability analysis tool (performance degradation model).

Where: Lifetime express the quantum efficiency degradation. It is linearly dependent as the equation shows to the product of the charge of the particle received by the ionization area divided by photon energy and initial quantum efficiency. It is expressed by year in seconds by ys constant. It also considers factors such as: The charge of the electron and photon.

6.6.4.2 Detectivity

The detectivity is a measure of the least detectable radiant power or detector signal to noise ratio. A higher detectivity indicates capability to detect lower levels of radiant power. When detectivity degradation is analyzed, it is referred to the loss of capability of semiconducting photodetectors to detect radiation. When programming Sakura, especifically detectivity degradation, we used the script, shown by Listing 6.17:

```
NEP = ((h.*c)./(N.*WaveL)).*(((2.*ID)./q).^1./2);
D = 1./NEP;
```

Listing 6.17: Screen capture of the script devoted to analyze the detectivity degradation of semiconducting photodetectors.

In order to calculate the detectivity of a semiconducting photodetector, the parameter NEP, or Noise Equivalent Power is necessary to be estimated. Moreover, the detectivity is the inverse of such a parameter.Note that Detectivity is express in percentage. Parameters such as h, c, and q are Planck's constant and c is the speed of light and q the elementary charge of the electron respectively. WaveL and ID are the wavelenght the photodetector (wavelength of interest) is designed to work in and ID is the dark current respectively.

6.6.4.3 Responsivity

The responsivity (R) expresses how much electrical signal is generated when a given amount of optical flux is incident on a detector. The electrical quantity can be current or voltage [4]:

Situation analyzed and expressed by Sakura reliability analysis tool at Listing 6.18

```
Ri = 1000000.*(((N.*q)./(h.*V))./685;%Responsivity; lumen=>(1/685)Watts=1
    lumen
```

Listing 6.18: Screen capture which express the way Sakura reliability analysis tool calculates the responsivity degradation of semiconducting photodetectors.

6.6.5 PMT Crystal window degradation model

Background radiation can be considered as one of the most important sources of performance degradation of crystals, specially PMT crystal windows -Browning effect of the crystal window and transmittance degradation-. Thorough this work, these effects were modeled and expressed in terms of reliability analysis and radiation hardness assurance.

- Browning effect
- Transmittance degradation of PMT crystal window

6.6.5.1 Browning effect

In terms of hardness to ionizing radiation of glass, two different radiation-induced effects are noted in glass: a permanent increase in transmission loss on exposure to darkening (browning effect) of the glass medium itself, and a larger transient loss. Sakura treats the browning effect of crystals exposed to radiation as defined by Listing 6.19:

```
%         Probability of Gamma ray interaction            %
MassAtt = str2double(get(hPpAbsorbOut,'string')); %photoelectric mass
   attenuation
Thi = str2double(get(hCrysIn,'string')); %glass thickness
fprob = 1 (exp( MassAtt.*Thi)); %Prob of gamma ray interaction
%         UV accumulated in the glass        %
Flux = str2double(get(hPhotonIn,'string')); %Photon Flux
UVA = (Flux.*fprob); %   Rate of UV accumulated in the PMT glass   %
%       Energy deposited per year       %
Pnrg = str2double(get(hPEiOut,'string')); %Photon Flux
Depo = (UVA.*Pnrg*31556926);
%       Dose per year       %
Densi = str2double(get(hCrysDenIn,'string'));%PMT Glass density
Vol = str2double(get(hVolu,'string')); %PMT Volume
MaSS = (Densi.*Vol.*1e3.*1e3); %Mass of the crystal in kg
```

```
%         Radiation received
Rx = get(hPpRad,'String');
Ry = get(hPpRad,'Value');
Rz = Rx{Ry};
DoSe = (((Depo./MaSS)./1e2).*str2double(Rz));
```

Listing 6.19: Screen capture of the script that describes browning effect estimation implemented in Sakura reliability analysis tool.

As shown in Listing 6.19 multiple steps are necessary when browning effect of the crystal is estimated. As first step there is Probability of gamma ray interaction (per unit distance travelled). Secondly, If there is a chance of interaction, UV accumulation and Energy deposited are determined in order to comprehend the effect of that radiation. Finally, when these parameters are estimated, total dose received is calculated, which certainly is the parameter used by Sakura to express browning effect.

6.6.5.2 Transmittance degradation

The main consequence of γ-ray induced radiation damage in scintillation crystals is radiation induced absorption, or color center formation. Radiation induced absorption causes degradation of optical transmittance and light output. The way of Sakura reliability analysis tool to express such a phenomena on crystals exposed to radiation is shown by Listing 6.20.

```
%       Transmittance degradation      %
%         Transmittance before irradiation
Trx = get(hPpGlassTr,'String');
Try = get(hPpGlassTr,'Value');
Trz = Trx{Try};
%       Radiation induction coefficient     %
RadICo = str2double(get(hGlassRadIn,'string'));
%         time elapsed
TImx = get(hPpTime,'String');
```

```
TImy = get(hPpTime,'Value');
TImz = TImx{TImy};
MiT = str2double(TImz);
%             Accumulated radiation dose
Accu = (1./RadICo);
%              Transmittance degradation
%Rz: the radiation received
TBIa = str2double(Trz).*(exp(str2double(Rz).*MiT./Accu));
TBI = ((str2double(Trz) TBIa).*100);
```

Listing 6.20: Screen capture of the part of the function to calculate transmittance degradation of crystals under the influence of radiation in Sakura reliability analysis tool.

According to Listing 6.20, transmittance degradation of crystals follow an exponential expression, where initial transmittance of the crystal and Accumulated dose received are the main parameters which to consider. Certainly distributed in time.

6.7 Tests

During Sakura Reliability Analysis tool development, the fundamentals of its design was creating a graphical user interface (GUI) based on criteria driven by user-friendliness and simplicity. In other words, these criteria were as follows:

- Most of the electrical and electronic components for modeling and assessing should be available.
- Easy way to find the components needed by clicking a drop-down button
- An intuitive criteria selection for assessing one component should be available; afterwards, calculation should be automatic performed by the computational tool and therefore displayed on the screen.
- Ability to comprehend the results by multiple plots displayed; to see this plots, it is just necessary to press plot button once the calculation is performed.
- Ability to export data obtained after calculation; User can take this data obtained and ply with it when needed; a basic report can be written with this data obtained.
- Multiple -as many as required- calculations, plots and data exporting can be done at almost the same time. There is no restrictions in terms of numbers of calculations.
- Multi tasking. Users can perform TID, SET, and multiple reliability analysis at the same time. Actually, data from these assessment can be exported and saved afterwards if needed.
- Ability and capacity of selecting what tool is needed. You, as user can select the model of analysis you need in order to perform your assessment.

Bibliography

[1] Vijay Madisetti, Chonlameth Arpnikanondt, A Platform-Centric Approach to System-on-chip (SOC) Design. Springer, 2006. ISBN 0387238964, 9780387238968. Chapter 3., page 42.

[2] Visual Paradigm home page: http://www.visual−paradigm.com /VPGallery/diagrams/UseCase.html.

[3] MATLAB, Creating Graphical User Interfaces.Mathworks 2014.

[4] K.Laqua, B. Schrader, G. G. Hoffmann, D. S. Moore and T. Vo-Dinh. Detection of radiation. International union of pure and applied chemistry. Analytical chemistry division commission on spectrochemical and other procedures for analysis. Pure & Appl. chem, Vol 67, No, 10, pp. 1745-1760, 1995.

Chapter 7

Conclusions and future work

7.1 Conclusions

This work greatly contribute to the identification of all steps necessary to be considered when evaluating and assessing electronics and optical components devoted for Space applications. These steps are related to the requirements, functionality, and performance of those components that will operate in Space.

Throughout this thesis, it has been shown that reliability analysis should not only be based on current standards and prediction models. Most of the models developed by companies such RIAC apply only for ground conditions and low altitude military conditions. Results obtained by using such models are in some cases far from accurate since the environmental condition in Space and parameters such as radiation are not or only partially included. Therefore, in this thesis, new models for the reliability prediction of space related products is been developed, as well as improved those existing model developed by RIAC.

In this work, a complete analysis of the reliability and radiation hardness assurance of the focal surface of the JEM-EUSO Space Telescope has been performed. In order to carry out such analysis, a computational tool has been developed. In principle, it was designed for the JEM-EUSO Space Telescope, however, it can be of use to any other instrument devoted for Space application. This model is called the SAKURA code: a flexible tool

which to assess the reliability of any electronic device developed for Space applications.

The main conclusions we can extract from the analysis of the JEM-EUSO focal surface electronics performed during this work, can be summarized as follows:

- The most common source of failure of PMTs is related to the high brightness effects. This effect leads to a reduction of the transmittance of the crystal window. Another well common source of failure is based on its performance degradation due to secondary electron emission by ionizing particles. This effect is finally perceived as a noise signal at the output of the PMT. Since JEM-EUSO will be part of the ISS instrumentation, its field of view is already known. Thus, the brightness of high luminous (light pollution) cities will be avoided by switching off the instrument when passing by these locations. JEM-EUSO is provided with an automatic shutdown system in case of high luminosity occurrence. These events can be: a big storms with high lighning occurrence or Moonlight reflection on Sea water. This system aims to protect the PMTs and thus protecting the instrument thus ensuring the optimal performance of the equipment. After an exhaustive evaluation of the contribution to failure due to lightning, it is possible to infer that the combined effects of background and TLEs has a negligible contribution to the TID and SETs lower than 0.2% in a worst-case scenario.
- According to this study, the transmittance of the glass of the PMTs during the 5-years duration of the mission is greater than 99.98%, thereby maintaining a quantum efficiency of 20% all over the mission duration.
- The contribution to degradation of the PMT performance due to ionization of the cathode and dynode by radiation dose (mainly based on proton), is negligible. The production of secondary electrons by these elements due to these events is limited and therefore negligible. It is important to note that this is because of the height of the orbit ($\sim$400 km) where ionizing particle flux is very little.
- In this thesis, the quantum efficiency degradation during the mission due to the PMT performance in normal conditions has been evaluated. The analysis shows a reduction of the quantum efficiency of 0.1% in 5 years operation. According to this work, the degradation of the quantum efficiency is negligible. This effect is because

of the reduced level of light intensity the PMTs are going to be exposed to during the time of the mission. The failure rate obtained by quantum efficiency degradation was as low as $\lambda_{QE} = 2.12 \times 10^{-2}$ Failures/10^6 h. In other words, about 5 PMTs of the JEM-EUSO focal surface will fail during the whole Mission duration.

- The main sources of radiation affecting the reliability of the JEM-EUSO focal surface will be TIDs and SETs. The evaluation of theses sources are essential when assessing the reliability of an electronic component designed for Space. The result of this study, taking into account TID effect, secondary electrons emission due to radiation, as well as the darkening of the glass, show similar values in terms of degradation or aging. As preliminary results, we can say that the TID model proposed herein give us an approach of possible radiation effects on these components. Only 7 ± 2.5 PMT are expected to fail from our analysis during the 5 years duration of the mission by the effect of TIDs. It means a 99.86% of reliability. It does suggest that the PMT designed for JEM-EUSO is robust and highly reliable against the influence of TIDs.
- The analysis of the impact of SETs on PMTs during 5 years of operation, shows a reliability of 99.98% for heavy ions and 99.70% in case of protons. However, the combination of the affected population of PMTs by both heavy ions and protons shows a reliability of 99.68%: around 16 PMTs are prone to fail during the JEM-EUSO time mission.
- The 217 Plus reliability prediction method has been followed to evaluate those failures that might affect the electronic components by non-radiative causes. The failure mechanisms considered herein were: electrical overstress, solder joints, temperature cycling and operational failure rate. 65.91% of this kind of failures are due to Solder Joint, 33.53% to Electrical Overstress, 0.54% to Temperature Cycling and only 0.017% to Operational Failure Rate.
- The total number of failures according to the reliability prediction by using the 217 Plus method is of about 3.2% of the total failures: 1 PMT is prone to fail.
- As a result of this analysis, we can conclude that of 4932 PMTs that compose the JEM-EUSO focal surface, 30 ± 2 PMTs will fail. From which, 23 will be due to Space radiation, 5 due to quantum efficiency degradation and 1 PMT due to performance

degradation according to 217 Plus Prediction Method.

- It is possible to guarantee (based on this work) that the focal surface of the JEM-EUSO telescope has a reliability of 99.4% over the 5 year duration of the mission. This reliability meet the performance requirements established by both the JEM-EUSO collaboration and the space agencies. Requirements that validate the performance and therefore the full success of the mission.
- SAKURA, the computational tool for reliability analysis developed in this work can be used for any electronic device devoted for Space applications. The SAKURA code includes the PMT characterization studies made by Hamamatsu.

7.2 Significance for the research field

The work developed herein is essential for the JEM-EUSO collaboration. The reliability of an instrument is of very high relevance for any experimental scientific project and becomes a key point of the technical requirements for space instrumentation. In Space, failures of components/systems can not be afforded. An immediate repair is, in normal condition, not an option.

The impact of this work in the research and development community would be important to:

- Maximize the PMTs and linear circuits performance through better radiation hardness assurance,
- Development of new products -electronic components- devoted to space applications,
- A more exhaustive way of assessing electronics components reliability for ground, Military and Space qualification.

7.3 Future work

Since part of this Thesis is related to the development of software, It is necessary to continue improving this SAKURA computational tool first version by adding new software design. We aim to do this by adding components not yet included in any standard used for

reliability analysis. Thereafter, we intend to continue as we did with PMTs: studying the elements as thoroughly as possible to find all critical parameters in order to comprehend its behavior under multiple circumstances.

Among the new features we are intending to include in further version of SAKURA reliability analysis tool, we pretend to change the current Integrated Development Environment (IDE) used to build this computational tool. SAKURA pretends to be open source, free code, available for everyone. Therefore, using Matlab, though its robustness and stability, it is not the best option since it is not a free code. We intend to spread the code without forcing potential users to buy Matlab in order to use this tool.

On the other hand, since radiation hardness assurance performed at laboratories are expensive and most of the time impossible to be performed by small research teams, we consider as future work that it is necessary to collect all possible (free) data from assessment done for electronic and optical components in order to create a database with which to enhance the application of SAKURA.

Afterwards we intend to develop new statistical models to perform reliability analysis using the data collected. Thereby, enhancing current models and reliability standards devoted for military and Space applications. This informations and further possible models will be available for any person, company or research team who intends to perform these type of analysis.

Finally, in order to improve SAKURA, we intend to implement an SQL database instead of text file currently used.